

JULY 2017

Ph.D. in Civil Engineering

ABBAS HARAJ MOHAMMED

**UNIVERSITY OF GAZIANTEP
GRADUATE SCHOOL OF
NATURAL & APPLIED SCIENCES**

**OPTIMUM DESIGN OF POST-TENSIONED CONCRETE FLAT
SLABS USING FINITE ELEMENT METHOD**

**Ph.D. THESIS
IN
CIVIL ENGINEERING**

**BY
ABBAS HARAJ MOHAMMED**

JULY 2017

Optimum Design of Post-Tensioned Concrete Flat Slabs Using Finite Element Method

Ph.D. Thesis

in

Civil Engineering

University of Gaziantep

Supervisor

Assoc. Prof. Dr. Nildem TAYŞI

by

Abbas Haraj MOHAMMED

July 2017



© 2017 [Abbas Haraj MOHAMMED]

REPUBLIC OF TURKEY
UNIVERSITY OF GAZİANTEP
GRADUATE SCHOOL OF NATURAL & APPLIED SCIENCES
CIVIL ENGINEERING DEPARTMENT

Name of the thesis: Optimum design of post-tensioned concrete flat slabs using finite element method

Name of the student: Abbas Haraj MOHAMMED

Exam date: 31.07.2017

Approval of the Graduate School of Natural and Applied Science.



Prof. Dr. Ahmet Necmeddin YAZICI

Director

I certify that this thesis satisfies all the requirements as a thesis for the degree of Doctor of Philosophy.



Prof. Dr. Abdülkadir ÇEVİK

Head of Department

This is to certify that we have read this thesis and that in our consensus opinion it is fully adequate, in scope and quality, as a thesis for the degree of Doctor of Philosophy.



Assoc. Prof. Dr. Nildem TAYŞI

Supervisor

Examining Committee Members:

Prof. Dr. Mustafa ÖZAKÇA

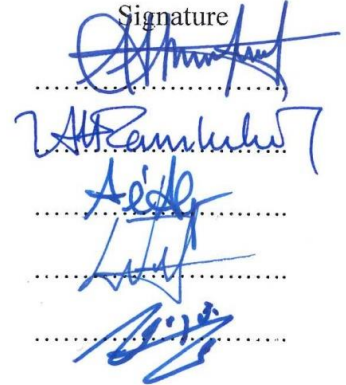
Assoc. Prof. Dr. Ali Hamza TANRIKULU

Assist. Prof. Dr. A. İlker AKGÖNEN

Assoc. Prof. Dr. Nildem TAYŞI

Assist. Prof. Dr. M. Tolga GÖĞÜŞ

Signature



I hereby declare that all information in this document has been obtained and presented in accordance with academic rules and ethical conduct. I also declare that, as required by these rules and conduct, I have fully cited and referenced all material and results that are not original to this work.

Abbas Haraj MOHAMMED

ABSTRACT

OPTIMUM DESIGN OF POST-TENSIONED CONCRETE FLAT SLABS USING FINITE ELEMENT METHOD

MOHAMMED, ABBAS HARAJ
Ph.D. in Civil Engineering
Supervisor: Assoc. Prof. Dr. Nildem TAYŞI
July 2017
151 pages

Post-tensioned slabs commonly used in building and bridge construction are grouped into two basic categories. These are the unbonded and bonded systems. This thesis investigates the structural behaviour of post-tensioned one-way concrete slabs. A nonlinear finite element model for the analysis of post-tensioned unbonded and bonded concrete slabs at elevated temperatures was developed. The numerical analysis was conducted by the finite element ANSYS software and was carried out on different one-way concrete slabs chosen from literature. A parametric study was conducted to investigate the effect of several selected parameters on the overall behavior of post-tensioned one-way concrete slab. These parameters include the effect of tendon bonding, thermal loading and tendon profile. The results showed that restrained post tensioned slab with bottom surface hotter has smaller failure load capacity.

Optimization in its wide sense can be used to solve many engineering problems. A three-dimensional finite element model for the optimization of bonded and unbonded post-tensioned concrete one-way slab was also developed in this study. The total weight of post-tensioned tendons was considered as the objective function. It is concluded that the tendon area design variable of post-tensioned slab is very effective due to, it enables us to find the optimum design of post-tensioned tendon with low cost under suitable service conditions.

Keywords: Post-tensioned slabs, computer modelling, finite element, unbonded tendon, bonded tendon, thermal loading, optimization.

ÖZET

SONLU ELEMANLAR YÖNTEMİYLE ARDGERİLMELİ DÜZ BETON DÖŞEMELERİN OPTİMUM TASARIMI

MOHAMMED, ABBAS HARAJ
Doktora Tezi, İnşaat Mühendisliği Bölümü
Danışman: Doç. Dr. Nildem TAYŞI
Temmuz 2017
151 sayfa

Binalarda ve köprülerde yaygın olarak kullanılan ard germeli döşemeler iki temel gruba ayrılmaktadırlar. Bunlar kenetlenmiş ve ayırık sistemlerdir. Bu çalışmada ard germeli, tek yönlü düz betonarme döşemelerin yapısal davranışları incelenmektedir. Sayısal analizler için doğrusal olmayan bir sonlu elemanlar modeli ANSYS yazılımı ile geliştirilmiş ve literatürden seçilen farklı tek yönlü betonarme döşeme üzerinden doğrulanmıştır. Ard germeli kenetlenmiş betonarme döşemelerin farklı sıcaklıklardaki analizi için doğrusal olmayan bir sonlu elemanlar modeli geliştirilmiştir. Çeşitli parametrelerin ard germeli tek yönlü betonarme döşemenin genel davranışı üzerindeki etkilerini araştırmak için bir parametrik çalışma yapılmıştır. Bu parametreler arasında halat bağlanma etkisi, termal yük etkisi ve halat profilinin etkisi bulunmaktadır. Sonuçlar, taban yüzeyi daha sıcak olan ard gerilmeli döşemenin daha düşük kırılma yük kapasitesine sahip olduğunu göstermektedir.

Genel anlamda optimizasyon, birçok mühendislik problemini çözmek. Bu çalışmada da, kenetlenmiş ve ayırık ard germeli betonarme tek yönlü döşemenin optimizasyonu için üç boyutlu bir sonlu elemanlar modeli geliştirilmiştir. Gerilimli tendonların toplam ağırlığı, amaç fonksiyon olarak düşünülmüştür. Ard germeli döşemenin germe halatlarının kesit alanının tasarım değişkeni olarak tanımlanmasının çok önemli olduğu sonucuna varılmaktadır, çünkü ard germe halatlarının optimum alanı uygun servis koşullarında düşük maliyeti vermektedir.

Anahtar Kelimeler: Ard germeli döşemeler, bilgisayar modeli, sonlu elemanlar, kenetlenmiş halatlar, ayırık halatlar, ısı yüklemeler, optimizasyon.



To My Parents

ACKNOWLEDGEMENT

I would like to express my special appreciation and thanks to my supervisor Assoc. Prof. Dr. Nildem TAYŞI, for all her help, patience, valuable advice, always providing and guiding me in the right direction. I'm very grateful and proudest to work under her academic guidance.

Special thanks to my family. Words cannot express how grateful I am to my mother for all of the sacrifice that have made on my behalf. Also to all my brothers. I am greatly indebted to my wife, for their strong encouragement during the years of my study. I cannot express my gratitude enough to sweetheart, my daughter Noor.

TABLE OF CONTENTS

	Page
ABSTRACT.....	v
ÖZET.....	vi
ACKNOWLEDGEMENT	viii
TABLE OF CONTENTS.....	ix
LIST OF TABLES	xiv
LIST OF FIGURES	xvi
LIST OF SYMBOLS/ABBREVIATIONS	xxii
CHAPTER 1	1
INTRODUCTION	1
1.1 General.....	1
1.2 Pre-Stressed Concrete Structures.....	2
1.2.1 Principle of pre-stressed concrete.....	3
1.2.2 Methods of prestressing.....	6
1.2.2.1 Pretensioned concrete.....	6
1.2.2.2 Post-tensioned concrete.....	7
1.2.3 Advantages of prestressed concrete.....	10
1.3 Analysis Method and Program.....	11
1.4 Problem Statement.....	11
1.5 Objective of the Thesis	12
1.6 Layout of the Thesis.....	12
CHAPTER 2	14
LITERATURE REVIEW.....	14
2.1 General.....	14
2.2 Post-Tensioned Method	15

2.2.1	Bonded post-tensioned.....	15
2.2.2	Unbonded post-tensioned	17
2.2.3	External post-tensioning	19
2.3	Analysis of Post-Tensioned Concrete Structures.....	21
2.4	Optimization of Post-Tensioned Concrete Structures.....	25
2.4.1	Optimum design of post-tensioned concrete structure	26
2.4.2	Optimum design of post-tensioned concrete slab	28
CHAPTER 3	31
FINITE ELEMENT FORMULATION AND MODELING OF MATERIAL		
PROPERTIES		
3.1	Finite Element Formulation	31
3.1.1	Basic steps in the finite element method	31
3.1.2	Outline of ANSYS	32
3.1.3	Finite element representation.....	32
3.1.4	Finite element model of concrete.....	33
3.1.5	Finite element model of reinforcement.....	33
3.1.5.1	Discrete representation	34
3.1.5.2	Embedded representation	34
3.1.5.3	Smearred (distributed) representation.....	34
3.1.6	Finite element model of steel plates	36
3.1.7	Finite element model of interface	37
3.1.8	Anchorage steel modeling	39
3.1.9	Thermal solid modeling	39
3.2	Nonlinear Solution Techniques.....	40
3.2.1	Initial-stiffness procedure	42
3.2.2	Full Newton-Raphson procedure	42
3.2.3	Modified Newton-Raphson procedure.....	42
3.3	Convergence Criterion	44
3.4	Analysis Termination Criterion	45
3.5	Modeling of Material Properties	45

3.5.1	General.....	45
3.5.2	The mechanical behavior of concrete	46
3.5.2.1	Uniaxial compression behavior of concrete	46
3.5.2.2	Uniaxial tension behavior of concrete	47
3.5.2.3	Biaxial stress behavior of concrete	48
3.5.2.4	Triaxial stress behavior of concrete.....	49
3.5.3	Concrete Modeling	50
3.5.3.1	Plasticity based models	50
3.5.3.2	Stress-strain relationship model	51
3.5.3.3	Failure criteria of concrete	52
3.5.3.4	Crack modeling	53
3.5.3.5	Crushing modeling	56
3.5.3.6	Modulus of elasticity	56
3.5.3.7	Poisson's ratio	56
3.5.4	Modeling of reinforcing bars	57
3.5.5	Material modeling of strands	57
CHAPTER 4		59
ANALYTICAL APPLICATIONS AND DISCUSSIONS		59
4.1	General.....	59
4.2	Finite Element Model	60
4.3	Analysis of Post Tensioned One-Way Slabs	62
4.3.1	Analysis of unbonded one-way slab 1-H35.....	62
4.3.2	Analysis of unbonded one-way slab T2.....	68
4.3.3	Analysis of bonded one-way slab TB2.....	74
CHAPTER 5		80
PARAMETRIC STUDIES		80
5.1	General.....	80
5.2	Effect of Bonding.....	80
5.3	Effect of Thermal Loading.....	85

5.4	Effect of Tendon Profile	89
5.5	Summary of Parametric Study	93
5.5.1	Stress distribution in the concrete	93
5.5.2	Crack patterns	101
5.5.3	Von-Mises stress in the concrete	106
CHAPTER 6		109
OPTIMIZATION OF POST-TENSIONED CONCRETE SLABS		109
6.1	General	109
6.2	Statement of an Optimization Problem	109
6.3	Objective Function and Constraints	112
6.4	Optimization of PT Slabs using Sub-Problem Approximation Method	113
6.4.1	Optimization strategy	113
6.4.2	Total weight of PT tendons minimization for bonded post-tensioned slab	114
6.4.2.1	Effect of the applied load on the optimization of bonded slab.	120
6.4.2.2	Effect of number of applied point loads on the optimization of BPT slab	121
6.4.3	Total weight of PT tendons minimization for UPT slab	123
6.4.3.1	Effect of the applied load on the optimization of UPT slab	129
6.4.3.2	Effect of number of applied point loads on the optimization of UPT slab	130
6.5	Optimization of Post-Tensioned Concrete Slabs Using Genetic Algorithm	132
6.5.1	Genetic algorithms	133
6.5.2	Interface MATLAB and ANSYS	134
6.5.3	Total weight of PT tendons minimization for the BPT slab using GA	136
CHAPTER 7		139
CONCLUSIONS		139
7.1	Conclusions	139
7.2	Recommendations for Future Study	142
REFERENCES		143

APPENDIX A	149
APPENDIX B	151



LIST OF TABLES

	Page
Table 3.1 FE representation of structural components	32
Table 4.1 Material properties of concrete, reinforcement and strand for the UPT slab 1-H35.	64
Table 4.2 Material properties of concrete, reinforcement and strand for UPT slab T2	70
Table 4.3 Material properties of concrete, reinforcement and strand for PT slab TB2.	76
Table 5.1 Parameters considered in the parametric study.	82
Table 5.2 Material properties of concrete, reinforcement and strand for proposed slab.....	82
Table 5.3 Stresses in the top and bottom fiber at center of proposed slab.	87
Table 5.4 Summery of the parametric study results.	94
Table 6.1 Constraints specified by the ACI 318.....	115
Table 6.2 Initial, optimum and limits of design variables and constraints of BPT slab.....	116
Table 6.3 Initial and design optimization values for BPT slab.	121
Table 6.4 Initial and design optimization values for BPT slab for different type of loading.	123
Table 6.5 Initial, optimum and limits of design variables and constraints of UPT slab.....	125
Table 6.6 Initial and design optimization values for UPT slab.	130
Table 6.7 Initial and design optimization values for UPT slab for different type of loading.	132
Table 6.8 Constraints specified by the ACI 318 for the optimization with GA.....	137

Table 6.9 Initial, optimum and limits of design variables and constraints for the optimization with GA. 138



LIST OF FIGURES

	Page
Figure 1.1 (a) Harped tendon. (b) Draped tendon (Nawy, 2010).....	4
Figure 1.2 Principle of PT reinforcement (Nawy, 2010).	5
Figure 1.3 Pretensioning procedure (Gribniak and Mickleborough, 1990)	7
Figure 1.4 DSI post-tensioning Jack (DSI)	9
Figure 1.5 Post-tensioning procedure (Gribniak and Mickleborough, 1990)	9
Figure 3.1 SOLID65 geometry (ANSYS, 2012).....	33
Figure 3.2 Models of reinforcement in reinforced concrete (Wolanski, 2004):	35
Figure 3.3 LINK8 geometry (ANSYS, 2012).....	36
Figure 3.4 SOLID45 geometry (ANSYS, 2012).....	36
Figure 3.5 TARGE170 geometry (ANSYS, 2012).	38
Figure 3.6 CONTA175 geometry (ANSYS, 2012).....	38
Figure 3.7 SHELL181 geometry (ANSYS, 2012)	39
Figure 3.8 SOLID70 geometry (ANSYS, 2012).....	40
Figure 3.9 Basic techniques for the solution of non-linear equations: (a) Iterative (b) Incremental (c) Incremental-Iterative (Zebun, 2006).....	41
Figure 3.10 Newton-Raphson procedures (Zebun, 2006).	43
Figure 3.11 Load step, sub steps, and time (ANSYS, 2012).	44
Figure 3.12 Typical uniaxial stress-strain curve for concrete in compression (Chen, 1982)	47
Figure 3.13 Typical uniaxial stress-strain curve for concrete in tension (Chen, 1982).	48
Figure 3.14 Biaxial state of loading (Kupfer et al., 1969).	49

Figure 3.15 Schematic failure surface of concrete in 3-D stress space (Zebun, 2006).	50
Figure 3.16 Simplified compressive uniaxial stress-strain curve for concrete (Desayi and Krishnan,1964).....	51
Figure 3.17 Failure surface in principal stress space with nearly biaxial stress (ANSYS, 2012).....	53
Figure 3.18 Smeared crack modeling (Zebun, 2006).....	55
Figure 3.19 Two-dimensional cracking representation in discrete cracking modeling approach (Zebun, 2006).....	55
Figure 3.20 Alternative bilinear stress-strain relationships (CEB, 1993)	57
Figure 3.21 Multi-linear stress-strain relationship for the strands.	58
Figure 4.1 Details of slab geometry and arrangement of reinforcement of UPT slab 1-H35 (Yang et al., 2013) (dimensions are in mm).	63
Figure 4.2 FE mesh of the concrete and the prestress strand for quarter of the UPT slab 1-H35.	64
Figure 4.3 Load- deflection curve for the UPT slab 1-H35.	65
Figure 4.4 First crack for the UPT slab 1-H35.....	66
Figure 4.5 Cracks and crushing patterns of the UPT slab 1-H35 at failure load.	66
Figure 4.6 Stress distribution of concrete for the UPT slab 1-H35 at failure load... ..	67
Figure 4.7 Von Mises stress for the UPT slab 1-H35 at failure load.	67
Figure 4.8 Details of UPT slab T2 geometry and loading (Bailey and Ellobody, 2009a) (dimensions are in mm).....	69
Figure 4.9 FE mesh of concretes and prestressing strand for quarter of the UPT slab T2.	71
Figure 4.10 Load- deflection curve for the UPT slab T2.....	71
Figure 4.11 First crack for the UPT slab T2.	72
Figure 4.12 Cracks and crushing patterns of the UPT slab T2 at failure load.	72
Figure 4.13 Stress distribution of concrete for the UPT slab T2 at failure load.	73
Figure 4.14 Von Mises stress for the UPT slab T2 at failure load.....	73

Figure 4.15	Details of BPT slab TB2 geometry and loading (Bailey and Ellobody, 2009b) (dimensions are in mm).	75
Figure 4.16	FE mesh of the concrete and the prestress strand for quarter of the BPT slab TB2.	76
Figure 4.17	Load- deflection curve for the BPT slab TB2.....	77
Figure 4.18	Deformed shape of the BPT slab TB2.....	77
Figure 4.19	Stress distribution of concrete for the BPT slab TB2 at failure load....	78
Figure 4.20	First crack for the BPT slab TB2.	78
Figure 4.21	Cracks and crushing patterns of the BPT slab TB2 at failure load.....	79
Figure 4.22	Von-Mises stress for the BPT slab TB2 at failure load.	79
Figure 5.1	Loading and boundary conditions of the proposed slab for the parametric study.	81
Figure 5.2	Load-deflection curves for the bonded and unbonded slabs.....	83
Figure 5.3	Load-stress curve of concrete of the bottom fiber at center of the slab..	83
Figure 5.4	Force in tendon at support for the bonded and unbonded slabs.....	84
Figure 5.5	Force in tendon at center of the slab for the bonded and unbonded slabs.	84
Figure 5.6	Thermal loading applied to proposed slabs.	86
Figure 5.7	Effect of thermal loading on central deflection for restrained unbonded slabs.....	86
Figure 5.8	Effect of thermal loading on central deflection for restrained bonded slabs.....	87
Figure 5.9	Effect of thermal loading on concrete stress at the bottom fiber at the center of restrained unbonded slab.....	88
Figure 5.10	Effect of thermal loading on concrete stress at the bottom fiber at the center of restrained bonded slab.	88
Figure 5.11	Effect of thermal loading on tendon force at the center of the free end slab.	89

Figure 5.12 Effect of thermal loading on tendon force at the center of the restrained slab.....	90
Figure 5.13 Proposed tendons profiles.....	90
Figure 5.14 Effect of tendon profile on central deflection for simply supported unbonded slab.	91
Figure 5.15 Effect of tendon profile on central deflection for simply supported bonded slab.	91
Figure 5.16 Effect of tendon profile on central deflection for fix supported unbonded slab.	92
Figure 5.17 Effect of tendon profile on central deflection for fix supported bonded slab.....	92
Figure 5.18 Stress distribution in the concrete at ultimate state for the slab S1.	95
Figure 5.19 Stress distribution in the concrete for the slab S2.....	95
Figure 5.20 Stress distribution in the concrete for the slab S6.....	96
Figure 5.21 Stress distribution in the concrete for the slab S7.....	96
Figure 5.22 Stress distribution in the concrete for the slab S10.....	97
Figure 5.23 Stress distribution in the concrete for the slab S13.....	97
Figure 5.24 Stress distribution in the concrete for the slab S16.....	98
Figure 5.25 Stress distribution in the concrete for the slab S18.....	98
Figure 5.26 Stress distribution in the concrete for the slab S20.....	99
Figure 5.27 Stress distribution in the concrete for the slab S22.....	99
Figure 5.28 Stress distribution in the concrete for the slab S24.....	100
Figure 5.29 Stress distribution in the concrete for the slab S26.....	100
Figure 5.30 Cracks and crushing patterns of the slab S2 at ultimate state.....	101
Figure 5.31 Cracks and crushing patterns of the slab S7.	102
Figure 5.32 Cracks and crushing patterns of the slab S10.	102
Figure 5.33 Cracks and crushing patterns of the slab S13.	103

Figure 5.34 Cracks and crushing patterns of the slab S16.	103
Figure 5.35 Cracks and crushing patterns of the slab S18.	104
Figure 5.36 Cracks and crushing patterns of the slab S20.	104
Figure 5.37 Cracks and crushing patterns of the slab S22.	105
Figure 5.38 Cracks and crushing patterns of the slab S24.	105
Figure 5.39 Cracks and crushing patterns of the slab S26.	106
Figure 5.40 Von-Mises stress in the concrete of the slab S2 at ultimate state.	106
Figure 5.41 Von-Mises stress in the concrete of the slab S7.	107
Figure 5.42 Von-Mises stress in the concrete of the slab S10.	107
Figure 5.43 Von-Mises stress in the concrete of the slab S13.	108
Figure 5.44 Von-Mises stress in the concrete of the slab S26.	108
Figure 6.1 Function plot depicting optimum solution for a 2 design variable set...	111
Figure 6.2 Optimization flow chart.	113
Figure 6.3 Dimensions of BPT slab (mm).	115
Figure 6.4 Loading of BPT slab for optimum design.	115
Figure 6.5 Evolution of optimal total weight of PT tendons for BPT slab versus number of iterations.	117
Figure 6.6 Evolution of the optimal area of PT tendons versus number of iterations.	117
Figure 6.7 Evolution of the eccentricity of the tendon profile versus number of iterations.	118
Figure 6.8 Evolution of mid-span deflection versus number of iterations.....	118
Figure 6.9 Evolution of maximum compression stress in concrete versus number of iterations.	119
Figure 6.10 Evolution of maximum tensile stress at mid-span in concrete versus number of iterations.	120
Figure 6.11 Loading of BPT slab for the load optimization.	120

Figure 6.12 Loading of BPT slab for the number of applied point load optimization.	122
Figure 6.13 Loading of UPT slab for optimum design.	123
Figure 6.14 Evolution of optimal total weight of PT tendons for the UPT slab versus number of iterations.	125
Figure 6.15 Evolution of optimal area of tendons for UPT slab versus number of iterations.....	126
Figure 6.16 Evolution of eccentricity of the tendon profile of UPT slab versus number of iterations.	126
Figure 6.17 Evolution of mid-span deflection of UPT slab versus number of iterations.....	128
Figure 6.18 Evolution of maximum compression stress in concrete of UPT slab versus number of iterations.....	128
Figure 6.19 Evolution of maximum tensile stress at mid-span in concrete of UPT slab versus number of iterations	129
Figure 6.20 Loading of UPT slab for the load optimization.	130
Figure 6.21 Loading of UPT slab for the number of applied point load optimization.	131
Figure 6.22 Optimization with GA.	135
Figure 6.23 Dimensions of BPT slab (mm) for the optimization with GA.....	136
Figure 6.24 Loading of BPT slab for optimum design for the optimization with GA.	136

LIST OF SYMBOLS/ABBREVIATIONS

P	Prestressing force.
f	Compressive stress.
A_c	Cross-sectional area of the beam section.
M	Maximum moment at midspan of beam.
f_b	Stress at the bottom fibers.
c	Centroid of the cross-section.
I_g	Gross-sectional moment of inertia.
f'_c	Ultimate uniaxial compressive strength of concrete.
f_t	Ultimate uniaxial tensile strength of concrete.
ε_1	Strain corresponding to $(0.3f'_c)$ of concrete.
ε_o	Strain at peak point for concrete.
ε_{cu}	Ultimate compressive strain of concrete.
E_c	Modulus of elasticity of the concrete.
σ	Stress
ε	Strain
β	Reduction factor to shear modulus of originally uncracked concrete.
β_o	Reduction factor to the shear modulus of opened crack concrete.
β_c	Reduction factor to the shear modulus of closed crack concrete.
ν	Poisson's ratio.
f_c	Compression stresses in concrete (obtained from FE analysis).
f_{pu}	Specified tensile strength of PT tendons.
f_{tendon}	Stresses in PT tendon (obtained from FE analysis).
V_r	Factored shear stress resistance.

V_f	Factored shear stress.
U_y	Displacement at mid-span of the slab (obtained from FE analysis).
l	Span length.
a	Area of PT tendons,
i	Initial stress in tendons
e	Eccentricity of the tendon profile.
GA	Genetic Algorithm
APDL	ANSYS Parametric Design Language.
FE	Finite Element.
3D	Three Dimensional.
PT	Post-Tensioned.
BPT	Bonded Post-Tensioned.
UPT	Unbonded Post-Tensioned.
ACI	American Concrete Institute.
PC	Prestressed Concrete.

CHAPTER 1

INTRODUCTION

1.1 General

Concrete is one of the most common building materials in civil engineering, due to its simple production, high compressive strength and versatility in form and application. However, concrete is a brittle material with a relatively low tensile strength, making it subjected to cracking. These problems are generally overcome by using reinforcement of various types; the most common is using regular reinforcement bars to carry tensile stresses where it is needed. Research has shown that labour on the construction site, such as preparation of formwork, placing of reinforcement bars and finishing of the concrete, can provide costs of the same magnitude as the material costs. Therefore, it is desirable to investigate new technologies that can contribute to saving labour time during construction and provide a more efficient solution.

Post-tensioning of concrete is a well-developed and common technology, which has proved to be a good solution regarding the brittleness and low tensile strength of the concrete. Benefits of post-tensioning include smaller crack widths and increased crack control, smaller deflections and more slender structures. Post-tensioning of flat slabs allows smaller slab thickness and larger spans, which is desirable in many typical flat slab structures such as industrial buildings and parking garages.

Post-tensioning is a method of reinforcing concrete using prestressed steel in combination with non-prestressed reinforcement. The post-tensioning Institute (PTI, 1976) explains post-tensioning in the post-tensioning Manual as a method in which the force and profile of the post-tensioning tendons is designed to produce loads that counteract a portion of the gravity loads which results in the reduction of flexural tensile stresses and deflections.

The costs of post-tensioning vary from project to project depending upon a number of factors. The length of tendon is the major influence in the cost of post-tensioning. Long tendons are relatively less expensive in comparison with short tendons. The fixed cost such as anchorages, stressing operation and establishment cause to the high cost of short tendons.

1.2 Pre-Stressed Concrete Structures

Concrete is strong in compression, but weak in tension allowing the formation of flexural cracks at early load stages. A longitudinal force can be imposed to the cross section of the concrete element, through the use of high-strength steel tendons, in order to reduce the tensile stresses that cause these cracks to develop. The longitudinal prestressing force, prestresses the sections along the span of the structural element before to the application of live and dead loads. This concept is not new, dating back to 1872 when P.H. Jackson patented a prestressing system using a tie rod to construct beams or arches from individual blocks (Nawy, 2010). The industry of Prestressed Concrete (PC) has come a long way through the years. Today it is used in underground structures, floating and offshore structures, buildings, numerous bridge systems and power stations including segmental and cable-stayed bridges.

PC has been commonly used as a cost-effective and effectual method of reinforced concrete slab construction. It offers unique benefits for improving structural performance over normal reinforced concrete in its capability to reach larger span-to-depth ratios. In Post-Tensioned (PT) segmental construction, steel tendons are the tensioning components that help as the major load-carrying components.

The prestressing tendons damage over time, mainly because of corrosion and the existence of initial imperfections. This problem can cause rupture of an individual wire in a strand or even the complete multi-wire strand causes to a loss of prestress. The loss of prestress effects in reduced slab performance and may finally lead to terrible failure. Therefore, it is imperative to controlling the decline rates of tendons and estimates the real-time conditions of slabs so that proactive renovation and maintenance measures can be taken.

Post-tensioning tendons are normally formed by casting hollow pipes into the concrete section. The wire prestressing strand are then passed through the pipes and attached to the concrete at the anchorage at each end. Normally in the U.S., in turn offers corrosion defense, a cement mortar is injected into the tendon and then allowed to harden. The grout also confirms a continuous bond between the concrete and tendon, which offers rather higher structural ability than unbonded structure (Abdullah, 2015).

1.2.1 Principle of pre-stressed concrete

The prestressing force that is applied is dependent on the geometry and loading of a specific element and is determined with the principles of mechanics and stress-strain relationships. The prestressing force (P) can be either concentric (along the axis of the member) or eccentric (a distance away from and parallel to the axis of the member). For the concentric case, the compressive stress (f) on the beam cross-section is uniform and equal to :

$$f = -P/A_c \quad (1.1)$$

where A_c is the cross-sectional area of the beam section. The minus sign denotes the state of compression. If external transverse loads are applied to the beam, causing a maximum moment (M) at midspan, the resulting stress is equal to:

$$f_t = -P/A_c - Mc/Ig \quad (1.2)$$

and

$$f_b = -P/A_c + Mc/Ig \quad (1.3)$$

where f_t is the stress at the top fibers, f_b is the stress at the bottom fibers, c is the centroid of the cross-section and Ig is the gross cross-sectional moment of inertia. The equation for stress at the bottom fibers shows that the presence of the compressive prestress force reduces the tensile flexural stress as intended in the design. The equation for stress at the top fibers shows that the prestress force induces compressive stresses in turn reducing the capacity for external loads to be applied. This situation is avoided by applying the prestress force eccentrically. For this case, the stresses become:

$$f_t = -P/A_c + Pec/Ig - Mc/Ig \quad (1.4)$$

and

$$f_b = -P/A_c - Pec/Ig + Mc/Ig \quad (1.5)$$

where e is the eccentricity of the force from the centroid of the cross-section. In order to avoid high tensile stresses in the top fiber over the support, tendons are draped or harped over the length of the member (Figure 1.1). The harped profile is usually used in pretensioned beams and the draped profile in PT beams.

Regular or mild reinforcement is added to concrete to provide tensile strength and limit crack widths. Regular reinforcement can be called a passive reinforcement because it does not carry loads until the concrete has started cracking. Post-tensioning, however, provides an active reinforcement. The pre-stressing reinforcement applies compression to the concrete in those regions that will be subjected to tensile stresses during loading.

These compressive stresses will offset the tensile stresses produced by the loads. Figure 1.2 illustrates the principle of PT reinforcement and shows regular reinforced concrete that cracks under loading, PT concrete before loading and PT concrete after loading.

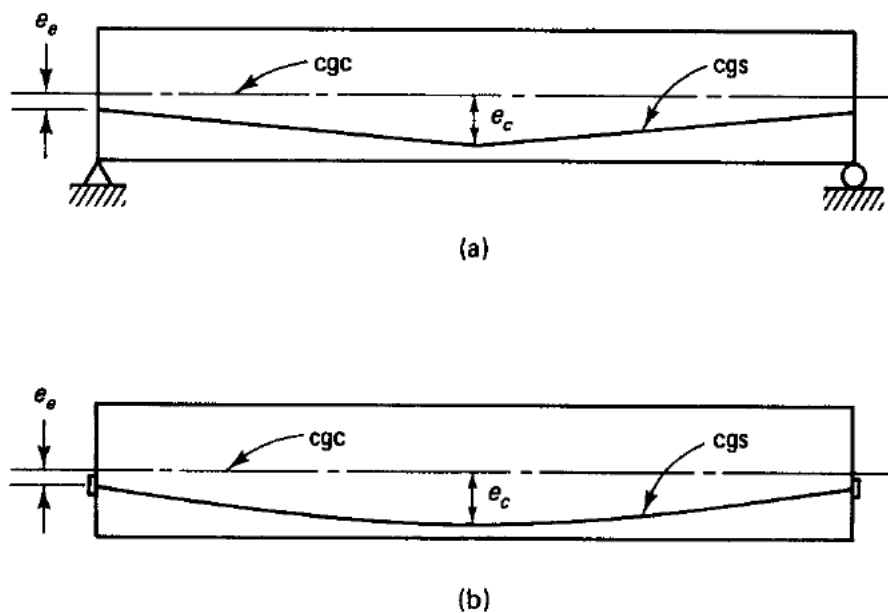


Figure 1.1 (a) Harped tendon. (b) Draped tendon (Nawy, 2010).

Thus, the total tensile stresses in the concrete will be significantly reduced, as will the crack propagation and crack widths. The deflections will also be reduced because the post-tensioning compressive stresses cause a negative deflection that will be balanced by the deflections induced by the self-weight and exterior loads (Nawy, 2010).

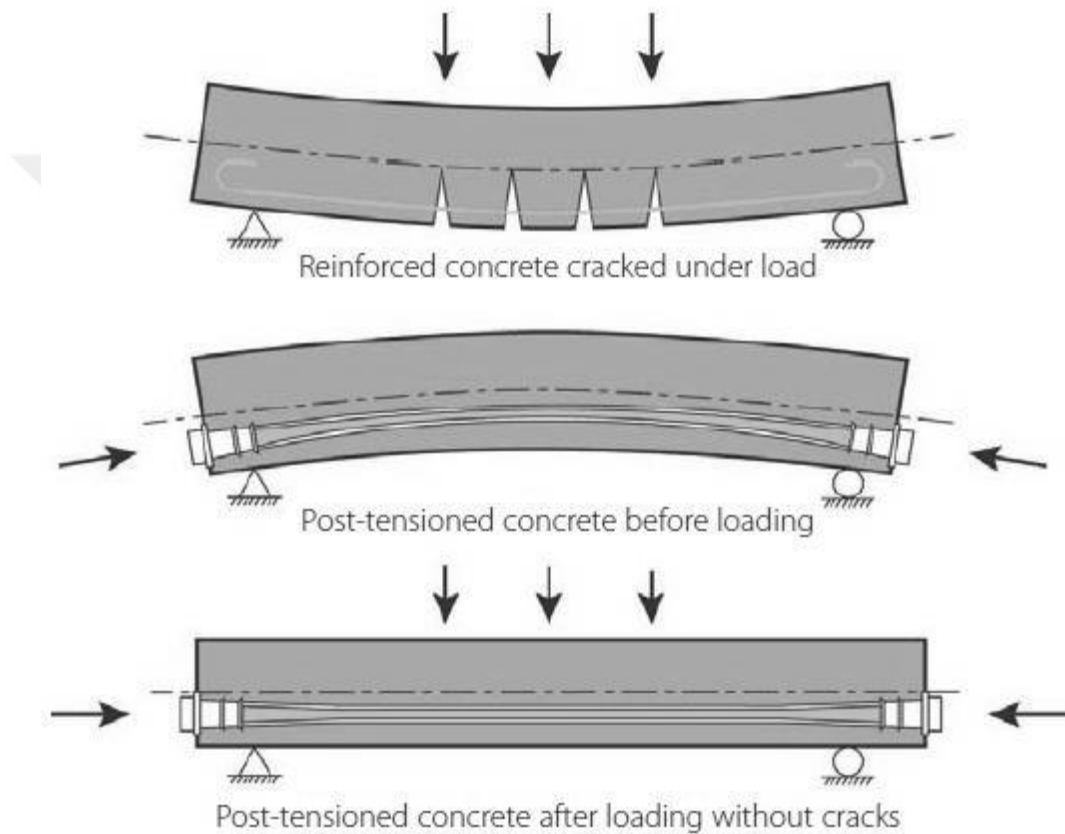


Figure 1.2 Principle of PT reinforcement (Nawy, 2010).

Pre-stressing the concrete by using PT reinforcement provides less cracking and smaller crack widths, causing better durability of concrete structures and preventing corrosion problems. Furthermore, pre-stressing leads to smaller deflections and allows for more slender structures and smaller overall construction heights. The concrete is prestressed by inserting post-tensioning reinforcement, which applies compressive stresses to the concrete. The compressive stresses are applied with a beneficial size and distribution in order to balance the effects of the external loads.

PT flat slabs are commonly used in industrial buildings, parking garages and other structures where large open areas are required. In comparison to normal reinforced concrete, post-tensioning allows for reduced slab thickness and larger spans.

1.2.2 Methods of prestressing

PC structures are widely used in construction building as wall and floor elements of bridges and buildings. Two types of pre-stressing are being employed requiring different technological procedures: pre-tensioned prestressing (Euser et al., 1983; Rabczuk and Eibl, 2004; Ayoub and Filippou, 2009; Hegger et al., 2010) and PT prestressing (Lou and Xiang, 2006; Zheng and Hou, 2008; Zhang et al., 2011; Vu et al., 2010; Bailey and Ellobody, 2009a; Bailey and Ellobody, 2009b). The present work discusses the PT concrete.

As mentioned in the past sections, prestress force is usually transported to a concrete member by highly PT tendons (strand, bar or wire) reacting on the concrete. The high strength prestressing tendons is most often tensioned using hydraulic jacks. The prestressing operation may occur before or after the concrete is cast and, accordingly, prestressed members are classified as either pretensioned or PT.

1.2.2.1 Pretensioned concrete

Pretensioning of the tendon occurs prior to the placement of concrete. Tendons are anchored at either end to large bulkheads. Then strands making up the tendon are stressed individually or simultaneously. The concrete is poured and once it reaches the required strength, the strands are cut at each end placing the member in a state of compression at the bottom fibers.

The procedures for pretensioning a concrete member is shown in Figure 1.3. Primarily, apply the tension force to the tendons and anchored at the both ends of the fixed abutments. After placing the formworks, concrete placing is done, the extremely stressed steel tendons are covered with concrete and then cured. Later, when the concrete reach hardening and sufficient strength the tendon wires are cut from the abutments. The highly stressed steel wires tries to shrink back to the initial strength this makes the concrete under compression (Gribniak et al., 2012).

To accommodate many identical units at the same time, usually, the pretensioned concrete members should be precast in pretensioning beds and long enough. Steam curing can be used to decrease the cycle time of construction and to facilitate the gaining of rapid concrete strength and the concrete is often stressed within 24 hours of casting. Because the concrete is usually stressed at such an early age, elastic shortening of the concrete and subsequent creep strains tend to be high. This relatively high time-dependent shortening of the concrete causes a significant reduction in the tensile strain in the bonded, prestressing steel and a relatively high loss of prestress.

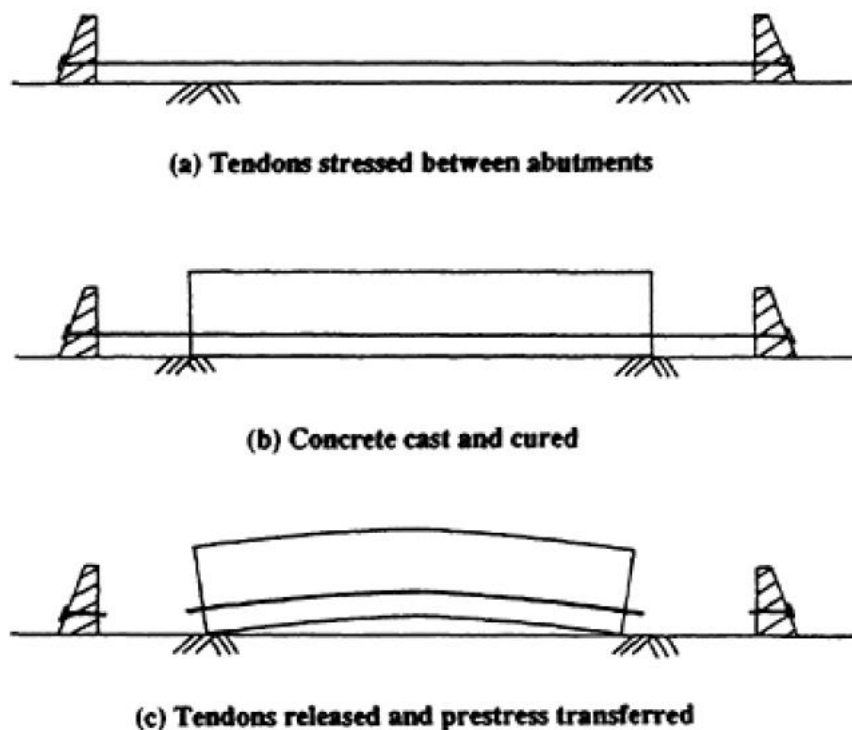


Figure 1.3 Pretensioning procedure (Gribniak and Mickleborough, 1990).

1.2.2.2 Post-tensioned concrete

Post-tensioning occurs after concrete has hardened. Anchorages and ducts are cast into the concrete. Once the concrete attains the required strength, tendons are threaded through the ducts and stressed with high-capacity hydraulic jacks (Figure 1.4). This creates the desired state of compression at the bottom fibers of the member.

Figure 1.5 shows the concrete post-tensioning procedure with the position of formworks. The concrete is cast around hollow ducts which are fixed to any desired profile. The steel tendons are usually in place, unstressed in the ducts during the concrete pour, or alternatively may be threaded through the ducts later. After the concrete has hardened and reached its required strength the tendons are tensioned. Tendons may be stressed from one end with the other end anchored or may be stressed from both ends, as shown in Figure 1.5(b).

Then anchored the tendons at each end. After anchored the tendons at the ends by plates onto the concrete ends, the prestressing stress is sustained, this stressing operation produces an internal stress in the concrete members and makes the concrete is under compression. The PT tendons also impose a transverse force to the member wherever the direction of the cable changes.

In the case of using bonding tendon types, after the tendons have been anchored and no further stressing is required, fill the ducts with grouting materials under pressure, which covers the tendons to increase bonding, to achieve more efficient in controlling cracks and providing ultimate strength. Bonded tendons are also less likely to corrode or lead to safety problems if a tendon is subsequently lost or damaged. In some situations, however, particularly in North America and Europe, tendons are not grouted for reasons of economy and remain permanently unbonded (Nawy, 2010).

Most in situ PC is PT. Relatively light and portable hydraulic jacks make on-site post-tensioning an attractive proposition. Also PT is used for large-span constructions of segmental bridge girders. Prestress may also be imposed on new or existing members using external tendons or such devices as flat jacks. These systems are useful for temporary prestressing operations but may be subject to high time-dependent losses

In bonded systems the tendons are fully bonded to the surrounding material. The tendons are inserted into ducts and after the pre-stressing load is applied, the ducts are filled with cementitious grout to provide bond between the tendon and the concrete. For bonded systems, there is in principle uniform steel-concrete force transfer along the length of the tendons and full strain compatibility is assumed, implying that steel strains are equal to the concrete strains.

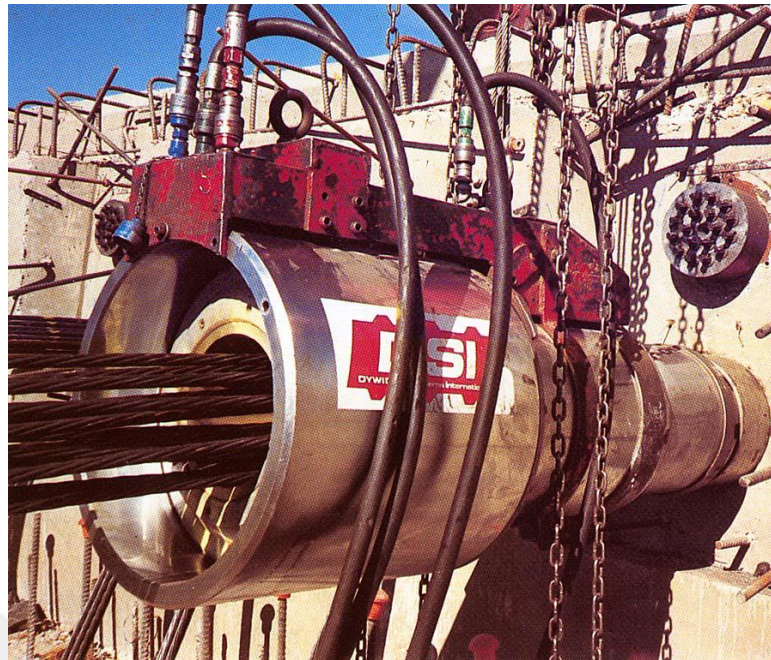


Figure 1.4 DSI post-tensioning Jack (DSI).

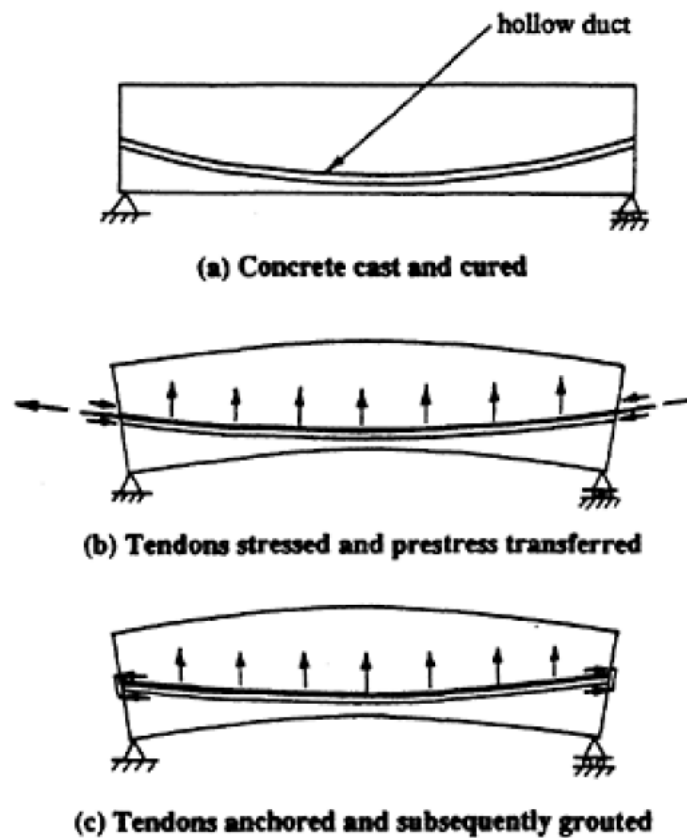


Figure 1.5 Post-tensioning procedure (Gribniak and Mickleborough, 1990).

For unbonded tendons, each tendon is greased and covered by a plastic tube, as to avoid corrosion and to provide minimum friction between the tendon and the concrete. However, if the tendon is damaged, it will lose all of its pre-stressing at once. For unbonded tendons, steel-concrete force transfer occurs only at the anchors and strain compatibility cannot be assumed at all sections.

1.2.3 Advantages of prestressed concrete

In comparison with other forms of constructions, for example steel and reinforced concrete, the PC offers excessive technical advantages. In the case of using members free from tensile stresses under working loads which is fully prestressed members, the cross section is more effectively utilized when compared with a reinforced concrete section which is cracked under working loads. Within certain limits, a permanent dead-load may be counteracted by increasing the eccentricity of the prestressing force in a prestressed structural element, thus effecting savings in the use of materials. PC members have great role in increasing the resistance to shearing force, because of the effect of compressive prestress, hence reduces the principal tensile stress. The use of curved cables, mainly in long-span members, helps to reduce the shear forces developed at the support sections.

A prestress concrete flexural member is stiffer response under working loads when compared with a reinforced concrete member with the same depth. However, after the first cracking, the flexural behavior of a prestressed member is similar to that of a reinforced concrete member. The use of the high strength concrete and steel in prestress members results in lighter and slender members than is possible with reinforced concrete. The two structural features of prestressed concrete namely high strength concrete and freedom from cracks, contributes to the improved durability of the structures under aggressive environmental conditions. PC have ability to improve the durability of material for energy absorption under impact loads. In addition, PC have the ability to resist repeated working loads has been proved to be as good in prestressed as in reinforced concrete.

Pre-stressing may be achieved either by pre-tensioning or by PT. Post-tensioning is that it allow using tendons that are draped or curved. Pretensioning can be achieved that but not so easily. The tensioned of tendons before the casting of concrete (pre-tensioning) is difficult compared to tensioned after the casting (post-tensioning).

1.3 Analysis Method and Program

The analysis and design of PT concrete flat slab was done by using the Finite Element (FE) method program ANSYS. The FE method is chosen for its ability and generality to model loading conditions and irregular structures.

The ANSYS computer program is a large-scale multipurpose FE program, which may be used for solving several classes of engineering analysis. It is capable of performing static, dynamic, heat transfer, fluid flow, and electromagnetism analysis.

Modern heuristic search algorithms are used in optimization problems as a powerful tools in different fields. On the other hand, structural design is the selection of design variables subject to strength and behavioral constraints; a process for which heuristic optimization techniques are very much suited. Two methods of optimization are considered in this study: the sub-problem approximation method and Genetic Algorithm (GA) method.

1.4 Problem Statement

When applying external load on the Bonded Post-Tensioned (BPT) one-way concrete slabs, the change in strain in tendons at any section is equal to the change in strain in adjacent concrete section. This tendon strain depends on the deformation of strain in concrete section. The profile of tendons affects the strain and failure loads of the PT one-way concrete slabs. In PT one-way concrete slab, tendons are classically placed continuously through the supports. The use of nonlinear FE modeling is limited, while little researches have been performed particularly for PT one-way concrete slab. This study provides a large overview of some of the key factors and the lacks for simple and reliable design procedures in the PT one-way concrete slab under flexural and thermal loading. The ultimate capacity of PT one-way concrete slab and failure loads cannot be evaluated by a local analysis of the critical section. A nonlinear analysis of the whole slab structural system is required. The FE was chosen for its ability to model irregular structures and loading conditions.

1.5 Objective of the Thesis

The purpose of the present Ph.D. study is to utilize the capabilities of modern algorithms for structural design and optimization of PT concrete slab; providing a flexible, and relatively easy tool for practicing engineers.

This research presents a FE model using ANSYS software to model the bonded and unbonded PT concrete slabs. The proposed models were validated with previous available experimental study was used to study the effects of the transverse, gravity and thermal loading on the flexural behavior of bonded and unbonded PT one-way concrete flat slabs. A thermal version of the model was used to calculate the temperature profile in the concrete slab, following by a structural version of the model, which reads the temperature profile to calculate thermal stresses. A parametric study was conducted to investigate the effect of several selected parameters on the overall behaviour of PT one-way concrete slab. These parameters include the effect of tendon bonding, the effect of thermal loading and the effect of tendon profile.

A numerical tool integrating analysis, design and optimization techniques are developed for the structural analysis, design and optimization of PT concrete slab. Optimum values of the area and number of tendons and tendon profile will be investigated subject to design constraints imposed by the relevant code of practice. The objective function is the total weight of PT tendons for concrete slab subjected to stress and displacement constraints.

1.6 Layout of the Thesis

This thesis composed of seven chapters; the current chapter (chapter one) presents a general introduction about PC one-way slabs, the aims of the study and the methodology.

In chapter two, most of previous researches carried out on analysis, behavior and properties of PT concrete one-way slabs, and review of experimental studies of PT concrete one-way slabs. Chapter three deals with the basics of FE method, the procedure adopted for the FE representation and the nonlinear solution techniques used to solve nonlinear equations. Also it deals with the FE modeling of material properties

Chapter four presents a comparison between the experimental results and the results obtained from the FE analysis. In chapter five, a parametric study was conducted to investigate the effect of several selected parameters on the overall behavior of PT one-way concrete slab.

Chapter six present the developed FE model using ANSYS to study the optimum design of bonded and unbonded PT concrete slab. In this chapter two methods of optimization are considered: the sub-problem approximation method and GA method.

Finally, Chapter seven gives conclusions drawn from this study, and recommendations for further studies.



CHAPTER 2

LITERATURE REVIEW

2.1 General

PT concrete flat slab systems are widely used for office buildings, hotels, residential, parking garages and hospitals. The system has proven its structural economy and efficiency. The use of PT allows for material savings due to reduced slab thickness. PT also reduces the deflection and cracking of the concrete structures under loads. The design process of the PT slab system to resist gravity loads is pretty well defined in codes of practice all over the world (Semelawy et al., 2012).

Prestressing method is define as concrete with embedded reinforcements in it to produce internal stress, this internal stress counteracts with external service loads to a preferred degree. This method is done by applying high stress to reinforced tendons in zones, which cracks takes place in it due to external loadings, and then it gives a section that has the ability to resist higher loads before cracking occurs. This system increases the external load capacity to crack (Abeles, 1965). The prestressed method has much application, especially in concrete constructions. A large part of bridges in the US is constructed by the prestressed system. Two different methods were used for prestressing concrete system: pre-tensioned and PT (Allouche, 1999).

In the pre-tensioned method, stress is applied to the tendons before concrete placing. In this method, tendons are tensioned in a stressing bed. The formwork gathering is placed with stressing beds and anchorages at the ends, then concrete placing is done. After concrete reaches adequate strength, strands must be released at the ends. This operation produces big internal forces, the forces produced by tendons are transmitted to the concrete member by bonds between tendon and concrete. This method usually used in precast constructions when many identical elements are required (Allouche, 1999).

In the PT method, stress is applied to the tendons after concrete placing. Ducts are used to obtain the desired profile and to allow free movement of tendons in the member. When the concrete has gained sufficient strength, each tendon is stressed to the desired load by using a stressing jack and anchored at each end of the member to maintain the prestressing force in the concrete. PT method is a widely used technic used all over the world for reinforced concrete structures, to prevent cracks and minimize deflections that produced by externally applied loads.

In this chapter, a review of published experimental and analytical studies carried out on internally and externally PT concrete structures will be provided. The main parameters affecting the behavior of PT concrete structures such as area and depth of non-prestressing steel, span-to-depth ratio, loss of prestressing force due to creep and shrinkage of the concrete, as well as relaxation of the prestressing tendons, location of tendons, force in tendons, and types of loading had been investigated, especially for PT one-way concrete slabs. This chapter points out the various researches related with the PT slabs and reviews the developed predictions of the stress at failure in the bonded and unbonded tendons through experimental works were undertaken by different researchers. As well as this chapter deals with previous studies related to the FE Method and the analytical models by ANSYS package program to investigate the flexural response of bonded and unbonded PC slabs.

2.2 Post-Tensioned Method

The PT method is a widely used technic all over the world used for structures, to prevent cracks and minimize deflections, which produced by externally applied loads. By PT method, greater applied loads, greater spans with the same member depth, crack controls and smaller member sizes can be attained. According to bond types, there are two different PT concrete members: (bonded and unbonded PT).

2.2.1 Bonded post-tensioned

In BPT, the stressing force in PT system is held by bonds between surrounding concrete and tendons. The adhesion between steel tendons and concrete significantly affects the resistance of the PT members. The bond between concrete and strands is mobilized by the transformation force of strands to concrete (Hoyer, 1939). In BPT system there is a space between the tendons and ducts, cement mortar is inserted in

under pressure to fill this space, which significantly increases the bond and strain compatibility between tendons and concrete, also totally it can protect the tendons against corrosion (Allouche, 1999). BPT can be used in all environmental conditions. BPT has not needed a large area of tendons to obtain the required strength as compared to Unbonded Post-Tensioned (UPT). The tensile stress moves from nearby concrete to the reinforcements, due to the adequate bonds. BPT can be precast or cast in place. The change in tendon strains at any section is equal to the change in strain in adjacent concrete section. The tendon strains depend on the strain changes in the concrete section.

Tao and Du (1985) in their experimental study twenty-six PC beams were tested, different amounts of bonded and unbonded steels were used. To predict the effects of changing amounts of non-prestressed reinforcements, prestressed steel, and concrete strength on the prestressed stress of tendons. Their results showed that by decreasing the total amount of reinforcements (bonded and unbonded) the tendon stress increased at failure. In the case of using a low amount of reinforcement, the beams behave more ductile as compared with beams with a high amount of reinforcement used. The same results were obtained by (Chakrabarti et al., 1994) who reported that by increasing the total amount of reinforcements at ultimate load the stress changes in the unbonded steel tendons were smaller.

Manalip et al. (1994) experimentally studied five beams of high strength concrete. Beams were subjected to pure bending and analyzed to measure their ductility and to realize the real strain-softening behavior of their compressed zones. For the experimentally tested beams, it was found that the use of high strength concrete instead of normal strength concrete effects the results by the doubling of the plastic rotation capacity.

Hussien et al. (2012) presented an experimental program to study the behavior of bonded and unbonded prestressed beams with high strength and normal strength concrete. Their results showed that by using partially PC beams with bonded tendons provide better behavior than those of unbonded tendons, and by Increasing the nominal compressive strength from 72 to 97 MPa for bonded prestressed beams, increase in the ultimate and cracking loads by 4 % and 18 %, respectively. The

analytical work was introduced and compared to the results of the experimental work and gives a good prediction.

Eight fire tests conducted on BPT one-way concrete slabs are presented by Bailey and Ellobody (2009b). Two additional tests at ambient temperature were augmented with the fire tests, carried out to failure on slabs with identical geometry and prestressing tendons. Detailed experimental data were provided from test in the form of horizontal and vertical displacements, temperature distributions within the slab and strains in the tendons.

2.2.2 Unbonded post-tensioned

When mortar or grout not used to fill the spaces between tendons and ducts, then it is called UPT system, instead, naturally filled with grease as a protection against corrosion. In UPT may be avoided the expensive of time-consuming of grouting operation, it is an economical alternative to conventional to bonded prestressed. This system has some problems, which stopped it from being more widely used, the unbonded system cannot be used in corrosive environments due to disposed of corrosion like bridges (Nowak, 1994), but may be used in parking structures with offering suitable protections against corrosion (Litvan, 1996). This system requires a larger area of tendons to obtain the required strength because of the ultimate strength of unbonded tendons about ten to thirty percent lower than bonded members (Park and Paulay, 1975). The behavior of UPT tendons does not wholly understand yet. Furthermore, it has not had a modest and accurate method for predicting the stress in unbonded tendons at failure. The tensile stress cannot be moved from nearby concrete to the reinforcements due to the lack of bonds, thus the cracking pattern at failure characterized by single or little cracks in the maximum moment region.

Chakrabarti and Whang (1989) experimentally published the cracking and ultimate strength behavior of simply supported reinforced concrete beams with partially prestressing of unbonded tendons. Eight beams have been tested. Their results showed that at the ultimate load the tensile steel bars reach yielding, failure occurs by concrete crushing at the ultimate load. By decreasing of partially prestressed ratio the stress in the steel bars increased. To predict the stress in the unbonded tendons at ultimate, the non-prestressed and compressive reinforcements should be taken into

account in the ACI 318-83 equation. Test results were reported with specific conclusions and recommendations for future design and code revisions.

Bums et al. (1991) experimentally tested two continuous PT concrete beams with internally unbonded tendons to predict change in the prestressing force in tendons. The results showed that the tendon forces under cycle service loads did not change up to the compressive stress level of $(12\sqrt{f_c})$. When the beams overloaded in just single span, tendons are tended to slide into a loaded span, this causes stress in tendons decreases on the end of the loaded beam span and increases stress in the unloaded span at the end. In the case of applying two spans loaded, the distributed stress in tendons did not change significantly. Furthermore predicted that by using of draped tendon profiles, the change in tendon stress for a given deflection was larger than the corresponding beam with less of severing draped profiles.

To study the effect of several parameters on the magnitude of the prestressing stress of steel, Harajli and Kanj (1991) tested twenty-six simply supported concrete beams with rectangular cross-sections, prestressed with unbonded tendons and with and without ordinary reinforcing steels. Their results showed that the application of the load types has no significant influence on the stress in prestressed tendons. Also, their results showed that the stress in prestressed tendons in single concentrated load was same in two third-point loads. By increasing the span-depth ratio from 8 to 20 effects in decreasing the stress in the tendons by 35 %. It means the load application was not significantly affected.

Campbell and Chouinard (1991) experimental used six partially unbonded PC beams with rectangular cross-sections, their results showed that by increasing the amount of non-prestressed bonded steels decreases the stress in the prestressing tendons at ultimate loads. Their test results were compared with predictions from two related design codes and identified some limitations of these code application to unbonded PC construction.

Chakrabati et al. (1994) experimentally tested thirty-three unbonded prestressed reinforced concrete beams. Their results showed that beams with enough reinforcement index and enough partial prestressing ratio have better load carrying capacity, better ductility, and performance in the post-cracking range. Using the high

amount of partial prestressing ratio caused sudden large cracking in the tension zones and high amount of combined reinforcing index cause crushing in the compression zones. To improve ductility, deflection, and cracking control the partial prestressing ratio should be reduced gradually. In the case of span-depth ratio above 35, post-cracking behavior and deflection control were enhanced. The tendon initial stress had no effect on overall beam behavior, however, the ultimate strength of prestressing steel increased.

Vu et al. (2010) calculated the structural response of UPT prestressed beams, including both the ultimate bearing capacity and the deflections under service loading, before or after cracking. They predicted the overall lengthening of the unbonded tendons at all loading stages: serviceability, cracking, and ultimate. The calculations of the bearing capacity and the deflection at failure were very accurate.

Under a symmetrical top two-point loading and a symmetrical top one-point loading, Yang et al. (2013) are tested twelve partially PT light weight concrete one-way slabs. For each loading type, unbonded prestressing three-wire strands were arranged with a harped profile of variable eccentricity and a straight profile of constant eccentricity. The ultimate stress and moment in unbonded tendons measured from the light weight concrete specimens are compared with those of PT normal-weight concrete beams and ACI 318-11 (ACI, 2011) predictions. From comparisons results, they found the ACI 318-11 design equations for the stress increase in unbonded tendons to be fairly conservative in both the normal-weight concrete and the light-weight concrete beams.

Four fire tests conducted on UPT one-way concrete slabs are presented by Bailey and Ellobody (2009a). Two additional tests at ambient temperature were augmented with the fire tests, carried out to failure on slabs with identical geometry and prestressing tendons. Detailed experimental data were provided from test in the form of horizontal and vertical displacements, temperature distributions within the slab and strains in the tendons.

2.2.3 External post-tensioning

Another method was introduced which was externally PT system, used in many parts of engineering structures, such as in segmental bridge constructions, rehabilitations,

strengthening of existing structures, and also used to replace the damaged tendons. By this method, the dimensions of the member sections and member self-weight can be reduced (Allouche, 1999).

Harajli (1993) experimentally studied the strengthening flexural members by external prestressing. For this purpose, he tested sixteen simply supported beams with rectangular cross-sections. The results of his tests showed that the nominal flexural strength of the beams was increased about 146 % by applying externally prestressing tendons, without a reduction in ductility, and the service load deflections were reduced by about 75 % under cyclic fatigue loading. Harajli (1993) found that by using draped tendon profile increases the flexural resistance as compared to straight tendon profile. Furthermore, Harajli (1993) assumed that by an increase in tendon elongation between the anchorage ends the strain in the external prestressing steel increases under applied loads, and the proportional between strain in strands and deflections were linear.

Tan and Ng (1997) tested six reinforced concrete beams with external prestressing tendons, the cross sections were T-section for all beams, and all beams were strengthened in flexure using external strands. Their test results showed that by using deviators for beam sections of maximum deflection had a significant effect on satisfactory service load behaviors (cracking, deflection, and steel stress) and had a higher load- carrying capacity as compared to the case where no deviators were used. Their results showed that by increasing eccentricity of straight tendons with a correspondingly smaller prestressing force had a significant effect on makes a larger internal steel stresses, service load deflections, and crack widths with a higher ductility. In the case of using draped tendon profile, significantly effects on stiffness, which was reduced, increase tendon stresses, makes more ductile behavior near failure. Also, the service load behavior was not changed by using a larger tendon area, which gives a lower ductility with higher ultimate strength.

Harajli et al. (1999) investigated a parametric study on concrete beams strengthened by externally straight steel tendons to find out the effect of deviators. Beams had been modeled with deviators and without deviators at mid-span. Harajli et al. (1999) mentioned a second order effect to change the tendon eccentricity with increasing member deformation. This effect can indicate the main differences between the

behavior of unbonded external tendons and unbonded internal tendons. By second order effect method the un-deviated external tendons to mobilizing has lower inelastic deformation and lower nominal flexural resistance as compared with deviated tendons. This has a significant effect on improving the service load behavior of the beams and reduces the stiffness due to applied load.

Naghypour et al. (2010) experimentally and numerically studied the behavior of reinforced concrete beams strengthened with externally prestressed tendons. They used a FEM program such as ANSYS to modeling PT reinforced concrete beams. They concluded that the strengthening method was very effective for beams with lower percentages of internal flexural tension reinforcement. Furthermore, they predict the increase in flexural strength caused by the used of unbonded external PT reinforcing bars was in reverse proportion to the percentage of internal flexural tension reinforcement.

2.3 Analysis of Post-Tensioned Concrete Structures

PT concrete is a method which is used for overcoming concrete's natural weakness tension. It is used to produce beams, floors or bridges with a longer span. Prestressing tendons are used to provide a holding load which produces a compressive stress that reverses the tensile stress which induced in the beam due to applied bending load. Traditional reinforced concrete structure is based on the use of steel reinforcement bars, rebar, inside concrete to counter the bending stress. More studies were concerned with analysis of PT concrete structure.

Concrete structural components exist in buildings and bridges in different forms. To the development of a general efficient and safe structure, consideration the response of these components during loading is very important. Different methods have been appeared to study and investigate the response of structural components. Experimental based testing has been widely used as a means to analyze individual elements and the effects of concrete strength under loading

FE analysis is a most suitable numerical method, used to solve and analyze complex problems, it is very important to engineering researchers. Recent developments in computer technology make it possible to use FE analysis computer programs in all engineering branches to dealing with different material properties, boundary

conditions, relationships between structural components, and statically or dynamically applied loads.

FE analysis can determine the response of linear and nonlinear structures with good accuracy. Problems require resolve of the Three Dimensional (3D) distribution of one or more dependent variables or elements, mathematically, then this element is express by differential equations or by integrations, these elements are connected at point nodes.

A 3D FE analysis is still the most general and comprehensive technique, which is used for static and dynamic analyses, capturing all aspects affecting the structural response. It becomes the numerical method of choice in many engineering and applied science areas (Kim, 2014).

A collection of papers were appeared by several researcher which explain the FE analysis for the behavior of reinforced concrete structures such as shear failure of beams, cyclic loading of columns, the behavior of structure to seismic, and bond models between concrete and steel.

The behavior of PT concrete structural members have previously been investigated experimentally by (Yang et al., 2013; Williams and Waldron, 1989; Ranzi et al., 2013; Bailey and Ellobody, 2009a; Bailey and Ellobody, 2009b; Ranzi et al., 2013; Aimin et al., 2013; Hussien et al., 2012; Kim and Lee, 2016) and others. Numerical and theoretical models have been previously developed by other researchers to study the behavior of bonded and unbonded PT concrete members.

Kim and Lee (2012) used nonlinear analysis method to finding the flexural behavior of continuous UPT members, this nonlinear analysis reflects the moment redistribution. The verification has been done to finding the accuracy of proposed analysis model, for this purpose the analysis test results was compared with experimental results. The results of their study showed that the loading type effect on the flexural behavior of continuous UPT, which was reflected by curvature distribution in the region of maximum moment and the accuracy of flexural behavior of the proposed analysis model were constant, irrespective of the type of applied loads, section shapes, and tendon profiles.

Fanning (2001) discussed a numerical model by ANSYS program, in his study the ordinary reinforced concrete beams with 3-meter-long spans and prestressed beams with long span 9 m have been tested. The load was applied up to failure to predict the response of ultimate reinforced concrete beams. The conclusion showed that a suitable numerical model for taking the flexural modes of failure in reinforced concrete members was dedicated smeared crack model.

Ellobody and Bailey (2008) investigated the structural behaviour of BPT one-way spanning concrete slabs in fire conditions. They developed a nonlinear FE model for the analysis of post-tensioned bonded concrete slabs at elevated temperatures.

A combination of the mesh-free and the FE methods was presented in Rabczuk and Belytschko (2006), where concrete was modelled by particles and the tendon by FEs. Zheng and Hou (2008) investigated the PC plate subject to fire using 3D solid FEs.

Ellobody and Bailey (2009) investigated the structural behaviour of UPT one-way spanning concrete slabs in fire conditions. They exploited ABAQUS to model the PT concrete slabs in fire with a combination of 6414 solid elements C3D8 and C3D6 to model the concrete, tendon, anchorage and interface elements. They employed the damaged plasticity model implemented within ABAQUS. The slabs are simply supported and reinforced with 15.7 mm nominal diameter seven-wire mono-strand tendons. They developed a nonlinear FE model for the analysis of post-tensioned unbonded concrete slabs at elevated temperatures. The mechanical and thermal material nonlinearities of the concrete, prestressing tendon and anchorages have been carefully inserted into this model. The interface between the tendon and surrounding concrete was also modelled, allowing the tendon to retain its profile shape during the deformation of the slab. The temperature distribution throughout the slab, time-deflection behaviour, time-longitudinal expansion, time-stress behaviour in the tendon, and the failure modes are predicted by the model and verified against test data. ABAQUS was also employed by Hegger et al. (2010).

PC beams using FE analysis was studied by Kasat and Varghese (2012) to understand the response of PC beams due to transverse loading. The scope of that study was limited to the determination of the structural static properties such as deflections and stress distributions. For that rectangular PC beam was taken for the analysis. The ANSYS package program was used as a tool of that FE analysis. The

PC beam was modeled as simply supported. Isotropic materials were used over the beam sections.

Computer software which allows the generation of a complete structural model of a PT concrete bridge with a voided slab deck is presented by Díaz et al. (2010). The code implements the orthotropic plate paradigm and provides a graphical user interface, which allows both preprocessing and post-processing, linked to a commercial FE package. A description of the code was presented, along with the formulation of the orthotropic plate. Verification and comparison examples demonstrate the performance and features of the software and also the applicability of the formulation. They used the FE package COSMOS/M to run the analysis.

For simulating the nonlinear flexural behavior of UPT beams and developing a 3D FE analysis, a study has been done by (Kim et. al. 2010) in their study the FE analysis by ANSYS program has been used to examine the effects of different prestressing forces on the flexural behavior of UPT concrete beams. Four PT concrete beams were tested in California state university. The results were compared with the analytical results by ANSYS program which showed that the 3-D FE analysis was able to simulate the PT concrete beam behavior, the strain produced by ANSYS program gives a good agreement with the strain by experimentally tested specimens.

Package ABAQUS program was used to model the PT structures with bonded and unbonded tendons by Kang and Huang (2012) three modeling approaches had been used to simulate unbonded and bonded tendons, compared all approaches with the analytical and experimental results. The first approach was based on contact technic which reflects tendons in concrete in true physical conditions. The second approach was a multiple-spring system that offers more flexibility in modeling and strength in convergence subjects. The third approach was the model using a contact formulation (surface-to-surface contact). Their results showed that the third method of the contact formulation was the most computationally efficient, and the developed model was capable of simulating for both bonded and unbonded tendons quite effectively.

A computer method based on the classical shell and plate theories is presented by Öztörün and Utku (2002) for the elastic analysis of cylindrical water tanks subjected

to axisymmetrical loading and post-tensioning loads. A spherical dome or circular plate roof, cylindrical container, top and bottom ring beams together with a circular plate foundation are considered as possible components of a water tank in the flexibility formulation. The program is based on the flexibility method of structural analysis. Flexibility coefficients of shell, plate and ring beam components are assembled into a system of flexibility matrices. Generalized displacements due to loads and temperature changes are computed for each component and assembled to form the constants of the compatibility equations.

Lou et al. (2016) analyzed the parametric study to predict the behavior of two-span continuous prestressed concrete beams with internal unbonded fiber reinforced polymer and steel tendons. A nonlinear model was verified by the experimental results. Their analytical results showed that the type of unbonded tendons has practically no influence on the cracking mode and moment redistribution, while it has limited effects on the development of deformation. They proved that, the type and amount of bonded steel bars affect significantly on the member behavior.

Zhang et al. (2011) developed a nonlinear analysis method to calculate ultimate stress in unbonded tendons. The analysis model was established by using the Reissner–Mindlin medium thickness plate theory allowing for the influence of the transverse shear deformation. The orthotropic increment constitutive model of concrete was extended to solve the medium thickness plate problem. The tension stiffening of the cracked concrete was considered in the nonlinear analysis model. The numerical formulation of calculating the stress increment in an unbonded tendon was established by using the spatial displacement relationship. They developed a computer program specifically for predicting the nonlinear response of a PC curved slab structure with unbonded tendons and calculating the ultimate stress in unbonded tendons. Six test models of PC curved slabs with unbonded tendons were reported.

2.4 Optimization of Post-Tensioned Concrete Structures

Optimization in its broad sense can be applied to solve any engineering problem. Having reached a degree of maturity over the past several years, optimization techniques are currently being used in a wide variety of industries, including aerospace, automotive, chemical, electrical and manufacturing industries. With the development of computer technology, complexity of problems being solved using

optimization methods is no longer an issue. Optimization methods coupled with modern tools of computer-aided design are also being used to enhance the creative process of conceptual and detailed design of engineering systems.

There is no single method or technique for solving all optimization problems efficiently. Hence a number of optimization methods have been developed for solving different types of optimization problems. It is in the entire discretion of the engineer to choose a method which is computationally efficient, accurate and appropriate for his design problem.

2.4.1 Optimum design of post-tensioned concrete structure

Large number of papers has been published on structural optimization in recent years. PC slab design involves large number of design variables and many practical constraints. Hence optimum design of a PC slab is challenging to the designers. It is computationally expensive to design manually. Hence optimization techniques are more suitable in such case.

Structural design optimization gained more popularity with the rapid development of optimization techniques together with the availability of powerful computers. In general, more studies were concerned with optimization of steel rather than concrete structures. Numerous studies were published addressing the design optimization of concrete structures and concrete structural elements.

Atabay and Gulay, (2009) carried out the cost optimization of the 3D shear-wall reinforced concrete structure using GA method. The design variables were the shear-wall dimensions. A computer program that can determine the optimum shear-wall dimensions required for the minimization of cost of structures was developed, for use in numeric applications. They optimize the 20-floored, 3-D shear-wall structure using the GA approach.

Two-stage hybrid optimization algorithms based on a modified GA are presented by Sahab et al. (2005). In the first stage, a global search was carried out over the design search space using a modified GA. In the second stage, a local search based on the GA solution was executed using a discretized form of Hooke and Jeeves method. The objective function was the total cost of the structure including the cost of

concrete, formwork, reinforcement and foundation excavation. The constraints were defined according to the British Standard BS8110 for reinforced concrete structures.

AI-Gahtani et al. (1995) reported an effective creation for optimum design of two-span continuous concrete beams with partially prestressed. Different forces on prestressed tendon profiles have been used along the beam length, tendons are anchored at the both beam ends with flexibility in the overlapping location. Their results showed that the design of partially PC beams was economic as compared to the designing of fully PC beams in two span continuous concrete beams, moreover, the same conclusion was verified by (Colin and MacRae, 1984) for simply supported concrete beams.

Gaelyn Krauser (2009) investigated a parametric study of a flat plate floor system designed using post-tensioning. Design was conducted by hand through a series of Excel spreadsheets and compared with the results found from the computer analysis program, ADAPT-PT.

Chaitanya et al. (2013) considered six design variables for optimization of the cost of simply supported prestressed concrete beam with all practical constraints using GA . Total cost of the beam was expressed in terms of cost ratio. Parametric study was done to observe the effect of size of population, number of generation, intensity of live load, cable profile and various practical beam lengths. Bending moment, shear force and deflection are calculated using MATLAB program.

Oded Amir (2013) presented an optimization procedure for reinforced concrete structures. The distribution of both concrete and reinforcement bars was optimized simultaneously. Concrete was modeled as a continuum exhibiting damage, into which reinforcement bars were embedded.

Rahul and Kumar (2014) designed and optimized portable footbridge. The basic emphasis has been given to minimize the total deformation of the structural member by optimizing the cross sections, material properties and weight. A 3D model was developed using SolidWorks. Six different cross sections (circular, rectangular and square with solid and hollow sections) of the beam with three different materials (Aluminium alloy, Structural steel and Titanium alloy) were analyzed in ANSYS

11.0 with similar loading and support conditions. The results obtained, after analysis of different cross sections and with different materials, were compared.

Peng and Liu (2013) presented the simulations of shrinkage tests of concrete blended with fly ash and ground granulated blast furnace slag based on the theory of 3D nonlinear moisture diffusion. The related parameters are identified by the inverse finite-element analysis approach using the design optimization module of ANSYS. The environmental humidity effect on shrinkage strain and the relationships between the identified parameters with the fly ash content are discussed.

Bennegadi et al. (2013) developed numerical model for the optimization of the external reinforcement of reinforced concrete beams by Hybrid Fiber Reinforced Polymer (HFRP) Plate. The model used a FE method adopted by ANSYS. To achieve this aim, a 3D nonlinear FE model is developed to study the behavior of concrete beams and plates with and without external reinforcement by FRP. Calibration and validation of the obtained results are compared to those given experimentally for different conditions from research. Next, the model was used to optimize the volume of the HFRP plate which is bonded externally to the concrete beam. The design of the HFRP plate volume considered as the objective function, the results are evaluated against specified design criteria, and the design is modified as necessary. The geometrical design variables are the height and width of the HFRP plate, and the state variables are the normal and shear stresses.

2.4.2 Optimum design of post-tensioned concrete slab

The design process can be described in many ways, but it must contain recognition of the need, an act of creation, and a selection of alternatives. Conventionally, the selection of the best possible alternative is the phase of design optimization. Optimization techniques play an important role in structural design, the very purpose of which is to find the best solutions from which a designer or a decision maker can derive a maximum benefit from the available resources. There can be large number of feasible designs but considering the resources the best is chosen. The best design could be in terms of minimum cost or minimum weight or maximum performance or a combination of these (Rahul and Kumar, 2014).

The existence of optimization methods can be traced to the days of Newton, Lagrange, and Cauchy. Optimization, in its broadest sense, can be applied to solve any engineering problem like design of aircraft and aerospace structures for minimum weight, optimum design of linkages, cams, gears, and other mechanical components, minimum weight design of structures for earthquake etc. (Sahab et al., 2005).

Few studies were concerned with the design of PC slab. One of the first attempts to consider the optimum design of PC slabs was carried out by Rozvany and Hampson (1963).

MacRae and Cohn (1987) used mathematical programming techniques for the solution of a comprehensive optimal design problem formulation. The formulation based on American codes of practice, includes constraints related to service, ultimate, and collapse limit states, as well as relevant technological constraints. Solutions to the nonlinear programming problem were obtained with an appropriate computer program, OPTIMAL.

Kuyucular (1991) considered several predefined cable profiles for a given section to minimize the prestressing cables weight. He carried out structural analysis by coupling FE and equivalent load method, the method involved a time consuming procedure of calculating several factors for each cable profile, hampering the automation of optimization process. In both studies, optimization was carried out for a given slab thickness. Excluding one of the main design variables would weaken the applicability of the design tool to engineering practice.

Lounis and Cohn (1993) considered minimization of two objective functions (cost and initial camber) by using one as the objective function and the other as a constraint using the e-constraint approach. They used Projected Lagrangian algorithm for optimization and sectional stress analysis and force-in-tendon method for analysis. Although all design variables were considered in optimization, their analysis method limits the application of their method to simple structures.

Semelawy et al. (2012) developed a numerical tool that was capable of finding the optimum design of a PC flat slab system using modern heuristic search algorithms. Structural analysis of the system carried out by using FE method. Concrete slab was

modeled by using a consistent triangular shell element that was originally developed by Koziey and Mirza (1995). The optimum design of a square prestressed flat slab supported on four columns at the corners and spanning 5.0 m was investigated. The Canadian code CSA A23.3 was chosen as the design code.

Sahab et al. (2005) presented cost optimization of reinforced concrete flat slab buildings according to the British Code of Practice (BS8110). The objective function was the total cost of the building including the cost of floors, columns and foundations. The structure was modelled and analysed using the equivalent frame method. The optimization process was handled in three different levels. In the first level, the optimum column layout is achieved by an exhaustive search. In the second level, using a hybrid optimization algorithm. In that hybrid algorithm, a GA was used for a global search. In the third level, an exhaustive search was employed to determine the optimum number and size of reinforcing bars of reinforced concrete members. Cost optimization for three reinforced concrete flat slab buildings was illustrated and the results of the optimum and conventional design procedures were compared.

CHAPTER 3

FINITE ELEMENT FORMULATION AND MODELING OF MATERIAL PROPERTIES

3.1 Finite Element Formulation

The FE method is a numerical procedure whereby the region or the continuum is discretized into small elements connected at nodes. The method can be applied to obtain approximate solutions to a variety of problems in various fields of engineering; in transient linear or nonlinear problems in stress analysis, heat transfer, fluid flow and electromagnetism problems (Bathe, 1996).

3.1.1 Basic steps in the finite element method

The basic steps involved in any FE analysis consist of the following (Moaveni, 1999):

1. The structure is created and divided into FE connected together at their nodes.
2. A shape function is assumed to represent the physical behavior of an element; that is, an approximate continuous function is assumed to represent the solution of an element.
3. Equations for stress distribution and stiffness are developed for an element.
4. Assemblage of FE equations to present the entire problem, then the global (or structural) stiffness matrix is constructed.
5. Boundary conditions, initial conditions, and loading are applied.
6. A set of linear or nonlinear algebraic equations is solved simultaneously to obtain nodal results, such as displacement values at different nodes, or other important information such as stresses and strains that can be obtained for the nodes or the elements.

3.1.2 Outline of ANSYS

The ANSYS (ANalysis SYStem) computer program is a large-scale multipurpose FE program, which may be used for solving several classes of engineering analysis. It is capable of performing static, dynamic, heat transfer, fluid flow, and electromagnetism analysis. In the present study, the ANSYS program was used for analyzing statically the PT concrete flat slabs.

One of the main advantages of ANSYS is the integration of the three phases of FE analysis: pre-processing, solution and post processing. Pre-processing routines in ANSYS define the model (element type, material properties and geometry modeling). Solution routines define boundary conditions, loadings and solution options. Displays may be created interactively on a graphics terminal as the data are input to assist the model verification. Post-processing routines may be used to display analysis results in a variety of ways such as plots of the structure's deformed shape and stress or strain, etc.

3.1.3 Finite element representation

The ANSYS computer program is utilized for analysis of all modeled slabs. Structural components encountered throughout the current study, corresponding FE representation and elements designation in ANSYS are presented in Table 3.1.

Table 3.1 FE representation of structural components.

Structural component	Element designation in ANSYS
Concrete	SOLID65
Reinforcement and tendon	LINK8
Steel plate	SOLID45
Interface surface	CONTA175 and TARGE170
Anchorage steel	SHELL181
Thermal	SOLID70, LINK33, SHELL131

3.1.4 Finite element model of concrete

In this study, 3D brick element with 8 nodes is used to model the concrete (SOLID65 in ANSYS). SOLID65 (or 3D reinforced concrete solid) is used for the 3D modeling of solids with or without reinforcing bars (rebar). The solid is capable of cracking in tension and crushing in compression. In concrete applications, for example, the solid capability of the element may be used to model the concrete, while the rebar capability is available for modeling reinforcement behavior. The element is defined by eight nodes having three degrees of freedom at each node: translations of the nodes in x, y, and z-directions. The most important aspect of this element is the treatment of nonlinear material properties. The concrete element is capable of cracking (in three orthogonal directions), crushing, plastic deformation, and creep (ANSYS, 2012). The geometry, node locations, and the coordinate system for this element are shown in Figure 3.1.

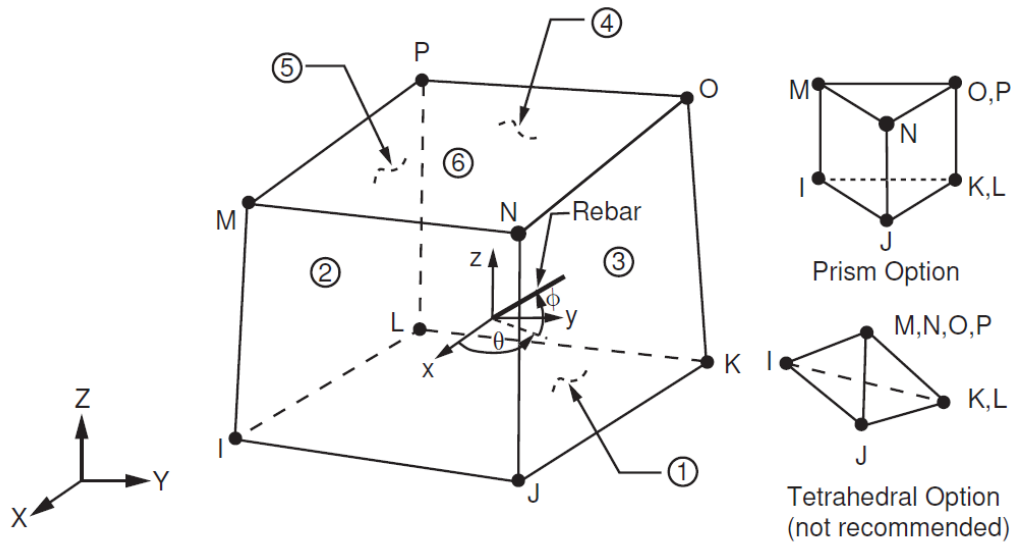


Figure 3.1 SOLID65 geometry (ANSYS, 2012).

3.1.5 Finite element model of reinforcement

Three techniques exist to model steel reinforcement in FE models for reinforcement (Wolanski, 2004), these are:

1. The discrete model.
2. The embedded model.

3. The smeared model.

3.1.5.1 Discrete representation

Discrete representation has been widely used. The reinforcement in the discrete model uses one dimensional bar or beam elements that are connected to concrete mesh nodes as shown in Figure 3.2a. Therefore, the concrete and the reinforcement mesh share the same nodes and the same occupied regions. Full displacement compatibility between the reinforcement and concrete is a significant advantage of the discrete representation. Their disadvantages are the restriction of the mesh and the increase in the total number of elements.

3.1.5.2 Embedded representation

The embedded representation is often used with high order isoparametric elements. The bar element is built in a way that keeps reinforcing steel displacements compatible with the surrounding concrete elements as shown in Figure 3.2b. When reinforcement is complex, this model is very advantageous. The stiffness matrix of the reinforcing steel is evaluated separately and then added to that of the concrete to obtain the global stiffness matrix.

3.1.5.3 Smeared (distributed) representation

The smeared model assumes that reinforcement is uniformly spread in a layer throughout the concrete element in a defined region of the FE mesh as shown in Figure 3.2c. This approach is used for large scale models where the reinforcement does not significantly contribute to the overall response of the structure.

The prestressing and nonprestressing reinforcements (tendon and reinforcement) were represented by using 2-node discrete representation (LINK8 in ANSYS) and included within the properties of 8-node brick elements. LINK8 is a spar (or truss) element which may be used in a variety of engineering applications. This element can be used to model trusses, sagging cables, links, springs, etc.

LINK8 is a discrete model and spar element, which is used for many engineering applications, by this element the trusses, links, sagging cables, and springs can model. This element is a 3D spar and uniaxial tension-compression element. LINK8

has 3 degrees of freedoms at each node, nodes in the x, y and z-directions are translated, no bending of the element is considered (ANSYS, 2012).

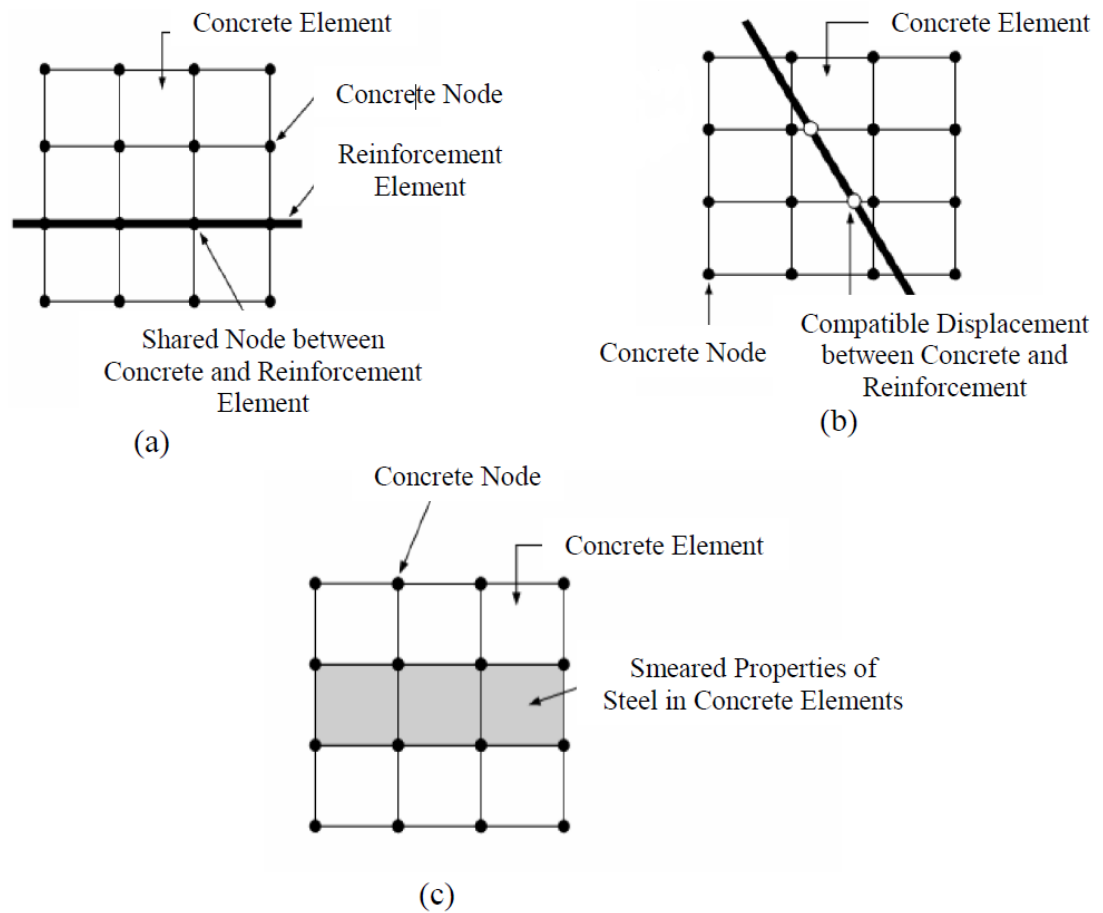


Figure 3.2 Models of reinforcement in reinforced concrete (Wolanski, 2004):
 (a) Discrete (b) Embedded and (c) Smeared.

The prestressing stress is the initial value of the strain in this link element. The PT force has transferred through the slab and connected at the ends by anchorages. The geometry, node locations, and the coordinate system for this element are shown in Figure 3.3.

For tendon cable, since it is located inside the concrete section (through the hole) and the prestressing force is transferred to concrete through end anchorages and profile of tendon, the cable is connected to slab only at the anchorages (ends).

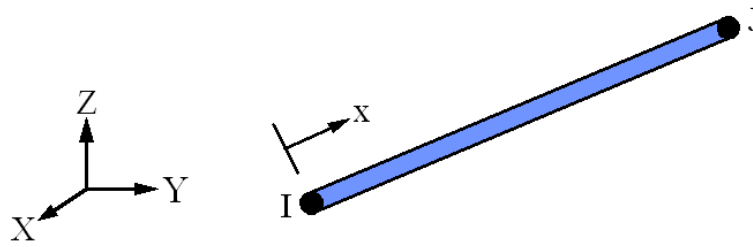


Figure 3.3 LINK8 geometry (ANSYS, 2012).

3.1.6 Finite element model of steel plates

To avoid crushing at point loads the bearing plates are used. SOLID45 is used for the 3-D modeling of solid structures. This element is defined by eight nodes having three degrees of freedom at each node, nodes in the nodal x, y, and z-directions are translated. This element has plasticity, creep, swelling, stress stiffening, large deflection, and large strain capabilities. The geometry, node locations, and the coordinate system for this element are shown in Figure 3.4 (ANSYS, 2012).

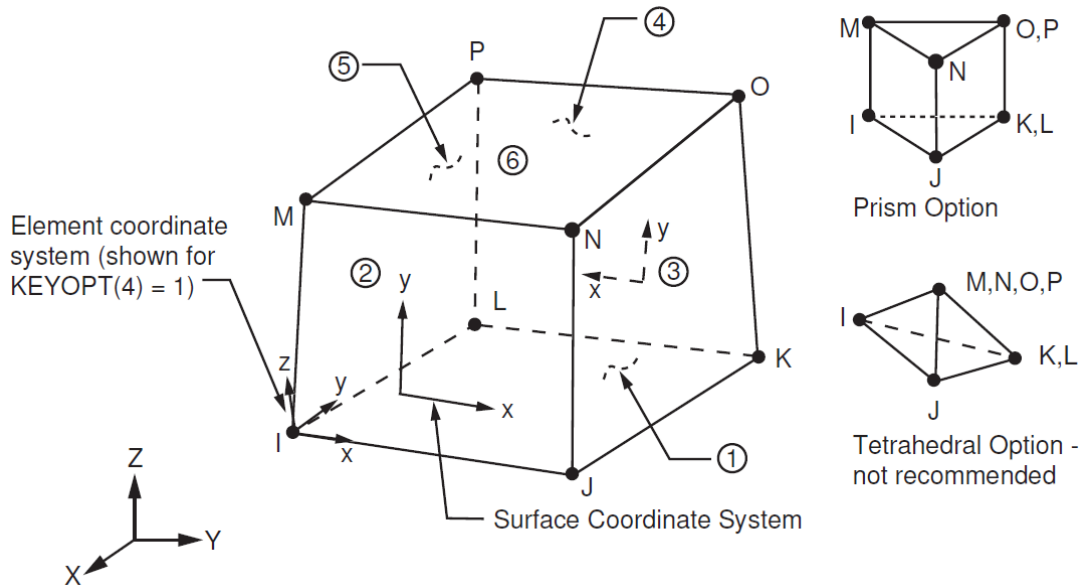


Figure 3.4 SOLID45 geometry (ANSYS, 2012).

3.1.7 Finite element model of interface

The contact between the concrete and the tendon was modeled by contact elements (using the CONTACT PAIR MANAGER) available within the ANSYS program element library. The method requires definition of two surfaces that are the target and contact surface. The target surface within this model (TARGE170 in ANSYS) represents rigid surface which is defined as the concrete surface surrounding the tendon and the contact surface (CONTA175 in ANSYS) represents contact, slid and deformable surface is defined as the tendon surface. The TARGE170 element has four corner nodes, and each node has three translation degrees of freedom (u, v and w) in x, y and z directions respectively. This element is located on the surface of 3D solid (such as 8-node brick element) and has the same geometric characteristics as the solid element face with which it is connected. The contact elements are formed using these two elements and monitors the displacement of the contact surface in relation to the target surface.

TARGE170 is used to represent various 3D "target" surfaces for the associated contact elements CONTA175, the contact elements themselves overlay the solid, shell, or line elements describing the boundary of a deformable body and are potentially in contact with the target surface, defined by TARGE170. This target surface discretized by a set of target segment elements TARGE170 and paired with its associated contact surface via a shared real constant set. It can impose any translational or rotational displacement, temperature, and magnetic potential on the target segment element. For rigid target surfaces, these elements can easily model complex target shapes. For flexible targets, these elements will overlay the solid, shell, or line elements describing the boundary of the deformable target body (ANSYS, 2012), as shown in Figure 3.5.

CONTA175 is used to represent contact and sliding between two surfaces (between node and surface, or between line and surface) in 2D or 3D. The geometry is shown in Figure 3.6. The element is applicable to 2D or 3D structural and coupled field contact analyses. This element is located on the surfaces of solid, beam, and shell elements. 3-D solid and shell elements with mid-side nodes supported for bonded and no separation contact. Contact occurs when the element surface penetrates one of the target segment elements TARGE170 on a specified target surface. This element

also allows separation of bonded contact to simulate interface delamination (ANSYS, 2012).

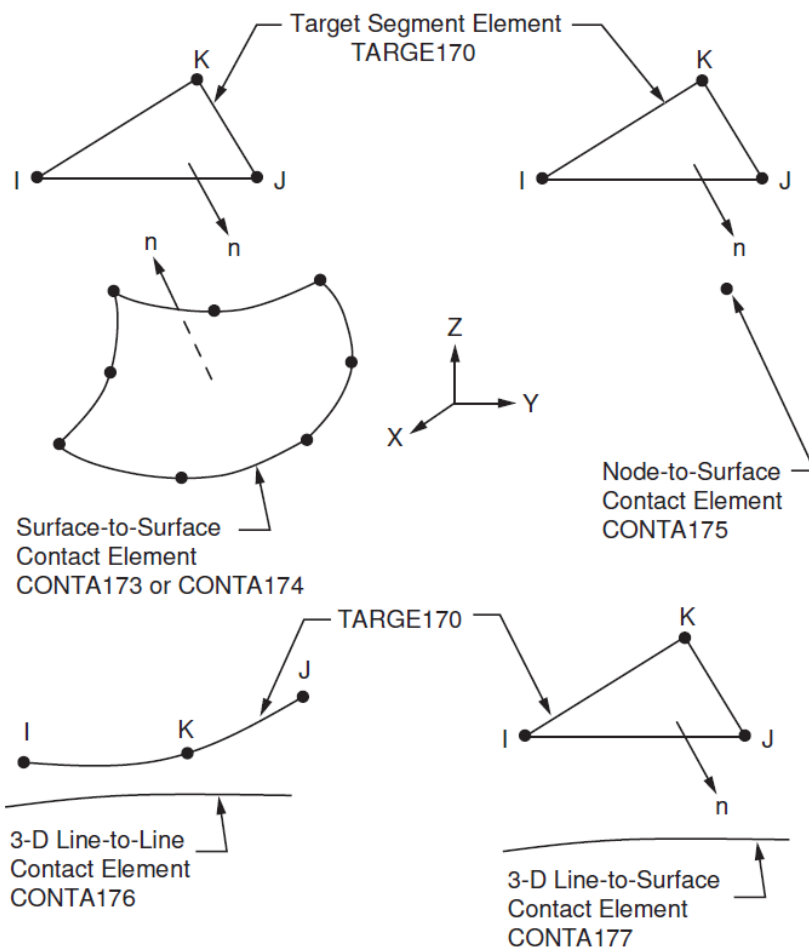


Figure 3.5 TARGE170 geometry (ANSYS, 2012).

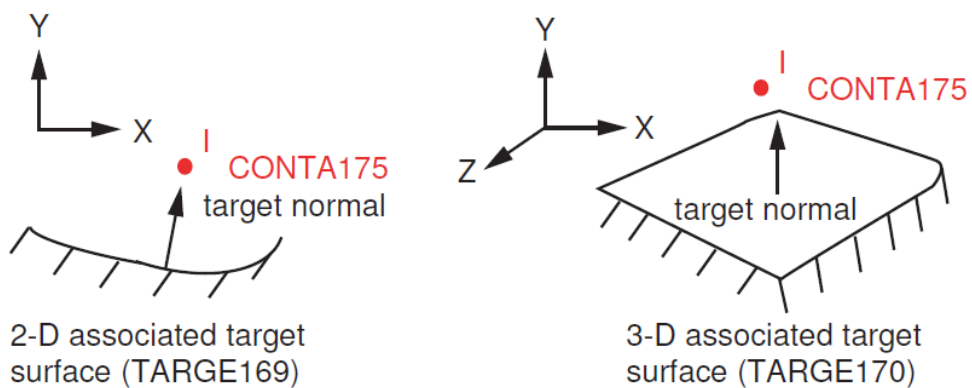


Figure 3.6 CONTA175 geometry (ANSYS, 2012).

3.1.8 Anchorage steel modeling

The tendons must be anchored at both ends of the beam members to maintain internal forces, these forces create high stress at both ends, to avoid the ends from crushing the shell plates must be applied at the ends.

SHELL181 is suitable for analyzing thin to moderately thick shell structures. It is a four node element with six degrees of freedom at each node, translations in the x, y, and z directions, and rotations about the x, y, and z-axes. The geometry, node locations, and the coordinate system for this element are shown in Figure 3.7 (ANSYS, 2012).

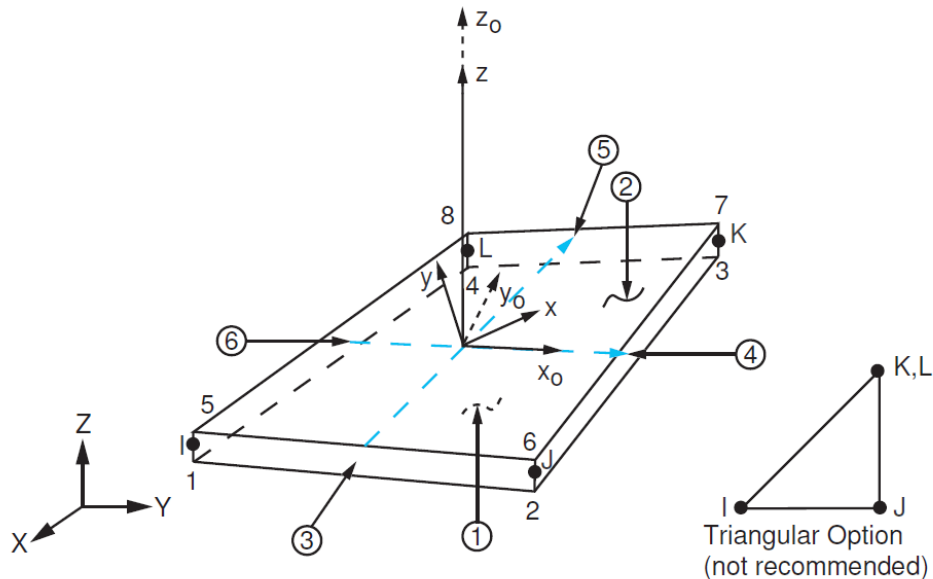


Figure 3.7 SHELL181 geometry (ANSYS, 2012).

3.1.9 Thermal solid modeling

Thermal-stress applications are treated in a so-called coupled-field analysis, which takes into account the interaction between thermal expansion/contraction and mechanical stress. The change from structural to thermal analysis is achieved in ANSYS as the elements are switched from structural SOLID65 to thermal SOLID70 type.

SOLID70 has a 3D thermal conduction capability. The element has eight nodes with a single degree of freedom, temperature, at each node. The element is applicable to a

three-dimensional, steady-state or transient thermal analysis. The geometry this element is shown in Figure 3.8 (ANSYS, 2012).

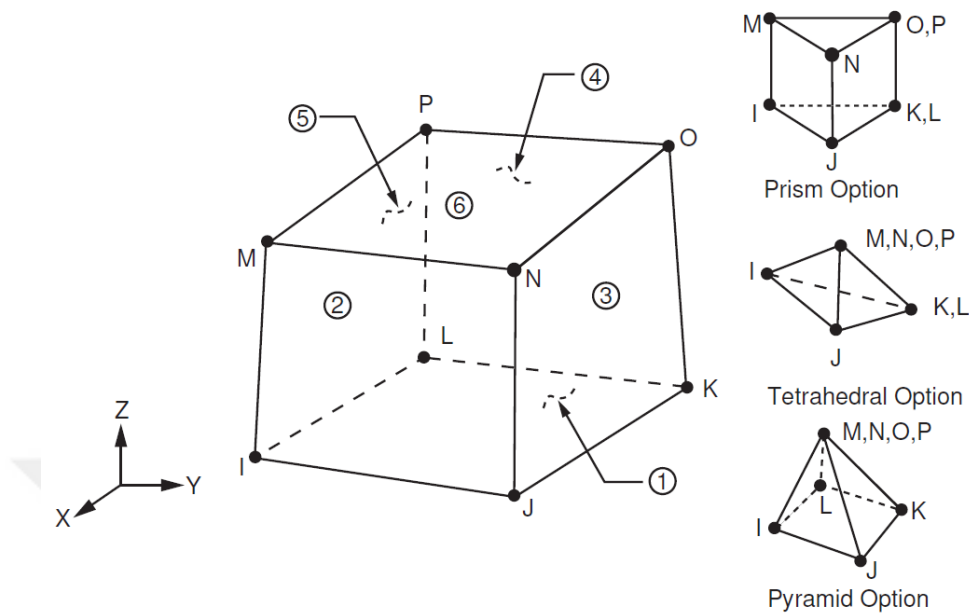


Figure 3.8 SOLID70 geometry (ANSYS, 2012).

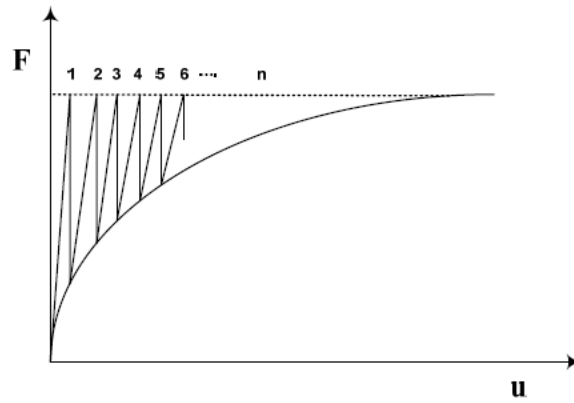
3.2 Nonlinear Solution Techniques

In nonlinear analysis, three basic solution techniques are usually used to solve the governing equations. These are the iterative, the incremental and the combined incremental-iterative approaches. These approaches are diagrammatically illustrated in Figure 3.9 for a single degree of freedom nonlinear analysis.

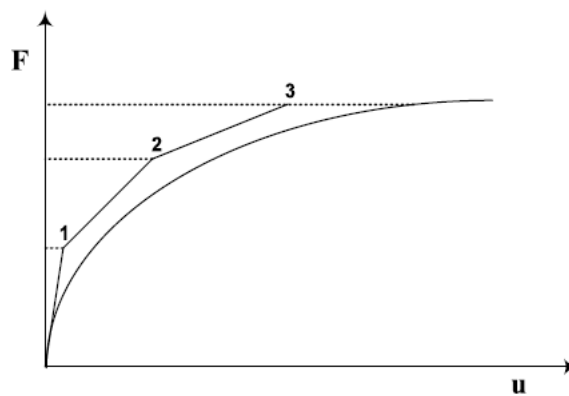
The purely iterative techniques imply the application of the total load in a single increment, as shown in Figure 3.9a. The out of balance force is used as an additional load. The total displacement is taken as the sum of the accumulated displacements from each iteration. The iterative corrections continue until the out of balance forces become negligibly small. This type of technique is not suitable for tracing the entire nonlinear equilibrium path because it fails to produce information about the intermediate stages of loading (Zebun, 2006).

The purely incremental techniques are usually carried out by applying the external loads as a sequence of sufficiently small increments, as shown in Figure 3.9b. Within each increment of loading, linear constitutive relationships are generally assumed. Because the purely incremental technique does not account for the redistribution of

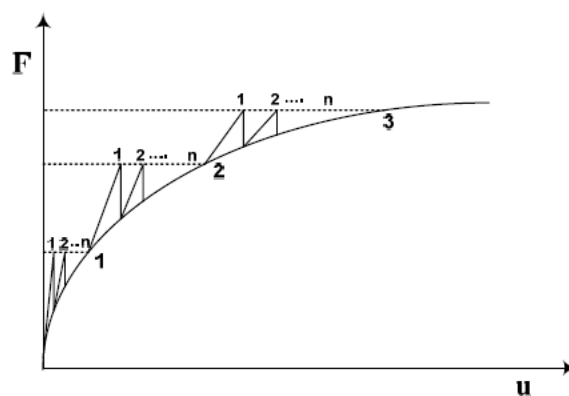
forces during the application of loading increments, the method suffers from a progressive and uncorrected tendency to drift from the true equilibrium path (Moaveni, 1999).



(a)



(b)



(c)

Figure 3.9 Basic techniques for the solution of non-linear equations: (a) Iterative (b) Incremental (c) Incremental-Iterative (Zebun, 2006).

The combined incremental-iterative technique implies the subdivision of the total external load into smaller increments, as shown in Figure 3.9c. Within each increment of loading, iterative cycles are performed in order to obtain a converging solution corresponding to the stage of loading under consideration. In practice, the progress of the iterative procedure is monitored with reference to a specified convergence criterion (Zebun, 2006).

ANSYS computer program employs "Incremental-Iterative Technique" to solve nonlinear problems. In this program, this technique uses one of the following procedures:

3.2.1 Initial-stiffness procedure

In this procedure, the stiffness matrix is formed and solved only once at the beginning of the analysis, and the program uses this initial stiffness matrix at every equilibrium iterations. For this procedure, the computation cost per iteration is significantly reduced, but in case of strong nonlinearities (such as large deformation analysis), the method often fails to converge, Figure 3.10a (Zebun, 2006).

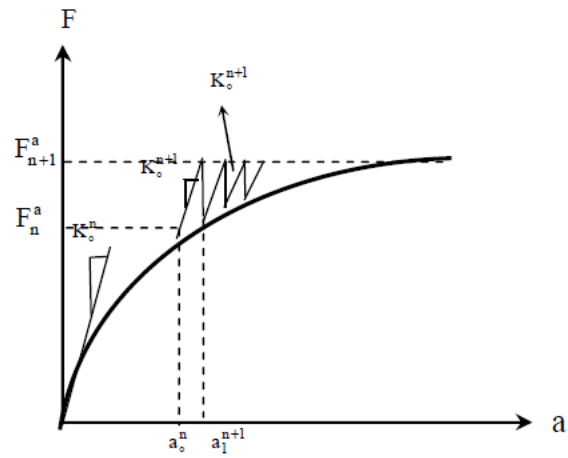
3.2.2 Full Newton-Raphson procedure

In this procedure, the stiffness matrix is updated at every equilibrium iteration, thus a large amount of computation may be required to form and solve the stiffness matrix, Figure 3.10b (Zebun, 2006).

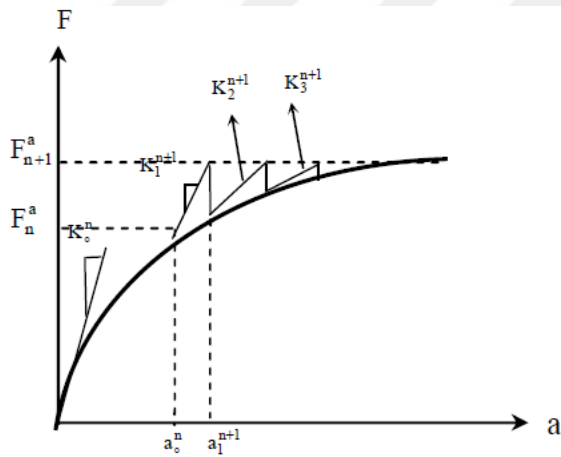
3.2.3 Modified Newton-Raphson procedure

The modified forms of the Newton-Raphson method are most common. In one method the stiffness matrix is updated at the beginning of the first iteration of every load increment (KT1 method). In case of two modifications, the stiffness matrix is calculated at the beginning of the second iteration (KT2 method), so that the nonlinear effects are more accurately represented in the stiffness matrix. These methods are more economical than the full Newton-Raphson method because they involve fewer stiffness matrix reformulations, but the convergence is slower and a

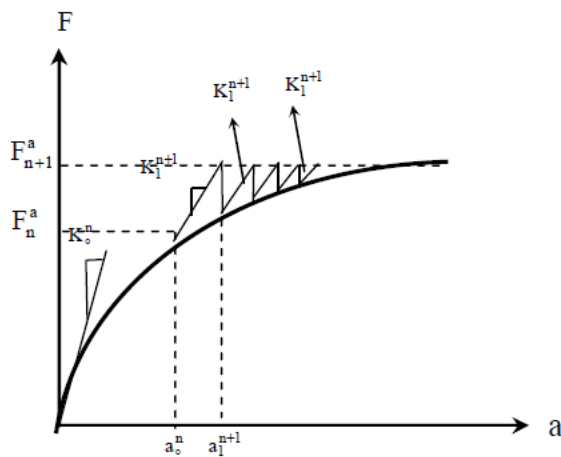
large number of iterations are required to achieve a converged solution, Figure 3.10c (Zebun, 2006).



(a) Initial stiffness method.



(b) Full Newton-Raphson method.



(c) Modified Newton-Raphson method

Figure 3.10 Newton-Raphson procedures (Zebun, 2006).

The initial-stiffness and the modified Newton-Raphson procedures converge more slowly than the full Newton-Raphson procedure, as they require fewer stiffness matrix reformulations (ANSYS, 2012). The full Newton-Raphson is adopted in the current study.

In the ANSYS computer program a nonlinear analysis can be organized into three levels of operation:

1. The top level consists of the load steps defined explicitly over a "time" span. Loads are assumed to vary linearly within load steps (for static analysis), as shown in Figure 3.11.
2. Within each load step, it can direct the program to perform several solutions (sub steps or time steps) to apply the load gradually.
3. At each sub step, the program will perform a number of equilibrium iterations to obtain a converged solution.

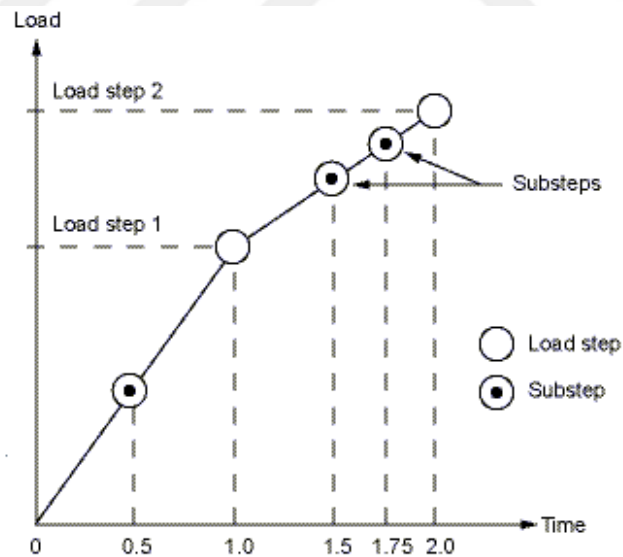


Figure 3.11 Load step, sub steps, and time (ANSYS, 2012).

3.3 Convergence Criterion

The program will continue to do equilibrium iterations until the convergence criteria are satisfied (or until the maximum number of equilibrium equations is reached).

Convergence checking can be based on forces, moment, displacements or rotations, or on any combination of these items. Additionally, each item can have a different convergence tolerance value. For multiple degree of freedom problems, it also has a choice of convergence norms.

In this study, the default of ANSYS program is used (convergence is checked by a displacements convergence criterion, tolerance equal to 0.05).

3.4 Analysis Termination Criterion

The nonlinear FE analysis used in simulating the response of PT flat slabs must include as well a criterion to terminate the analysis when failure of the structure is reached. In a physical test under load control, collapse of a structure takes place when no further loading can be sustained; this is usually indicated in the numerical tests by successively increasing iterative displacements and a continuous growth in the dissipated energy. Hence, the convergence of the iterative process cannot be achieved and therefore it is necessary to specify a suitable criterion to terminate the analysis.

In this study, a maximum number of iterations for each increment of load are specified to stop the nonlinear solution if the convergence tolerance has not been achieved. A maximum number of iterations (100) are used, because it is observed and found that this range is generally sufficient to predict the solution's divergence or failure.

3.5 Modeling of Material Properties

3.5.1 General

The performance of any structure under loads depends, to a large degree, on the stress-strain relationship of the material. Reinforced concrete slabs are made of different materials (concrete and reinforcing steel) which are brought together to work as a reinforced concrete slab system. That system is made to exploit the material relationship of each constituent material according to its designation.

In order to obtain an accurate analysis with FE method, proper material models are needed. In general, the steel can be considered as a homogeneous material that exhibits similar stress-strain relationship in compression and tension and its

properties are generally well defined. On the other hand, the behavior of concrete is very much dependent on the properties of each of its components; namely, cement mortar, aggregates and air voids. Therefore, concrete is a grossly heterogeneous material and has completely different properties in compression and tension. Mainly, because of this heterogeneity, it is difficult to define its properties accurately.

A description of the constitutive relationships for the materials comprising reinforced concrete slabs are given in this section.

3.5.2 The mechanical behavior of concrete

Concrete itself can be considered as a composite system made up of cement, aggregate, sand and water and it is because of the difference in stiffness of these materials that the interface zones between them create weak points in the materials which make up and develop micro cracks. This property is decisive for the mechanical behavior of concrete (Chen, 1982), in that, the mathematical behavior of concrete is associated with internal micro-cracking, also the fact that these aggregate-mortar links have a low tensile strength is the sole reason why concrete has a low tensile strength itself and is considered as a good compression bearing material. From the above, it can be concluded that the constituents which make up concrete have a significant effect on the way concrete behaves under different loading and this is mathematically represented by a stress-strain curve.

Experimental observations showed that concrete could behave as either a linear or nonlinear material depending on the level and the nature of the stresses to which it is subjected under low level of stress concrete behaves as a linear elastic material, while for higher values of stress and for sustained loading, it exhibits highly non-linear properties (Al-Thebhawe, 2001).

The concrete may be subjected to uniaxial, biaxial and triaxial stresses. The behavior of concrete under these states of stresses is described in the following sections.

3.5.2.1 Uniaxial compression behavior of concrete

A typical uniaxial compressive stress- strain curve is shown in Figure 3.12. It can be noted that the concrete behaves as linear elastic material when the stress level is less than about (0.3-0.5) times of the uniaxial compressive strength (f'_c), and for stress

above this point, the curve shows a gradual increase in curvature up to about (0.75-0.9) (f'_c) upon where it bends more sharply and approaches the peak point at (f'_c). Thereafter the stress-strain curve descends until failure occurs due to the crushing of concrete at the ultimate strain (Chen, 1982).

The observed stress-strain relationship of concrete has to be expressed analytically to be useful in the analysis and design of structural members.

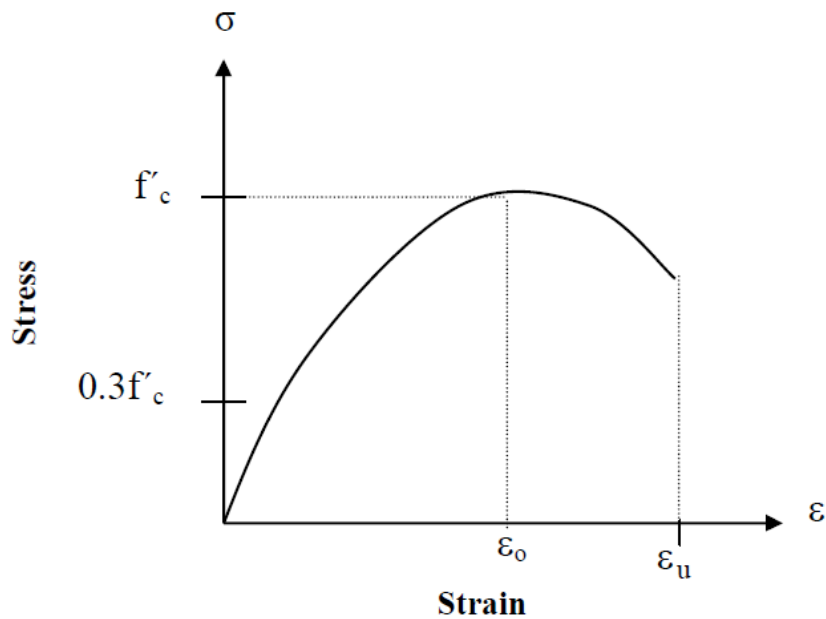


Figure 3.12 Typical uniaxial stress-strain curve for concrete in compression (Chen, 1982).

3.5.2.2 Uniaxial tension behavior of concrete

The general mechanical behavior of concrete under uniaxial tensile stress shows that the stress-strain response of concrete is linear up to about 60 percent of cracking stress (f_t) as shown in Figure 3.13. Beyond this level, bond micro cracks start to grow and the curve starts to increase as the stress level increases until peak stress is reached (Chen, 1982).

The tensile strength of concrete can be estimated using either the modulus of rupture test, split cylinder test or direct tension test.

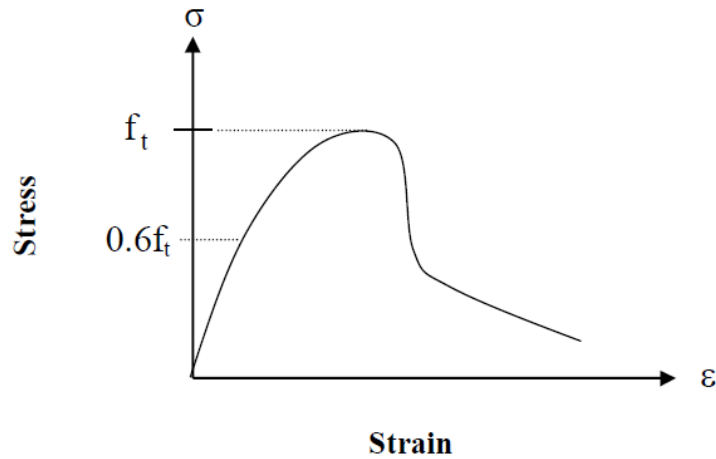


Figure 3.13 Typical uniaxial stress-strain curve for concrete in tension (Chen, 1982).

3.5.2.3 Biaxial stress behavior of concrete

The failure of concrete members usually occurs under combined loading conditions, and the state of stress at failure is generally complex. Biaxial and triaxial states of stress- strain behavior are somewhat different from that of uniaxial state. Extensive experimental tests on concrete under biaxial stress state have been performed by many investigators amongst them (Kupfer et al., 1969).

The test results show that the ultimate strength of concrete in biaxial compression is greater than in uniaxial compression, and it depends on the principal stress ratio. The ultimate strength data are reported in terms of biaxial stress envelope as shown in Figure 3.14.

The maximum strength increase is approximately (25 %) of the uniaxial strength is achieved at a stress ratio of ($\sigma_1/\sigma_2 = 0.5$), and this is reduced to about (16 %) at an equal biaxial-compression state ($\sigma_1/\sigma_2=1$). Under biaxial compression-tension the compressive strength decreases almost linearly as the applied tensile stress is increased. While under biaxial tension, the strength is almost the same as that of the uniaxial tensile strength (Chen and Saleeb, 1982).

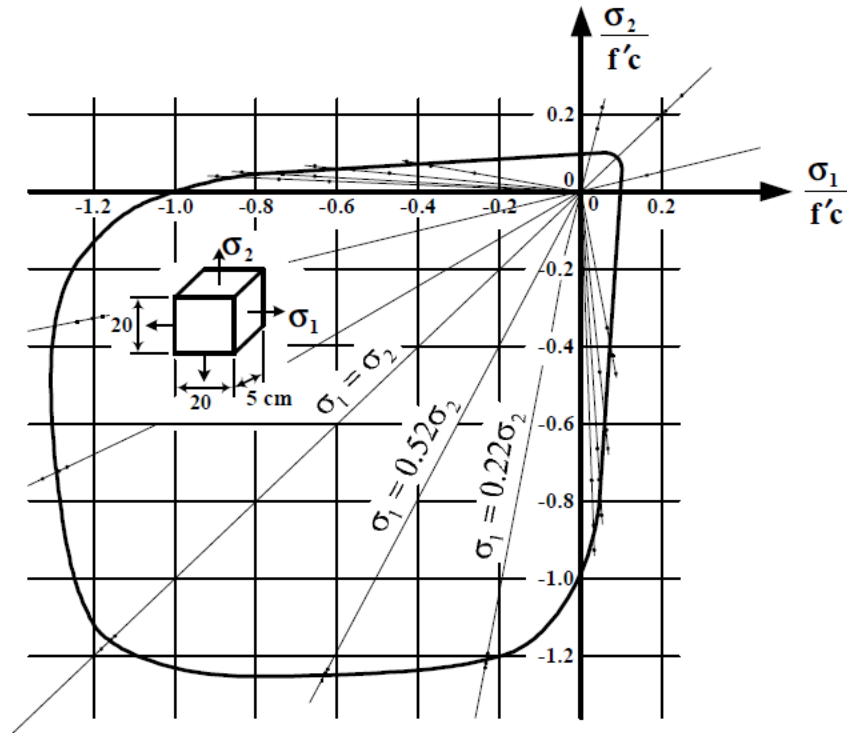


Figure 3.14 Biaxial state of loading (Kupfer et al., 1969).

3.5.2.4 Triaxial stress behavior of concrete

Under a triaxial stress state the failure surface of concrete is a function of the three principal stresses. Because isotropy for concrete is assumed, the elastic limit, the onset of unstable crack propagation and the failure limit all can be represented as surfaces in 3D principal stress spaces, as shown in Figure 3.15. When the hydrostatic compressions along the line ($\sigma_1=\sigma_2=\sigma_3$) increase, the deviatoric sections (planes perpendicular to the line ($\sigma_1=\sigma_2=\sigma_3$)) of the failure surface are more or less circular, which indicates that the failure in this region is independent of the third stress invariant (Chen, 1982). But for smaller hydrostatic pressures, these deviatoric cross sections are convex and noncircular.

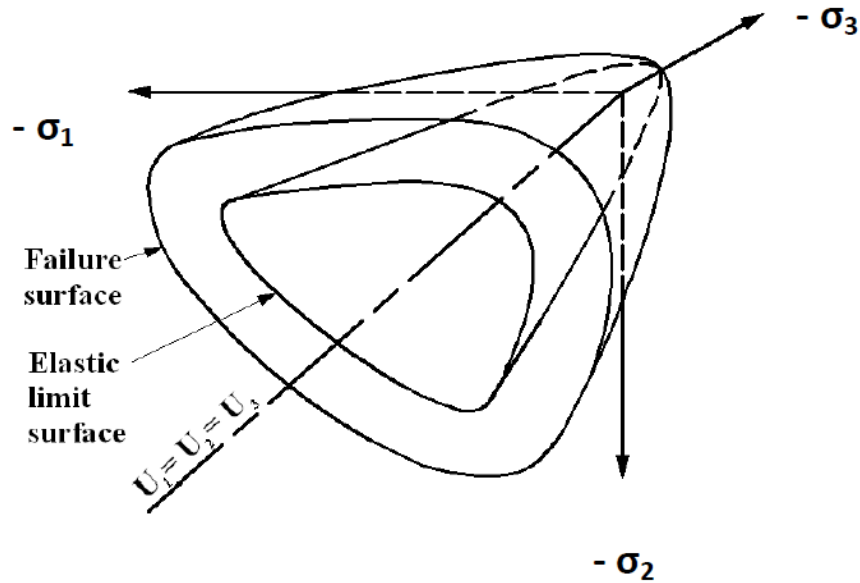


Figure 3.15 Schematic failure surface of concrete in 3-D stress space (Zebun, 2006).

3.5.3 Concrete Modeling

3.5.3.1 Plasticity based models

Plasticity based models have been used extensively in the recent years to model concrete in compression. Plasticity theory provides a mathematical relationship that characterizes the elasto - plastic response of materials.

ANSYS program provides several options to characterize different types of material behavior, such as bilinear isotropic (with work hardening) and multi linear isotropic hardening. For concrete, the crushing of concrete in compression algorithm is akin to a plasticity law (Fanning, 2001). This algorithm is similar to a multi linear work hardening of uniaxial stress-strain curve based on rate independent Von- Mises yielding criterion.

Rate independent plasticity constitutes an irreversible straining that occurs in a material once the yield surface is reached. There are three ingredients in the rate independent plasticity theory in the ANSYS program:

- 1- Yield criterion (elastic-limit surface).
- 2- Flow rule.
- 3- Hardening rule (loading surface).

The yield criterion determines the stress level at which yielding is initiated, while the flow rule determines the direction of plastic straining. The hardening rule describes the changing of the yield surface with progressive yielding so that the stress states for subsequent yielding can be established (ANSYS, 2012). In the present study, plasticity based models are used to model stress-strain relationship of concrete in compression.

3.5.3.2 Stress-strain relationship model

In this study, the concrete is assumed to be homogeneous and initially isotropic; the adopted stress-strain relation is based on work done by Desayi and Krishnan (1964); as shown in Figure 3.16.

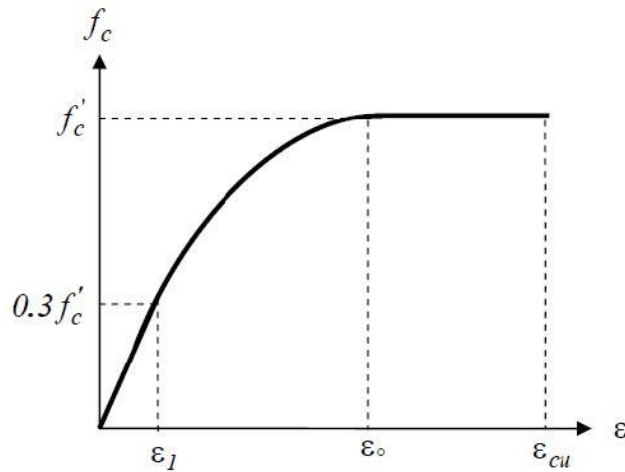


Figure 3.16 Simplified compressive uniaxial stress-strain curve for concrete (Desayi and Krishnan,1964).

Compressive uniaxial stress-strain relationship for concrete model was obtained by using the following equations to compute the multi-linear isotropic stress-strain curve for the concrete (Desayi and Krishnan,1964).

$$f_c = \varepsilon E_c \quad \text{for } 0 \leq \varepsilon \leq \varepsilon_1 \quad (3.1)$$

$$f_c = \frac{\varepsilon E_c}{1 + \left(\frac{\varepsilon}{\varepsilon_1}\right)^2} \quad \text{for } \varepsilon_1 \leq \varepsilon \leq \varepsilon_0 \quad (3.2)$$

$$f_c = f'_c \quad \text{for } \varepsilon_0 \leq \varepsilon \leq \varepsilon_{cu} \quad (3.3)$$

And

$$\varepsilon_1 = \frac{0.3f'_c}{E_c} \quad (\text{Hooke's law}) \quad (3.4)$$

$$\varepsilon_o = \frac{2f'_c}{E_c} \quad (3.5)$$

Where:

ε_1 = strain corresponding to $(0.3f'_c)$.

ε_o = strain at peak point.

ε_{cu} = ultimate compressive strain.

The multi-linear curves are used to help with convergence of the nonlinear solution algorithm (Tavarez, 2001). In the present study, take more from five points between $(\varepsilon_1, 0.3f'_c)$ and (ε_o, f'_c) (i.e. construct the multi-linear isotropic stress-strain curve for concrete in Figure 3.16).

3.5.3.3 Failure criteria of concrete

In the present study, the model to be used is capable of predicting failure of concrete materials. Both cracking and crushing failure modes are accounted. For the two input strength parameters (i.e. ultimate uniaxial tensile strength f_t and compressive strength f'_c) are needed to define a failure surface for the concrete. Consequently, criterion for failure of the concrete due to a multiaxial stress state can be calculated by (Willam and Warnke, 1975).

The 3D failure surface for states of stress that is biaxial or nearly biaxial is represented in Figure 3.17. The most significant nonzero principal stresses are in the σ_{xp} and σ_{yp} directions, the three surfaces are shown as projections on the $(\sigma_{xp} - \sigma_{yp})$ plane. The mode of failure is a function of the sign of σ_{zp} (principal stress in the z direction). For example if and are both negative and is slightly positive, cracking would be predicated in a direction perpendicular to σ_{zp} , However, if is σ_{zp} zero or slightly negative, the material is assumed to crush (ANSYS, 2012).

If the crushing capability of the concrete is turned on the FE slab models fail prematurely. Crushing of the concrete starts to develop in elements located directly under the loads. Subsequently, adjacent concrete elements crush within several load steps as well, significantly reducing the local stiffness (Zebun, 2006). Convergence

problems have been repeated when crushing capability was turned on (Wolanski, 2004).

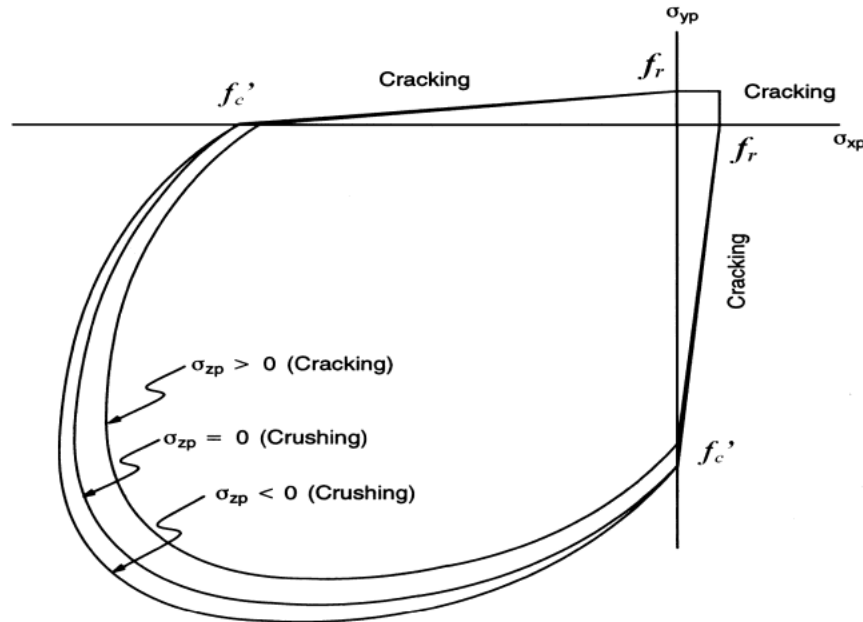


Figure 3.17 Failure surface in principal stress space with nearly biaxial stress (ANSYS, 2012).

Therefore, in part of this study, the crushing capability is turned off and cracking of the concrete controls the failure of the FE models (as suggested by previous researchers (Wolanski, 2004; Zebun, 2006).

3.5.3.4 Crack modeling

Three different approaches for crack modeling have been employed in the analytical studies of concrete structures using the numerical technique of FE method. These are:

- 1- Smearred cracking modeling (as shown in Figure 3.18).
- 2- Discrete cracking modeling (as shown in Figure 3.19).
- 3- Fracture mechanics modeling.

The particular cracking model to be selected from the three alternatives depends on the purpose of the analysis. In general, if overall load-deflection behavior is desired,

the smeared crack modeling is probably the best choice. If detailed local behavior is of interest adaptations of the discrete cracking modeling are useful. For the special class of problems in which fracture mechanics is the appropriate tool, a specialized fracture model may prove to be necessary.

For ANSYS computer program (ANSYS, 2012), crack modeling, depends on smeared cracking modeling. Therefore, general description for this modeling is given below.

Smeared cracking modeling

In this approach, the cracked concrete is assumed to remain as a continuum; that is the cracks are smeared out (as shown in Figure 3.18) in a continuous fashion-rather than representing a single discrete crack (as shown in Figure 3.19). The present approach has the effect of representing an infinite number of parallel fissures across the cracked concrete element. These parallel fissures are assumed to form in the planes (or surfaces for axisymmetric problems) perpendicular to the maximum principal stress (or strain) direction. After the first cracking has occurred, it is assumed that the cracked concrete becomes orthotropic or transversely isotropic, with one of the material principal axes being oriented along the direction of cracking.

Before cracking, the uncracked concrete is assumed to be an isotropic linear elastic material. However, the onset of cracking introduces orthotropic material properties and new incremental constitutive relationships must be derived. This is accomplished by modifying elasticity matrix.

In ANSYS computer program (ANSYS, 2012), the presence of a crack at an integration point is represented through modification of the stress-strain relations by introducing a plane of weakness in directions normal to the crack face. Also, a shear transfer coefficient is introduced which represents a shear strength reduction factor for those subsequent loads, which induce sliding (shear) across the crack face.

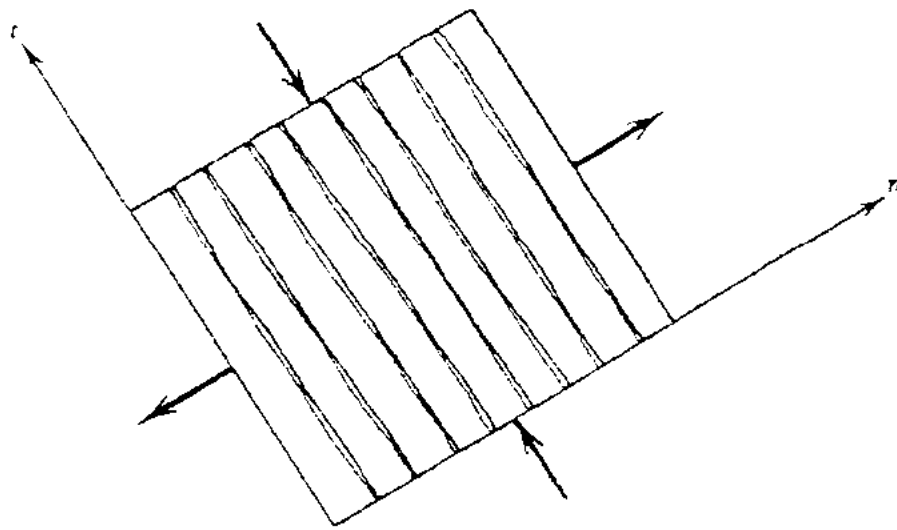


Figure 3.18 Smeared crack modeling (Zebun, 2006).

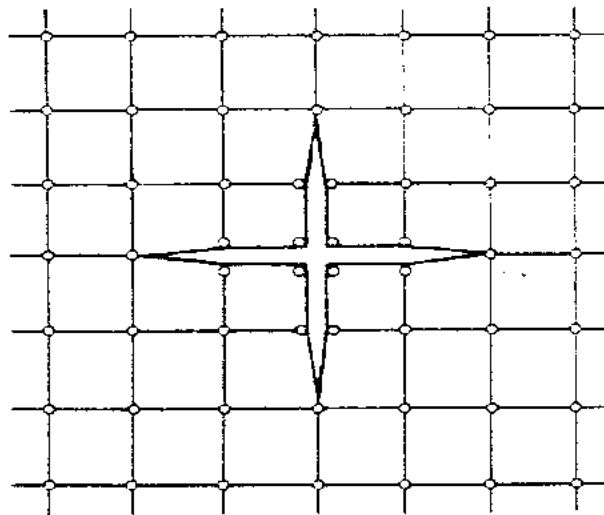


Figure 3.19 Two-dimensional cracking representation in discrete cracking modeling approach (Zebun, 2006).

Shear transfer coefficients

The concrete is assumed to behave linearly elastic in tension up to the ultimate tensile strength. After this point, the concrete cracks and the shear stiffness is reduced. Furthermore, once cracking has developed, the opposite faces of opened crack will be interlocked when they are subjected to parallel differential movement. This interlock depends on the texture of the cracked surface as well as the

constrained force that can keep the cracked surfaces from moving apart. The rough surfaces of the cracked concrete can partially transmit shear across the crack due to aggregate interlock and dowel action of the crossing reinforcement as the reinforcing bars provide some constraint somewhere along the cracked surface.

In the current model, the ability of concrete to transfer shear forces across the crack interface is accounted for by introducing a reduction factor (β) to the shear modulus of originally uncracked concrete. Two coefficients of shear strength reduction are used, thus (β_o) is introduced for the case of opened crack and (β_c) is introduced for the case of closed crack. The values of (β_o) and (β_c) are always in the range of ($1 > \beta_c > \beta_o > 0$) (ANSYS, 2012).

3.5.3.5 Crushing modeling

In ANSYS computer program (ANSYS, 2012), if the material at an integration point fails in uniaxial, biaxial or triaxial compression, the material is assumed to crush at that point. In concrete brick element, crushing is defined as the complete deterioration of the structural integrity of the materials (e.g. material palling). Under conditions when crushing has occurred, material strength is assumed to have degraded to an extent such that the contribution to the stiffness of an element at the integration point in question can be ignored.

3.5.3.6 Modulus of elasticity

The modulus was based on the equation,

$$E_c = 4700\sqrt{f'_c} \quad (3.6)$$

where E_c is the modulus of elasticity of the concrete and f'_c in MPa.

3.5.3.7 Poisson's ratio

Poisson's ratio, (ν), is the ratio of the transverse strain to longitudinal strain. For concrete under uniaxial compressive stress it ranges between (0.15-0.22) up to a stress level of (80) percent of (f'_c) as it was reported by many researchers. Beyond this level, this value increases rapidly and excess of (0.5) has been measured (Al-Thebhawe, 2001). In this study, a value of (0.2) is adopted for analyzing concrete slab (Merritt and Ricketts, 2001).

3.5.4 Modeling of reinforcing bars

Since the steel bars are slender, they can be assumed to transmit axial force only. Modeling of steel in FE is much simpler. The stress-strain relationship for reinforcing steel bars can be represented as shown in Figure 3.20. In this study the Poisson's ratio for steel is taken as 0.3 (Merritt and Ricketts, 2001).

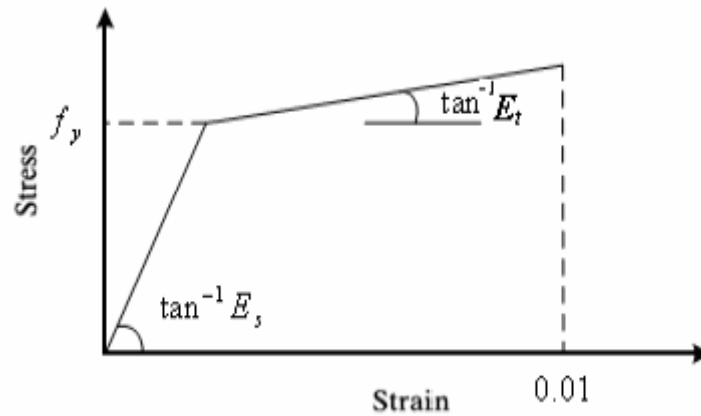


Figure 3.20 Alternative bilinear stress-strain relationships (CEB, 1993).

3.5.5 Material modeling of strands

Material properties of the strands were input as multi-linear isotropic material properties. Figure 3.21 illustrates the stress-strain curve of the strands.

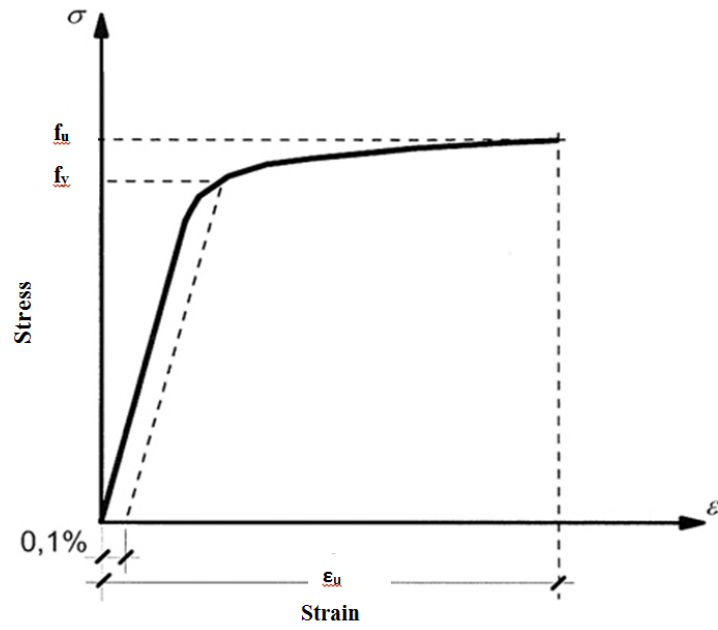


Figure 3.21 Multi-linear stress-strain relationship for the strands.

CHAPTER 4

ANALYTICAL APPLICATIONS AND DISCUSSIONS

4.1 General

The post tensioned slabs commonly used in building and bridge construction are grouped into two basic categories. These are the unbonded and bonded systems. PT concrete is a method for overcoming the natural weakness of concrete in tension. It is used to produce beams, floors or bridges with longer spans. Post-tensioning of concrete slabs can be conducted using unbonded or bonded tendons. In bonded systems, the tendons are fully bonded to the surrounding material. The tendons are inserted into the ducts and after the pre-stressing load is applied, the ducts are filled with cementitious grout to achieve the required bond between the tendon and the concrete. For bonded systems, there is in principle uniform steel-concrete force transfer along the length of the tendons and full strain compatibility is assumed, implying that steel strains are equal to concrete strains.

For unbonded tendons, each tendon is greased and covered by a plastic tube, as to avoid corrosion and to provide minimum friction between the tendon and the concrete. However, if the tendon is damaged, it will lose all of its pre-stressing at once. For unbonded tendons, steel-concrete force transfer occurs only at the anchors and strain compatibility cannot be assumed at all sections.

The prestressing force that is applied is dependent on the geometry and loading of a specific element and is determined with the principles of mechanics and stress-strain relationships. The prestressing force can be either concentric (along the axis of the member) or eccentric (a distance away from and parallel to the axis of the member). For the concentric case, the compressive stress on the beam cross-section is uniform. The presence of the compressive prestress force reduces the tensile flexural stress at bottom fibers and induces compressive stresses in top fibers. This situation is avoided by applying the prestress force eccentrically.

In order to avoid high tensile stresses in the top fiber over the support, tendons are draped or harped over the length of the member.

The behavior of PT concrete structural members have previously been investigated experimentally by Williams and Waldron (1989), Yang et al. (2013), Ranzi et. al. (2013), Bailey and Ellobody (2009a,b) and others.

This chapter presents a FE model using ANSYS software to model the bonded and unbonded PT concrete slabs. The proposed models were validated with previous available experimental study tested by Bailey and Ellobody (2009a,b) and Yang et al. (2013) and was used to study the effects of the transverse, gravity and thermal loading on the flexural behavior of bonded and unbonded PT one-way concrete flat slabs. A thermal version of the model was used to calculate the temperature profile in the concrete beam, following by a structural version of the model, which reads the temperature profile to calculate thermal stresses.

4.2 Finite Element Model

The ANSYS computer program is utilized for analysis of all modeled slabs. 3D brick element with 8-nodes is used to model the concrete. SOLID65 (or 3D reinforced concrete solid) is used for the 3D modeling of solids with or without reinforcing bars, which is capable of cracking in tension and crushing in compression.

Tendons and reinforcement were represented using 2-node discrete representation (LINK8) and included within the properties of 8-node brick elements. The link element is assumed to be capable of transmitting only axial forces, and perfect bond is assumed to exist between the concrete and the reinforcing bars. For tendon cable, since it is located inside the concrete section (through the hole) and the prestressing force is transferred to concrete through end anchorages and profile of tendon, the cable is connected to slab only at the end anchorages. Steel plates are added at the loading location to avoid stress concentration problems. This provides a more even stress distribution over the load area. The solid element (SOLID45) was used for the steel plates, which is used for the 3D modeling of solid structures.

The contact between the concrete and the tendon is modeled by contact elements (using the CONTACT PAIR MANAGER) (ANSYS, 2012). The method requires the definition of two surfaces that are the target and the contact surfaces. The target

surface within this model (TARGE170) represents rigid surface which is defined as the concrete surface surrounding the tendon. The contact surface (CONTA175) represents contact, slid and deformable surface, which is the tendon surface in this case. The TARGE170 element has four corner nodes, and each node has three translation degrees of freedom (u, v and w) in x, y and z directions respectively. This element is located on the surface of a 3D solid element such as the 8-node brick element and has the same geometric characteristics as the solid element face with which it is connected. The contact elements are formed using these two elements and monitors the displacement of the contact surface in relation to the target surface.

Thermal-stress applications are treated in a so-called coupled-field analysis, which takes into account the interaction between thermal expansion/contraction and mechanical stress. The change from structural to thermal analysis is achieved in ANSYS as the elements are switched from structural SOLID65 to thermal SOLID70 type. The distributions of thermal elastic stress components are then calculated by switching the SOLID70 thermal element to SOLID65 structural element which is used for 3-D modelling of solid structures. The FE solution performed via ANSYS calculates nodal temperatures, and then use the nodal temperatures to obtain other thermal quantities. The elastic stresses, induced by mechanical constraints and thermal strains resulting from the previous analysis, are calculated.

Material plays an important role in ANSYS modeling. Correct values of material properties have to be given as input in ANSYS. Cube compressive strength and yield strength of reinforcing bars are found experimentally and these values are given as inputs. In tension, the stress-strain curve for concrete is approximately linearly elastic up to the maximum tensile strength. After this point, the concrete cracks and the strength decrease gradually to zero.

ANSYS has its own non-linear material model for concrete. Its reinforced concrete model consists of a material model to predict the failure of brittle materials, applied to a 3D solid element in which reinforcing bars may be included. The material model is capable of cracking in tension and crushing in compression. It can also undergo plastic deformation and creep. The multi-linear stress-strain relationship is considered for concrete in compression in this study. Since the steel bars are slender, they can be assumed to transmit axial force only. Modeling of steel in FE is more

simple. The bilinear stress-strain relationship is considered for reinforcing steel bars in this study. On the other hand, the strands are considered as multi-linear isotropic material in this study.

4.3 Analysis of Post Tensioned One-Way Slabs

4.3.1 Analysis of unbonded one-way slab 1-H35

For the verification of the current numerical model, experimental UPT concrete slab tested by Yang et al. (2013) was chosen. The slab was designated as 1-H35 with f'_c of 32.64 MPa, which was simply supported and subjected to concentrated point load at the center of the span (Yang et al., 2013). The general layout of the UPT one-way concrete is shown in Figure 4.1. The unbonded tendons were arranged with variable eccentricity (harped profile) generating a prestressing moment opposite to the external moment. The eccentricity of harped tendons varied linearly from zero at both ends of the specimens to 37.5 mm at the harping points. The specimen has the section width of 600 mm and overall depth of 125 mm, as shown in Figure 4.1. To achieve the minimum amount of mild longitudinal tensile reinforcement specified in ACI 318-11, two deformed bars, each with a diameter of 10 mm, were arranged over the full length of the slab and welded to end anchorage plates. The closed stirrups, each with a diameter of 6 mm, were arranged at 50 mm intervals between the anchorage plate and the end support in order to prevent anchorage failure of the prestressing strands owing to high bursting and spalling stresses. The three-wire strands coated with a greased sheath were arranged for post-tensioning tendons. The tendon was a plain mono-strand with each strand made of three high-strength steel wires. The tendon had a nominal diameter of 2.9 mm, an area of 19.82 mm².

The tensile strength and equivalent yield strength of the low relaxation three-wire mono-strand were 2048 MPa and 1741 MPa, respectively. The yield strengths of the mild reinforcing bars with diameters of 10 mm and 6 mm were 383 MPa and 399 MPa, respectively. The average dry density of the concrete mixed was approximately 1770 kg/m³. The one-way slab specimen was supported on a hinge at one end and on a roller at the other end. Immediately before the test, a designed prestressing force was applied to unbonded tendons and subsequently anchored using a wedge set at both ends of the slab.

As an initial step, a FE analysis requires creating a mesh of the model. In other words, the model is divided into a number of small elements, and after loading, stress and strain are calculated at integration points of these small elements (ANSYS, 2012). An important step in FE modeling is the selection of the mesh density. A convergence of results is obtained when an adequate number of elements are used in a model. Combination of 3D solid elements (SOLID65, LINK8, SHELL181 and SOLID45) available within ANSYS (ANSYS, 2012) was used to model the concrete, tendon and anchorage elements. The elements have three degrees of freedom per node. Due to symmetry, only one-quarter of the slab was modelled (Figure 4.2), with 14760 elements, including the interface elements. The boundary conditions and load application were identical to that used in the tests. The measured post-tensioning stress in the tendons (26.38 kN) was initially applied in a separate step. The dead load representing the weight of the slab was applied as a body load. For the tests the jack load was applied in increments as a distributed load over the area of the spreader plates. The material properties adopted in the analysis are given in Table 4.1.

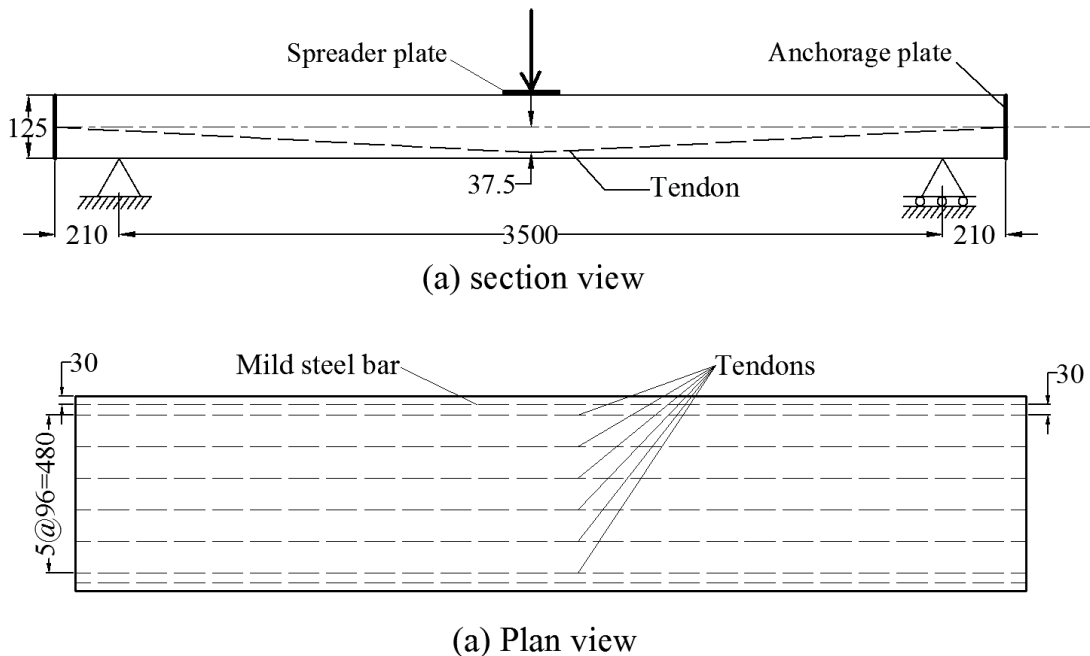


Figure 4.1 Details of slab geometry and arrangement of reinforcement of UPT slab 1-H35 (Yang et al., 2013) (dimensions are in mm).

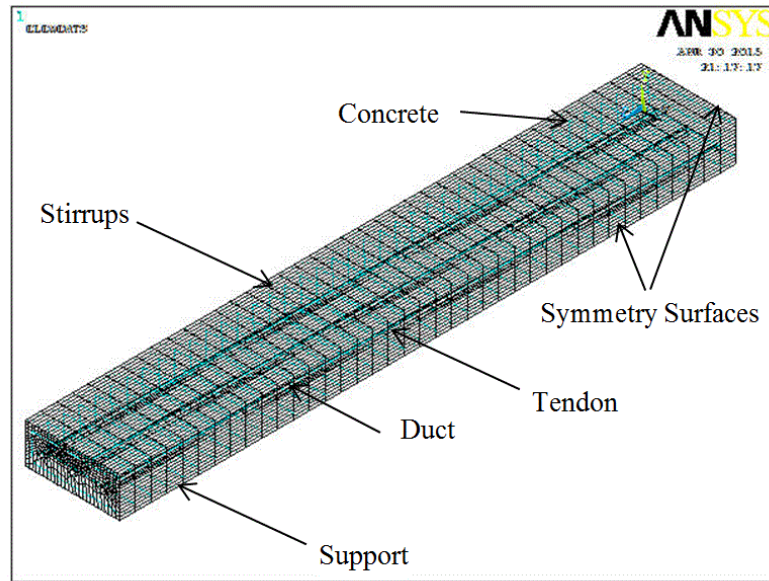


Figure 4.2 FE mesh of the concrete and the prestress strand for quarter of the UPT slab 1-H35.

Table 4.1 Material properties of concrete, reinforcement and strand for the UPT slab 1-H35.

	Concrete	Reinforcement		Strand
		10 mm	6 mm	
Ultimate compressive strength (MPa) (f'_c)	32.64	—	—	—
Ultimate tensile strength (MPa) (f_t)	3.2	—	—	—
Modulus of elasticity (MPa)	30000	205000	204000	202000
Poisson's ratio (ν)	0.2	0.3	0.3	0.3
Yield strength (MPa)	—	383	399	1741

The current analysis of a one way slab is a static nonlinear analysis under vertical live, dead and prestress loads. The analysis is carried out up to failure, thus it enables determination of failure load. In nonlinear analysis, the total load applied to a FE model is divided into a series of load increments called load steps. At the completion of each incremental solution, the stiffness matrix of the model is adjusted to reflect nonlinear changes in the structural stiffness before proceeding to the next load increment. ANSYS uses the Newton-Raphson equilibrium iterations for updating the model stiffness. For the reinforced concrete solid elements, convergence criteria were based on displacement, and the convergence tolerance limit is 5% in order to obtain convergence of the solutions. If the convergence behavior is smooth,

automatic time stepping will increase the load increment up to a selected maximum load step size and if the convergence behavior is abrupt, automatic time stepping will bisect the load increment until it is equal to a selected minimum load step size.

The load-central deflection curves from the FE analysis were compared with those from the experimental results. The experimental and numerical load deflection curves obtained for slab 1-H35 are shown in Figure 4.3, which shows the good agreement between the experimental and the FE results. At ultimate state, the numerical load was slightly smaller than the experimental load. The failure load of the experimental slab was 28.5 kN with a central deflection of 83.5 mm, compared to 28 kN and 90 mm obtained from the FE model. The failure load predicted using the model was 1.8 % smaller than that observed from the test. The mode of failure in the FE analysis was concrete crushing corresponded to the mode of failure in experimental. The first flexural cracking was initiated at 71 % of the ultimate load and was observed in the tension zone of the slab.

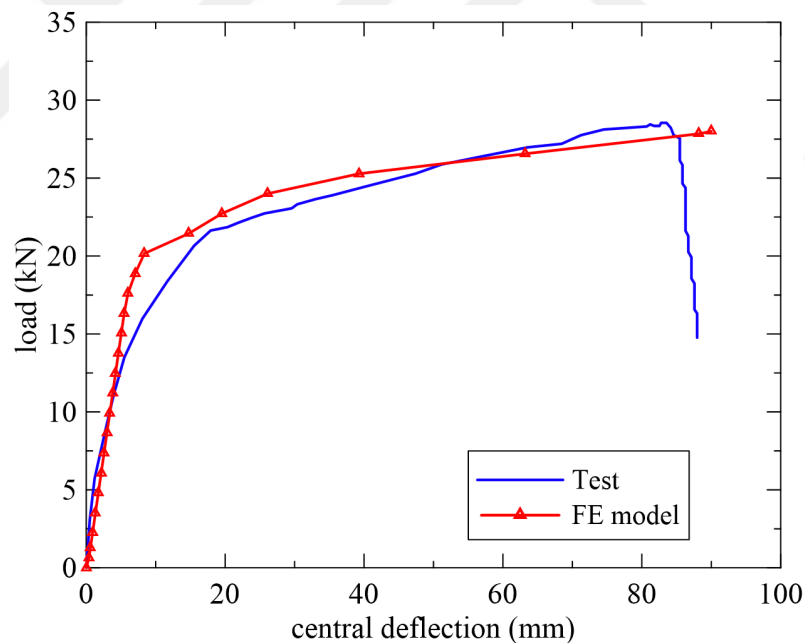


Figure 4.3 Load- deflection curve for the UPT slab 1-H35.

The initial cracking of the slab in the FE model corresponds to a load of 17 kN that creates stress just beyond the modulus of rupture of the concrete. The first crack can be seen in Figure 4.4. This first crack occurs in the constant moment region, and is a flexural crack.

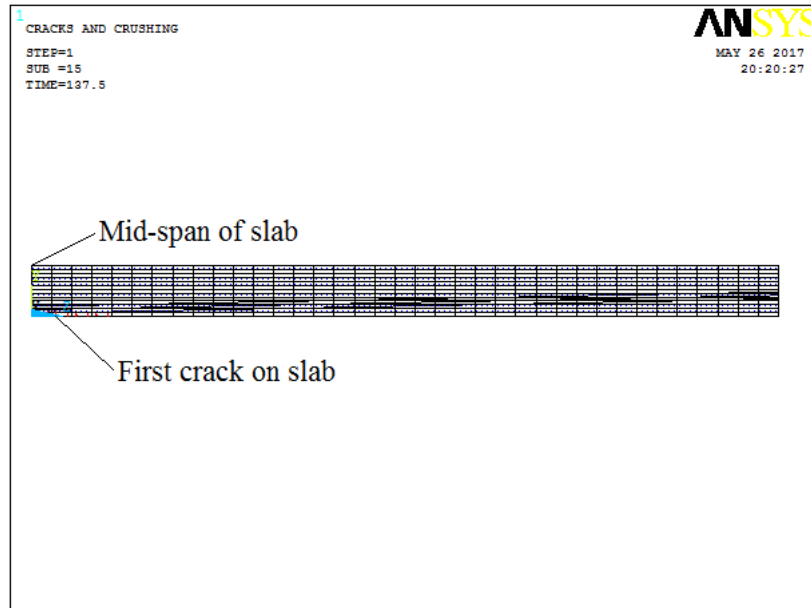


Figure 4.4 First crack for the UPT slab 1-H35.

Figure 4.5 shows the crack and crushing patterns of slab at failure load. The stress distribution in the concrete at failure for the PT slab 1-H35 is shown in Figure 4.6. The mode of failure of concrete crushing in the model, which corresponded to the mode of failure observed experimentally. The Von Mises stress for the unbonded slab 1-H35 at failure load are shown in Figure 4.7.

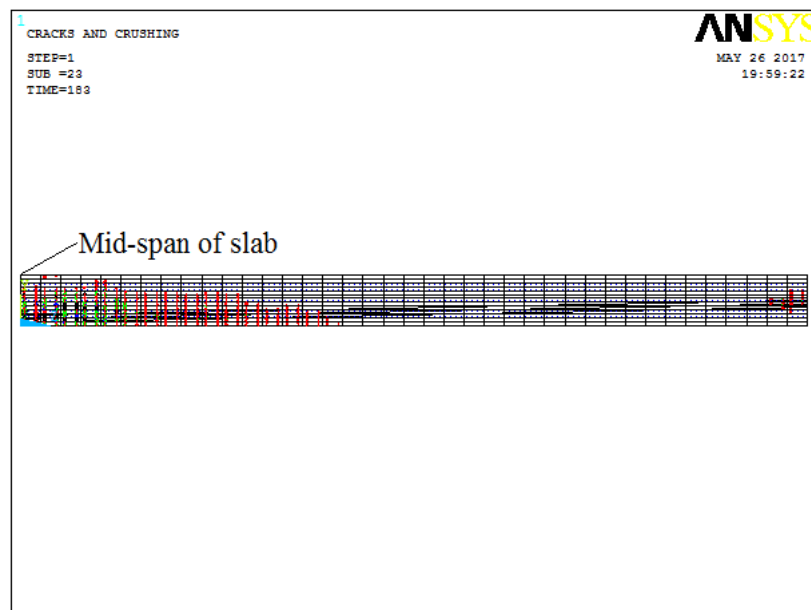


Figure 4.5 Cracks and crushing patterns of the UPT slab 1-H35 at failure load.

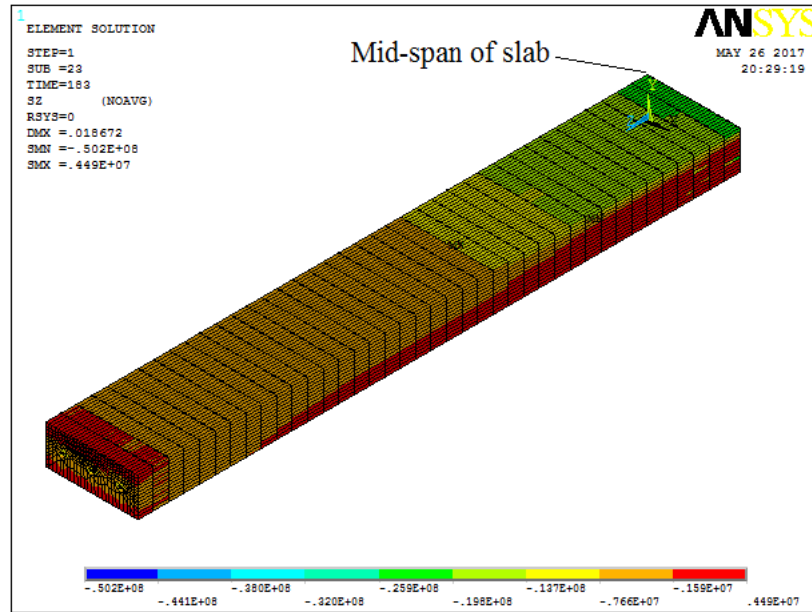


Figure 4.6 Stress distribution of concrete for the UPT slab 1-H35 at failure load.

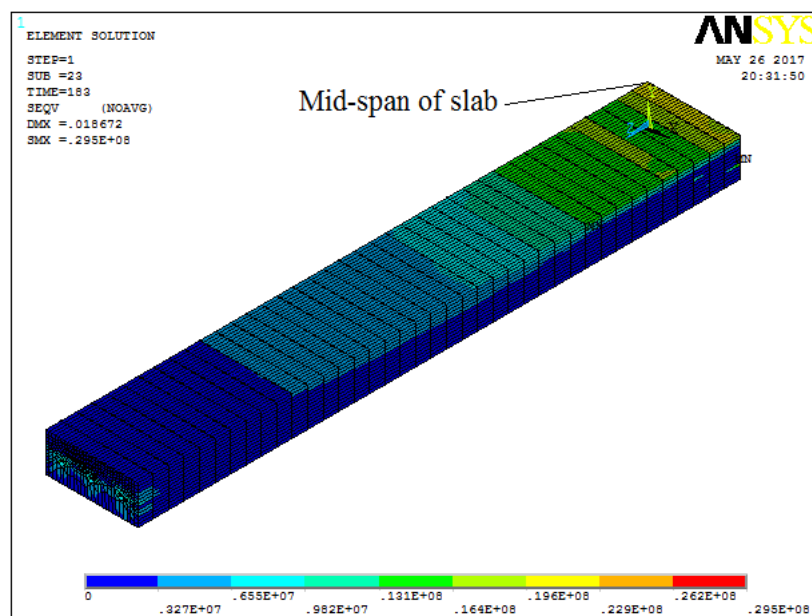


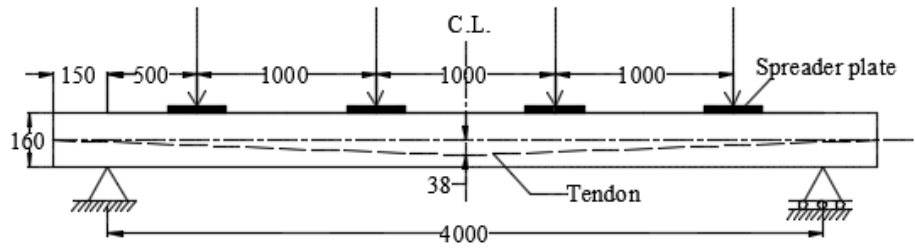
Figure 4.7 Von Mises stress for the UPT slab 1-H35 at failure load.

4.3.2 Analysis of unbonded one-way slab T2

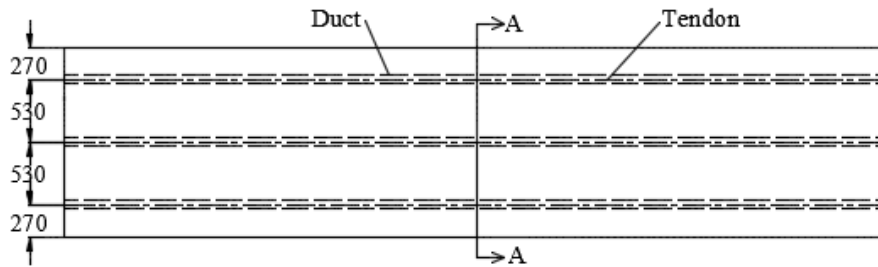
UPT concrete slab (T2) tested by Bailey and Ellobody (2009a) was chosen for numerical analyses verification. The designated compressive strength of the used concrete was 48.2 MPa. The slab was simply supported at both ends and subjected to four concentrated point loads. PT slab was designed according to BS8110-1. The general layout of the UPT one-way concrete is shown in Figure 4.8(a). The tendons were plain mono-strands with each strand made of seven high-strength steel wires. The tendons had a measured tensile strength of 1846 MPa, diameter of 15.7 mm and area of 150 mm². The load was applied gradually in equal increments of 5 kN. Three longitudinal ducts have been used in the slab (one in the middle and the other two were on both sides, at a spacing of 530 mm) as illustrated in Figure 4.8(b). At the middle of the slab height, the duct ends were fixed. The full applied design PT force to the slabs was 195 kN, with the average measured force in the three tendons being 169 kN, equating to 13 % losses (Bailey and Ellobody, 2009a).

The one-way slab specimen was supported by a hinge at one end and on a roller at the other end. Immediately before the test, a designed prestressing force was applied to unbonded tendons and subsequently anchored using a wedge set at both ends of the slab.

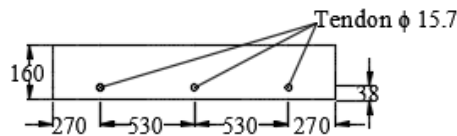
In this study, the UPT concrete slab was modeled using 3D solid elements available within ANSYS (ANSYS 2012). Because of symmetry, only one-quarter of the slab was modeled with 12300 elements, including the interface elements. Load applications and boundary conditions were the same as that utilized in the test. The measured post-tensioning force in the tendons (169 kN) was initially applied in a separate step. The dead load representing the weight of the slab was applied as a static body load.



(a) Loading and general layout of slab



(b) Plan view of slab



(c) Section at maximum moment region (A-A)

Figure 4.8 Details of UPT slab T2 geometry and loading (Bailey and Ellobody, 2009a) (dimensions are in mm).

Bailey and Ellobody (2009a) observed that there was no slip at the interface between the duct and concretes. Hence, only the contact between the tendon and duct was modeled utilizing interface elements (using the contact pair option) available within the ANSYS element library. The interface elements composed of two matching contact faces from the tendon elements and surrounding duct elements. The material properties adopted in the analysis are given in Table 4.2. The FE mesh of the concrete and PT strand for a quarter of the slab T2 are shown in Figure 4.9.

The results observed from the FE analysis in terms of the ultimate loads and load-central deflection curves were compared against the test results (Bailey and Ellobody, 2009a). Figure 4.10 represents the load–deflection curve obtained from FE analysis and experimental results for the slab T2, and good agreement can be noticed from the figure. The failure load and central deflection obtained from the experiment were 178.2 kN and 93 mm respectively, while the failure load and central deflection

obtained from FE analysis were 174.5 kN and 109 mm respectively. The failure load predicted from FE analysis was 2.1 % less than that obtained from the experiment.

Table 4.2 Material properties of concrete, reinforcement and strand for UPT slab T2

	Concrete	Steel plate	Strand
Ultimate compressive strength, f_{cu} (MPa)	48.2	—	—
Ultimate tensile strength, f_r (MPa)	3.0	—	—
Modulus of elasticity, E (MPa)	30000	200000	202000
Poisson's ratio, ν	0.2	0.3	0.3
Yield strength (MPa)	—	400	1846

The initial cracking of the slab in the FE model corresponds to a load of 111 kN that creates stress just beyond the modulus of rupture of the concrete. The first crack can be seen in Figure 4.11. This first crack occurs in the constant moment region, and is a flexural crack.

Figure 4.12 shows the crack and crushing patterns of slab at failure load. The stress distribution in the concrete at failure for the PT slab T2 is shown in Figure 4.13. The mode of failure of concrete crushing in the model, which corresponded to the mode of failure observed experimentally. The Von Mises stress for the unbonded slab T2 at failure load are shown in Figure 4.14.

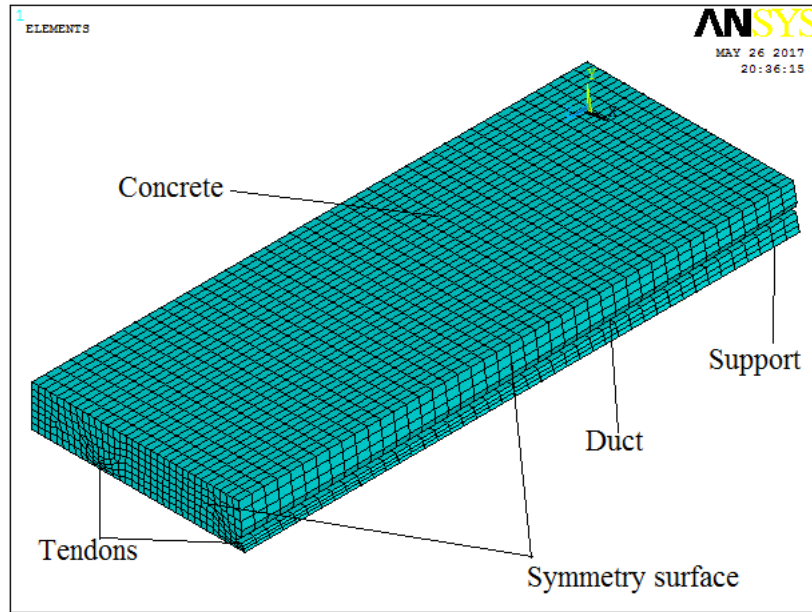


Figure 4.9 FE mesh of concretes and prestressing strand for quarter of the UPT slab

T2.

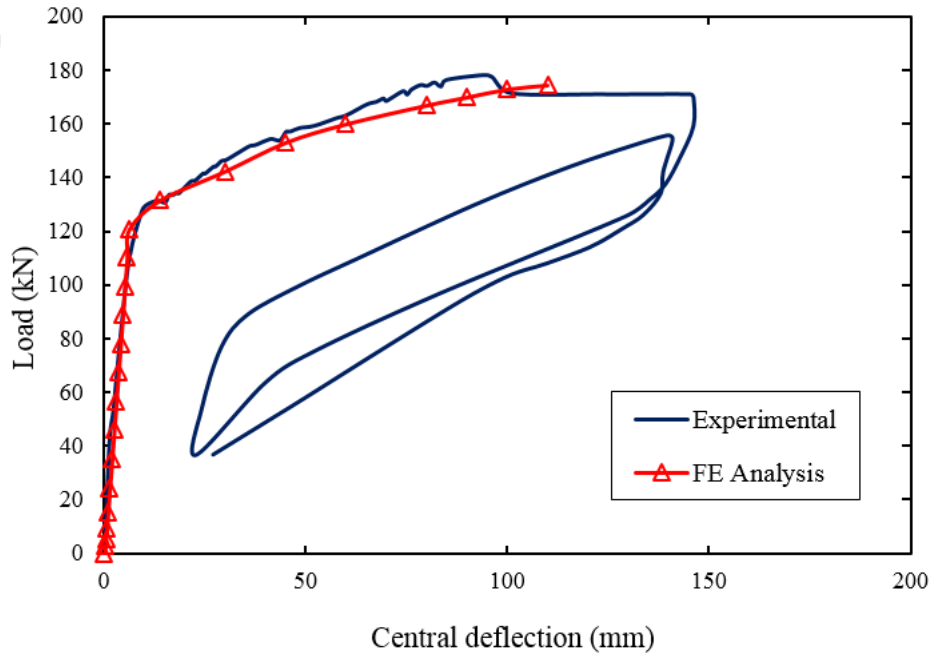


Figure 4.10 Load- deflection curve for the UPT slab T2.

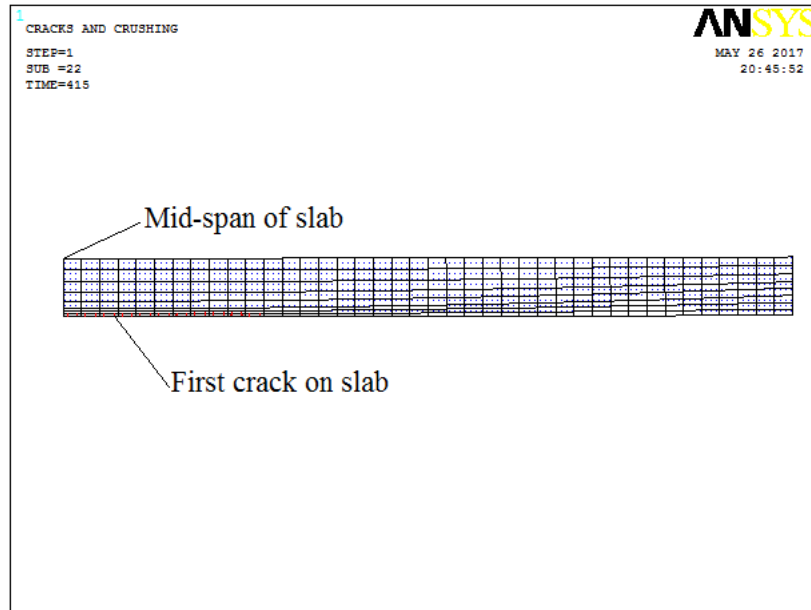


Figure 4.11 First crack for the UPT slab T2.

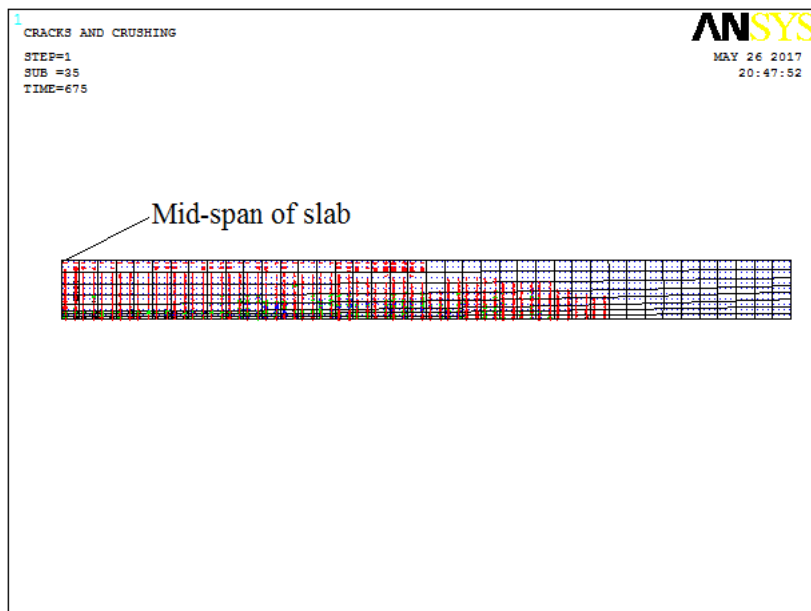


Figure 4.12 Cracks and crushing patterns of the UPT slab T2 at failure load.

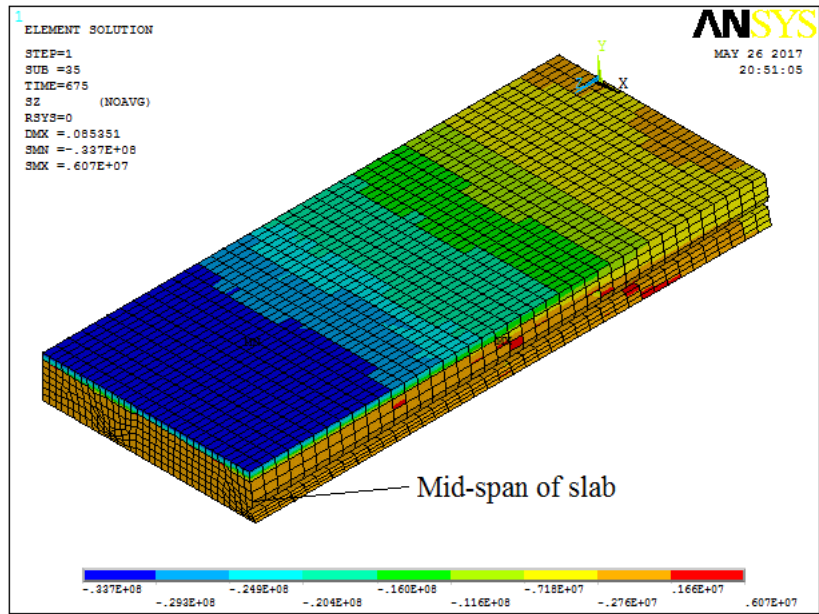


Figure 4.13 Stress distribution of concrete for the UPT slab T2 at failure load.

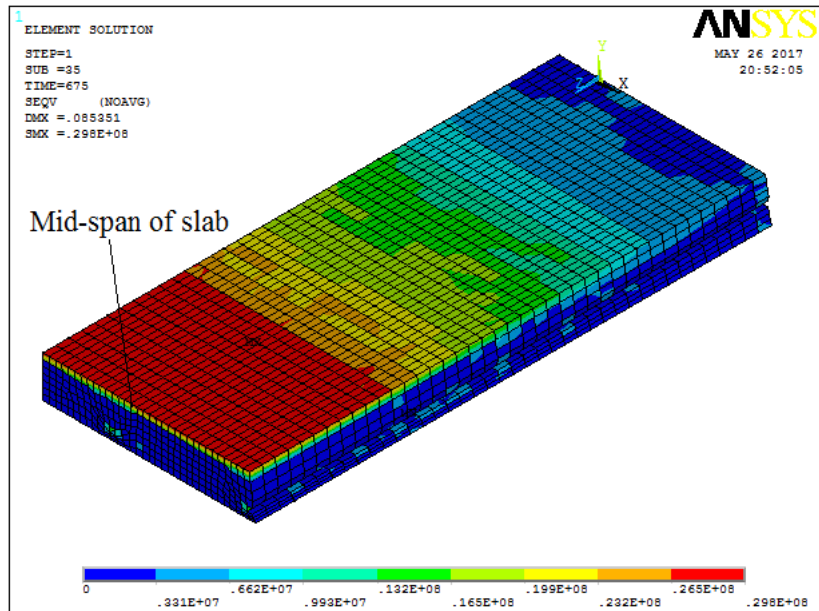


Figure 4.14 Von Mises stress for the UPT slab T2 at failure load.

4.3.3 Analysis of bonded one-way slab TB2

The behaviour of BPT concrete slabs is more complicated by reason the presence of ducts, the bond between concretes and ducts, the bond between ducts and grout, and the bond between grout and tendons.

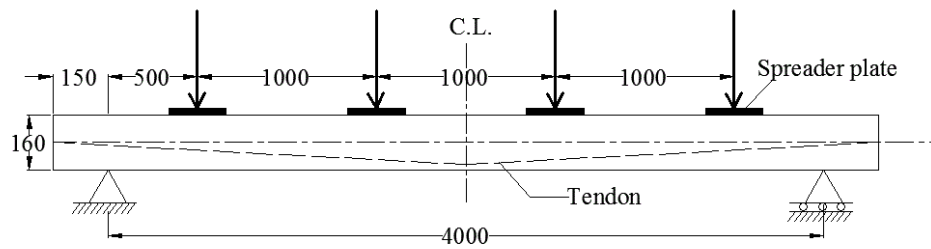
Two stages of analysis are needed for bonded slabs. At the first stage the slab is analyzed as unbonded post tensioned slab under prestress loading and gravity loading only. Next the slab is analyzed as bonded post tensioned slab. The two stages are needed because the grout is added after the prestressing of the strands.

BPT concrete slab (TB2) tested by Bailey and Ellobody (2009b) was chosen for numerical analyses verification. The designated compressive strength of the used concrete was 30.0 MPa. The slab was simply supported at both ends and subjected to four concentrated point loads. PT slab was designed according to BS8110-1. The general layout of the BPT one-way concrete is shown in Figure 4.15 (a). The tendons were plain mono-strands with each strand made of seven high-strength steel wires. The tendons had a measured tensile strength of 1846 MPa, diameter of 15.7 mm and area of 150 mm². The load was applied gradually in equal increments of 5 kN. Three longitudinal ducts have been used in the slab (one in the middle and the other two were on both sides, at a spacing of 530 mm) as illustrated in Figure 4.15 (b). At the middle of the slab height, the duct ends were fixed. The full applied design PT force to the slabs was 195 kN, with the average measured force in the three tendons being 169 kN, equating to 13 % losses (Bailey and Ellobody, 2009b).

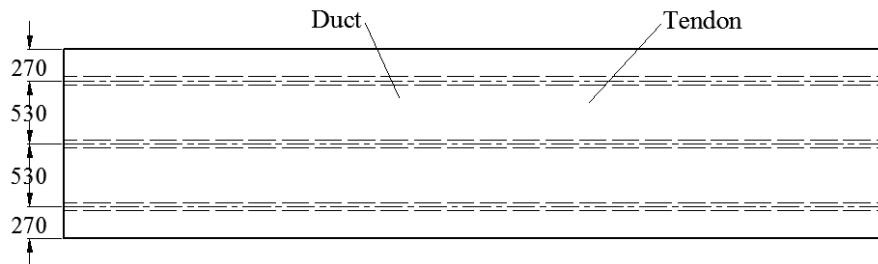
The one-way slab specimen was supported by a hinge at one end and on a roller at the other end. Immediately before the test, a designed prestressing force was applied to unbonded tendons and subsequently anchored using a wedge set at both ends of the slab.

In this study, the BPT concrete slab was modeled using 3D solid elements available within ANSYS (ANSYS 2012). Because of symmetry, only one-quarter of the slab was modeled with 11100 elements, including the interface elements. Load applications and boundary conditions were the same as that utilized in the test. The measured post-tensioning force in the tendons (169 kN) was initially applied in a

separate step. The dead load representing the weight of the slab was applied as a static body load.



(a) Loading and general layout of slab



(b) Plan view of slab

Figure 4.15 Details of BPT slab TB2 geometry and loading (Bailey and Ellobody, 2009b) (dimensions are in mm).

Bailey and Ellobody (2009b) observed that there was no slip at the interface between the duct and concrete. Hence, only the contact between the tendon and duct was modeled utilizing interface elements (using the contact pair option) available within the ANSYS element library. The interface elements composed of two matching contact faces from the tendon elements and surrounding duct elements. The FE mesh of the concrete and PT strand for a quarter of the slab TB2 are shown in Figure 4.16. The material properties adopted in the analysis are given in Table 4.3.

The results observed from the FE analysis in terms of the ultimate loads and load-central deflection curves were compared against the test results (Bailey and Ellobody, 2009b). Figure 4.17 represents the load-deflection curve obtained from FE analysis and experimental results for the slab TB2, and good agreement can be noticed from the figure. The failure load and central deflection obtained from the experiment were 187.9 kN and 107 mm respectively, while the failure load and central deflection obtained from FE analysis were 186 kN and 117 mm respectively.

The failure load predicted from FE analysis was 1.06 % less than that obtained from the experiment.

The deformed shape at failure for slab TB2, obtained from the model, is shown in Figure 4.18. The stress distribution in the concrete at failure for the PT slab TB2 is shown in Figure 4.19. The mode of failure of concrete crushing in the model, which corresponded to the mode of failure observed experimentally.

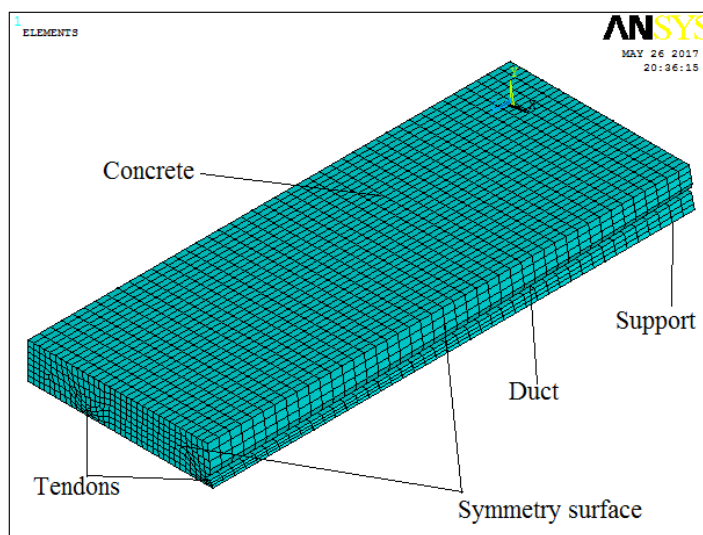


Figure 4.16 FE mesh of the concrete and the prestress strand for quarter of the BPT slab TB2.

Table 4.3 Material properties of concrete, reinforcement and strand for PT slab TB2.

	Concrete	Steel plate	Strand
Ultimate compressive strength (MPa) (f_c')	30.3	—	—
Ultimate tensile strength (MPa) (f_t)	3.0	—	—
Modulus of elasticity (MPa)	30000	200000	202000
Poisson's ratio (ν)	0.2	0.3	0.3
Yield strength (MPa)	—	400	1846

The initial cracking of the slab in the FE model corresponds to a load of 105 kN that creates stress just beyond the modulus of rupture of the concrete. The first crack can be seen in Figure 4.20. This first crack occurs in the constant moment region, and is a flexural crack. Figure 4.21 shows the crack pattern of slab at failure load. The Von Mises stress for the bonded slab TB2 at failure load are shown in Figure 4.22.

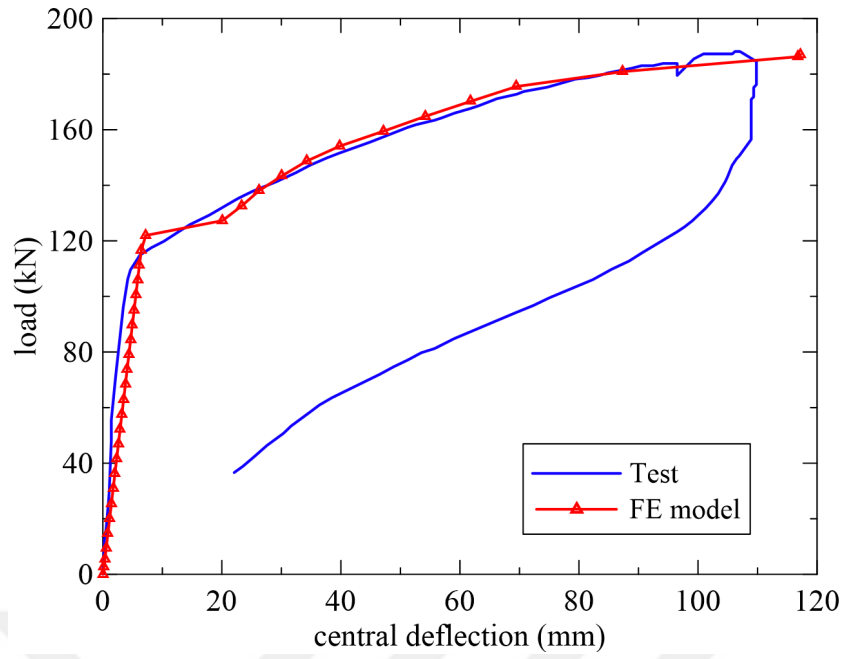


Figure 4.17 Load- deflection curve for the BPT slab TB2.

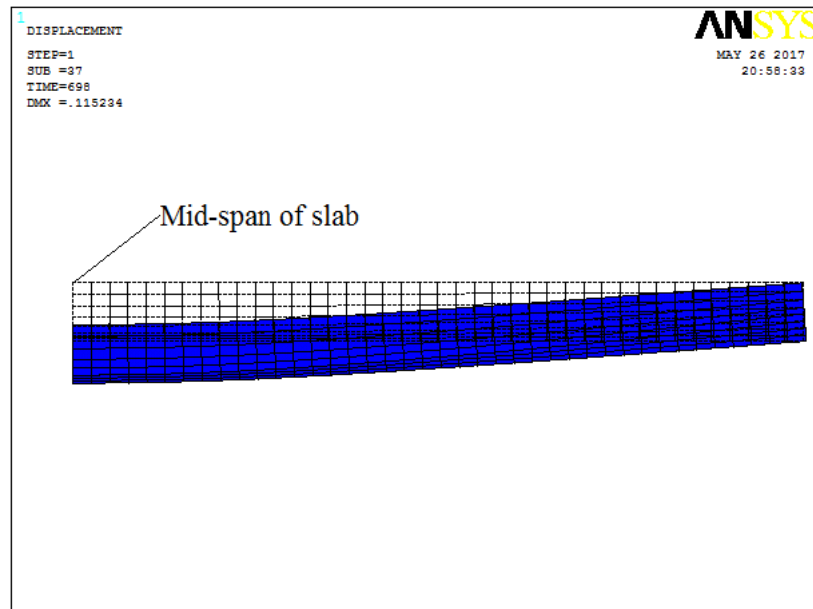


Figure 4.18 Deformed shape of the BPT slab TB2.

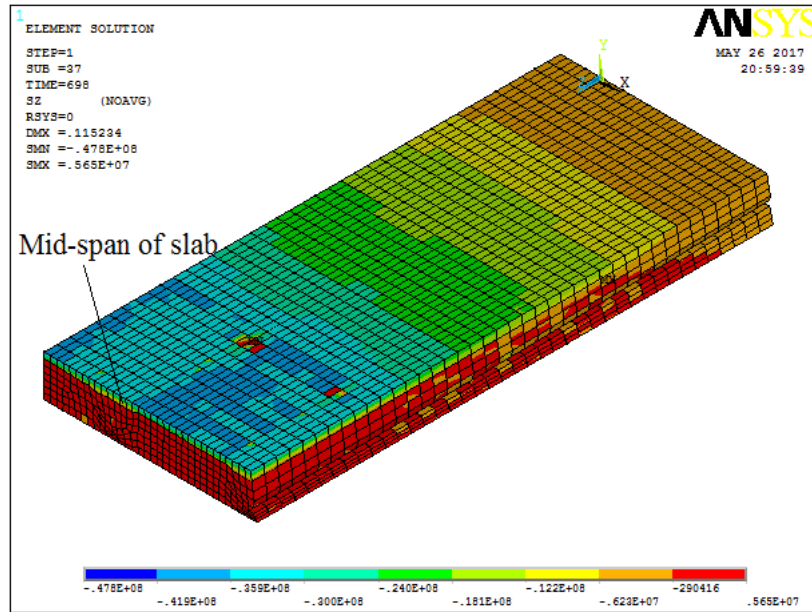


Figure 4.19 Stress distribution of concrete for the BPT slab TB2 at failure load.

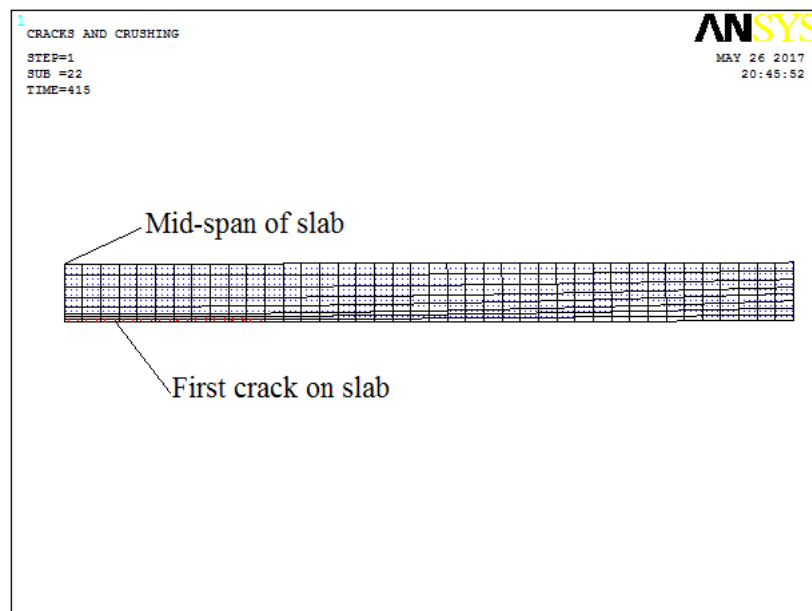


Figure 4.20 First crack for the BPT slab TB2.

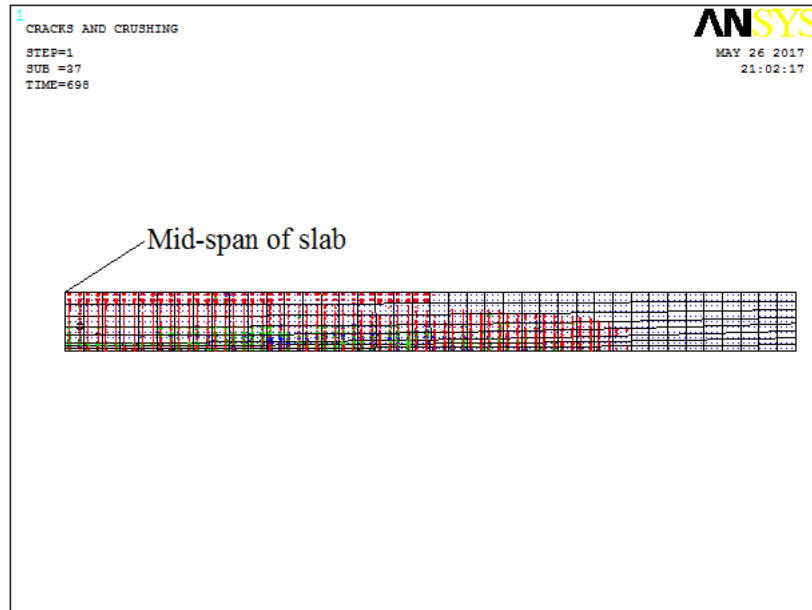


Figure 4.21 Cracks and crushing patterns of the BPT slab TB2 at failure load.

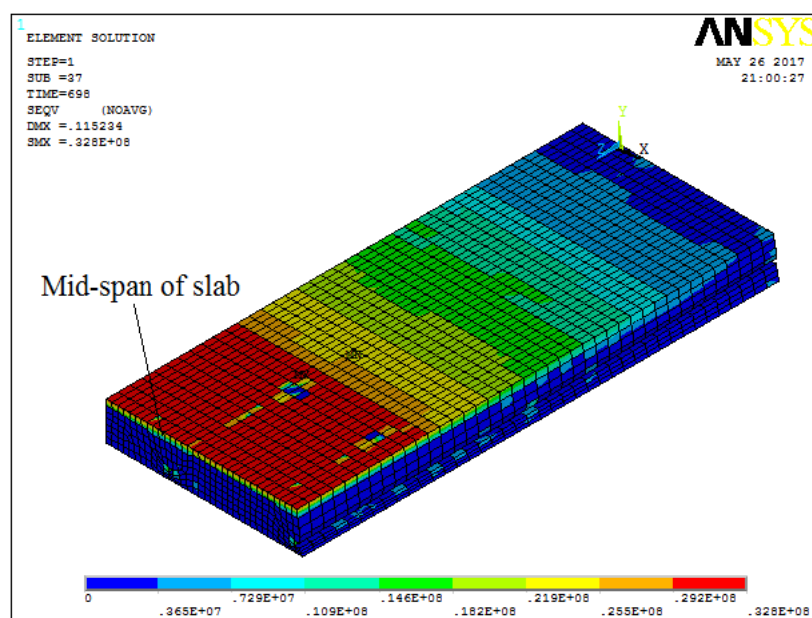


Figure 4.22 Von-Mises stress for the BPT slab TB2 at failure load.

CHAPTER 5

PARAMETRIC STUDIES

5.1 General

The verified FE model was used to investigate the effect of several selected parameters on the overall behaviour of PT one-way concrete slabs. These parameters include the effect of tendon bonding, the effect of thermal loading and the effect of tendon profile. The geometry of proposed slab for the parametric study is shown in Figure 5.1. The loading and boundary conditions considered for the proposed study for proposed slab are shown in Figure 5.1. The different parameters considered in the parametric study are summarized in Table 5.1. Group G1 included two slabs that used to study the effect of bonding. Groups G2 and G3 were subjected to thermal loading. To study the effect of tendon profile, three different tendon profiles are included in groups G4 and G5. The material properties adopted in the proposed study are given in Table 5.2.

5.2 Effect of Bonding

Group G1 included two slabs S1-S2 that used to study the effect of bonding. The load-deflection responses for both bonded slab S1 and unbonded slab S2, from the FE analysis, are plotted in Figure 5.2. It was observed that the ultimate load capacity for the slab with bonded tendon is 9.4 % higher than the slab with unbonded tendon. The higher ultimate capacity for bonded slab is due to additive stiffness comes from bonding with concrete. It is clear from the FE analysis that the response of the slabs is linear until the first crack has formed at approximately 62 kN. The ultimate central deflection of the bonded and unbonded slabs were 52.2 mm and 41.4 mm respectively. From Figures 5.2, it can be seen that the deflection of the unbonded slab is greater than the deflection of bonded slab at the same load after the cracking, which means that the stiffness of bonded slab is greater than the stiffness of the unbonded slab after cracking.

Figure 5.3 shows that the maximum tensile stress in concrete at the bottom fiber of the center of the bonded slab is greater than that of the unbonded slab. At higher loads, and due to the presence of the crack, the stress becomes zero or near the zero.

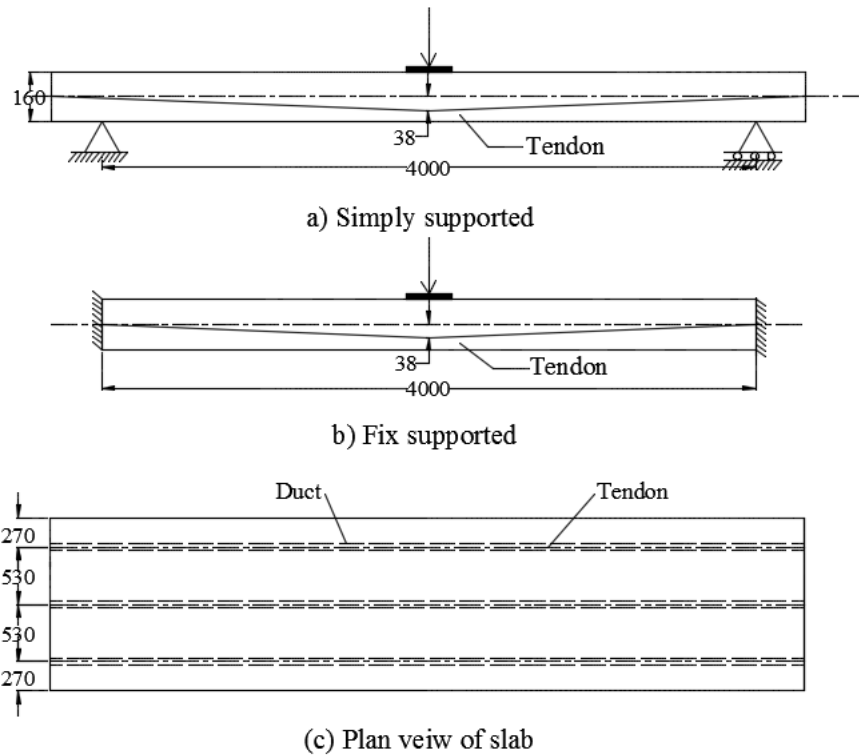


Figure 5.1 Loading and boundary conditions of the proposed slab for the parametric study.

The forces in post tensioned tendons for both bonded and unbonded tendons are shown in Figures 5.4-5.5. From the figures it can be found that the force in the bonded tendons is higher than the force in unbonded tendons in the center of the slab, while the opposite stands at the support. Note that the force in the unbonded tendon does not change along the slab.

Table 5.1 Parameters considered in the parametric study.

Group	Slab	Type of slab	Type of supported	Tendon profile	Thermal loading	Longitudinal expansion
G1	S1	Bonded	Simply	Parabolic	No thermal load	—
	S2	Unbonded				
G2	S3	Bonded	Fixed	Parabolic	Top hotter	Restraint
	S4				Bottom hotter	
	S5				Uniform	
	S6		Simply		Top hotter	Free
	S7				Bottom hotter	
	S8				Uniform	
G3	S9	Unbonded	Fixed	Parabolic	Top hotter	Restraint
	S10				Bottom hotter	
	S11				Uniform	
	S12		Simply		Top hotter	Free
	S13				Bottom hotter	
	S14				Uniform	
G4	S15	Bonded	Simply	Straight Bottom	No thermal load	—
	S16		Fixed			
	S17		Simply	Parabolic		
	S18		Fixed			
	S19		Simply	Straight Middle		
	S20		Fixed			
G5	S21	Unbonded	Simply	Straight Bottom	No thermal load	—
	S22		Fixed			
	S23		Simply	Parabolic		
	S24		Fixed			
	S25		Simply	Straight Middle		
	S26		Fixed			

Table 5.2 Material properties of concrete, reinforcement and strand for proposed slab.

	Concrete	Steel plate	Strand
Ultimate compressive strength (MPa) (f'_c)	30.3	—	—
Ultimate tensile strength (MPa) (f_i)	3.0	—	—
Modulus of elasticity (MPa)	30000	200000	202000
Poisson's ratio (ν)	0.2	0.3	0.3
Yield strength (MPa)	—	400	1846

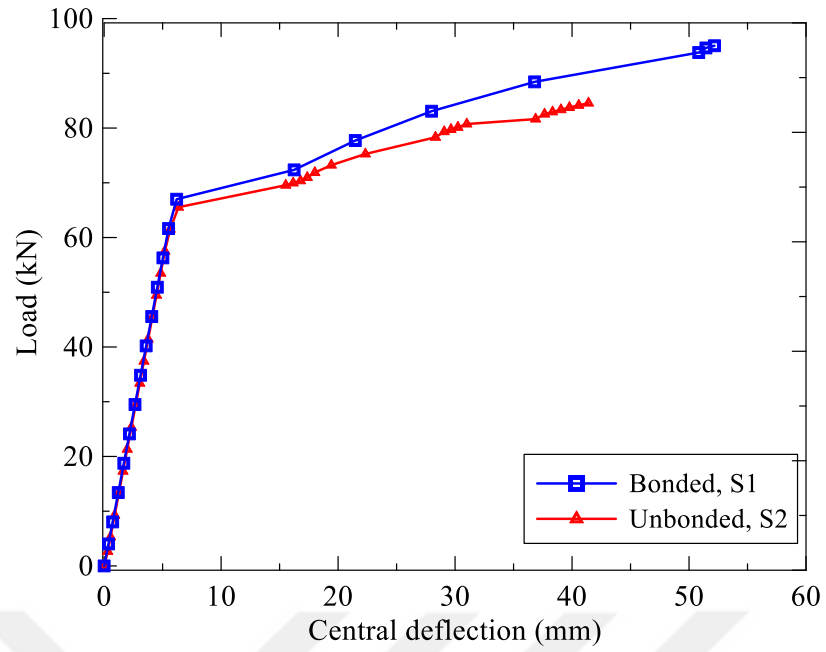


Figure 5.2 Load-deflection curves for the bonded and unbonded slabs.

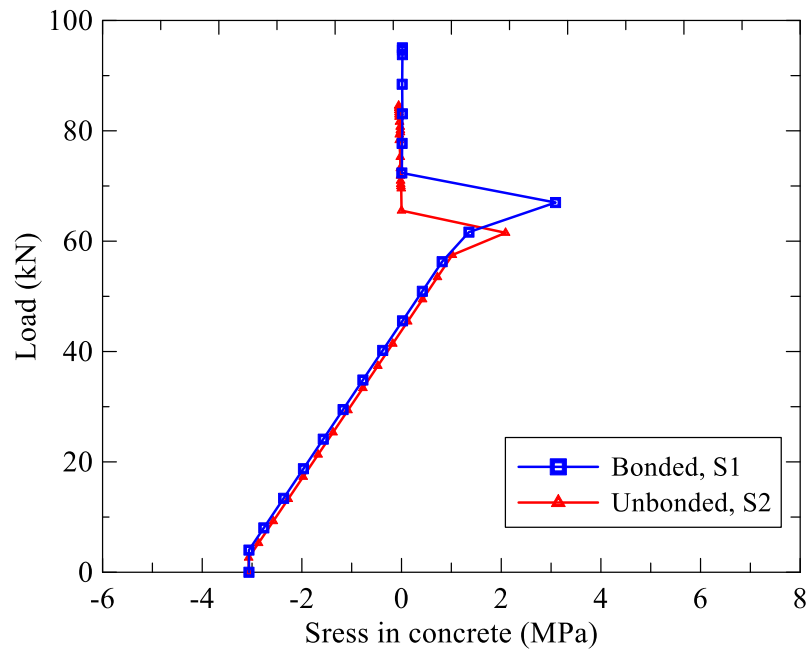


Figure 5.3 Load-stress curve of concrete of the bottom fiber at center of the slab.

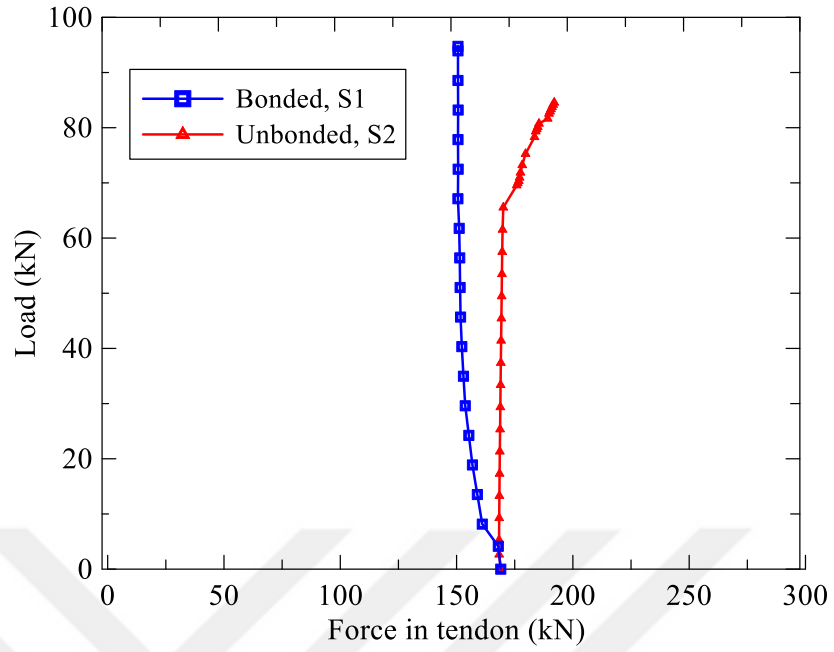


Figure 5.4 Force in tendon at support for the bonded and unbonded slabs.

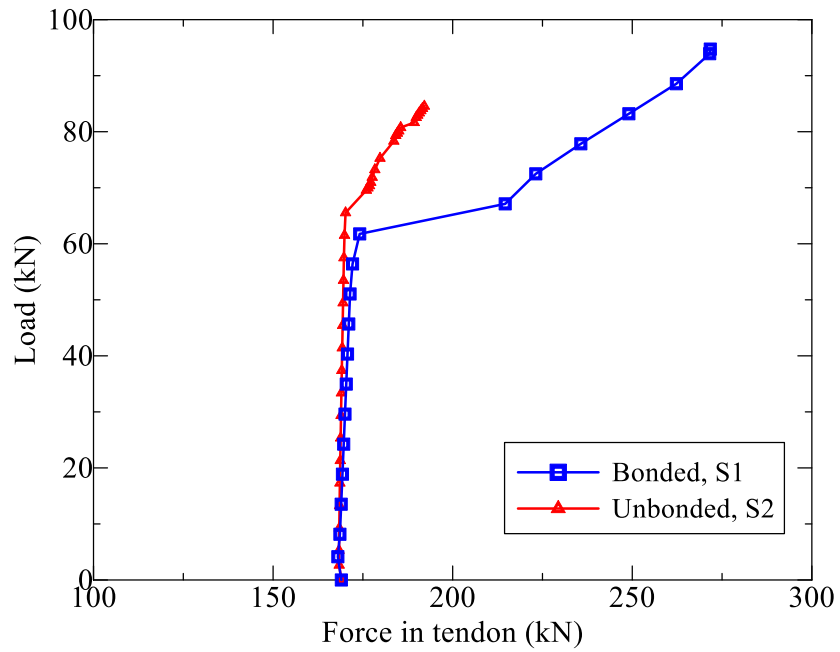


Figure 5.5 Force in tendon at center of the slab for the bonded and unbonded slabs.

5.3 Effect of Thermal Loading

The effect of the thermal loading was investigated by modelling twelve slabs S3–S14 as shown in Table 5.1. The groups of slabs are denoted as G2 and G3. Three types of thermal load are applied. The three types of thermal load are top surface hotter, bottom surface hotter and uniform temperature. In the top surface hotter, a temperature of 65°C is applied in the top of the slab and 15°C is applied on the bottom of the slab, while the bottom surface hotter case is the inverse. In the uniform temperature, a temperature of 65°C is applied uniformly to slab as shown in Figure 5.6. The concrete initial temperature is set to 15°C. The temperatures 65°C and 15°C are near the actual maximum and minimum environmental temperatures that the slabs are possibly exposed to.

The slab is analyzed under the effect of change in temperature together with the prestress, self-weight and live loading. The slabs are loaded under all loading to the failure. The effect of thermal loading was also applied on the tendon. The thermal load was applied as an initial strain to tendon elements. The thermal strain decreases the total prestressing force of tendons if change in temperature is positive and the inverse is right.

The plots of load versus central deflection are displayed in Figures 5.7-5.8. For the restrained bonded slab, the failure loads were 261 kN, 227 kN and 187 kN for uniform, top surface hotter and bottom surface hotter cases respectively. On the other hand, for restrained unbonded slab, the failure loads were 284 kN, 216 kN and 186 kN for top surface hotter, uniform and bottom surface hotter cases respectively. From the figure it can be seen that the failure load capacity for restrained post tensioned slab with bottom surface hotter load is the lowest due to the effect of thermal strain. The thermal strain coming from bottom surface hotter load causes tensile stress at top and compressive stress at bottom. From Figures 5.7-5.8, it is also obvious that the failure load capacity of unbonded slab is greater than the failure load capacity of bonded slab under the same top surface hotter load. The higher failure load capacity is due to the higher compressive stress in the bottom fiber for unbonded slab as shown in Table 5.3. From this table, it can be seen that the compressive stresses in the bottom fiber were 3.1 MPa and 10.5 MPa for bonded and unbonded restrained slabs, respectively.

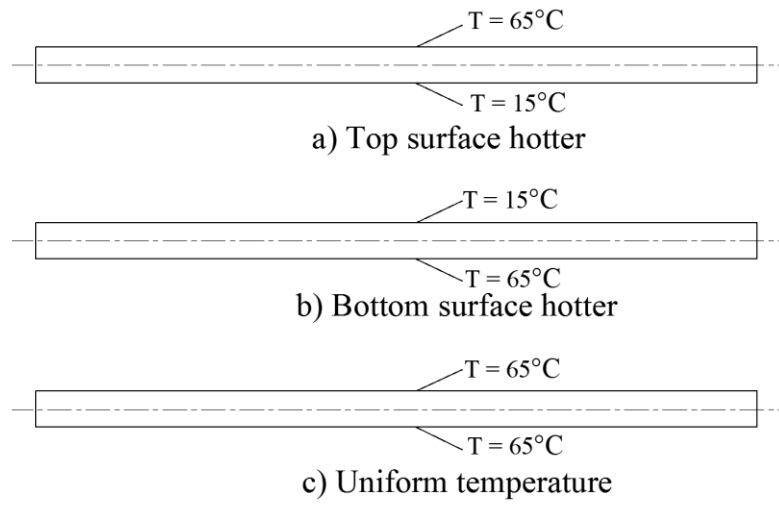


Figure 5.6 Thermal loading applied to proposed slabs.

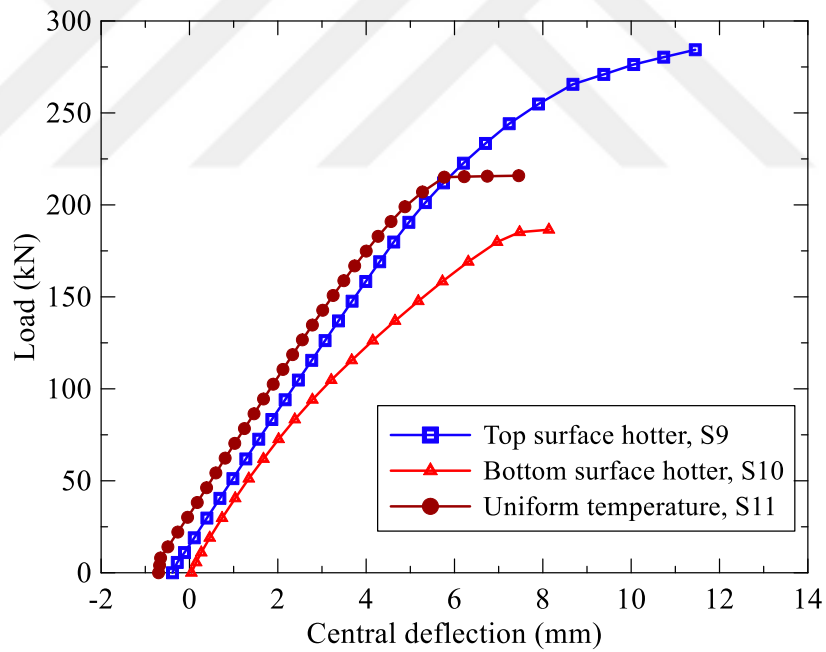


Figure 5.7 Effect of thermal loading on central deflection for restrained unbonded slabs

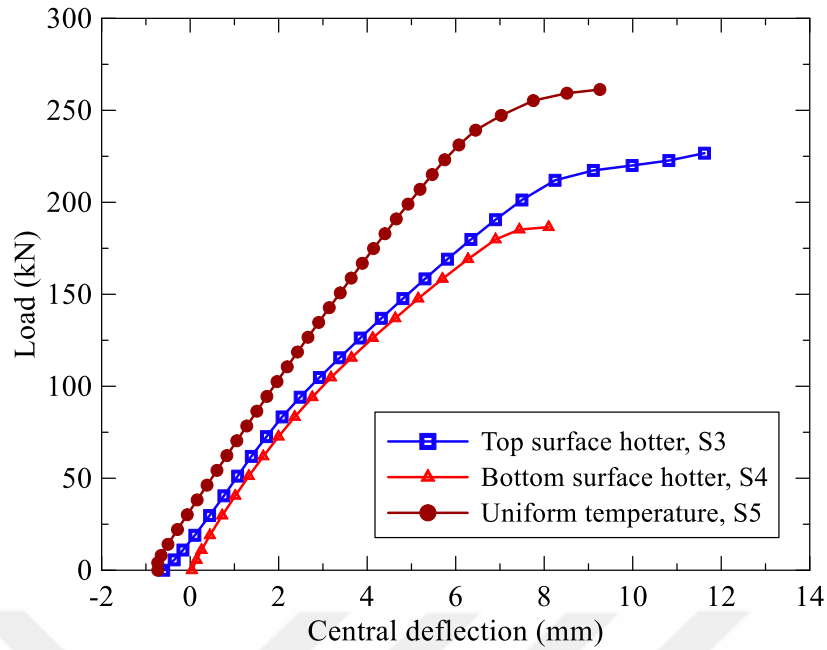


Figure 5.8 Effect of thermal loading on central deflection for restrained bonded slabs.

Table 5.3 Stresses in the top and bottom fiber at center of proposed slab.

		Stress in the top fiber (MPa)				Stress in the bottom fiber (MPa)			
		Bonded slab		Unbonded slab		Bonded slab		Unbonded slab	
		Restrained	Free	Restrained	Free	Restrained	Free	Restrained	Free
Due to prestress and self weight only		0.24	-1.1	0.17	-1.2	-3.5	-3.1	-3.4	-3.1
Due to prestress, self weight and temperature	Top surface hotter	-20.4	-1.8	-20.1	-1.9	-3.1	-4.0	-10.5	-3.5
	Bottom surface hotter	0.84	-0.87	0.84	-0.9	-16.1	-2.8	-16.0	-2.7
	Uniform temperature	-19.3	-0.17	-18.4	0.08	-19.4	-4.3	-16.8	-4.5

Figures 5.9-5.10 show the load-stress curves of concrete at the bottom fiber of the mid-span for the restrained slabs. The stress increases proportionally with loading until the crack or the crash occurs. After that, the stress decreases rapidly downward to zero value and continues with an approximately constant value near the zero. Zero values mean that the concrete is cracked at this fiber or at least the element beside this element is cracked. The figure shows that the stresses start with compressive stress due the effect of the positive temperature strain. The compressive stress occurs only in constrained slab.

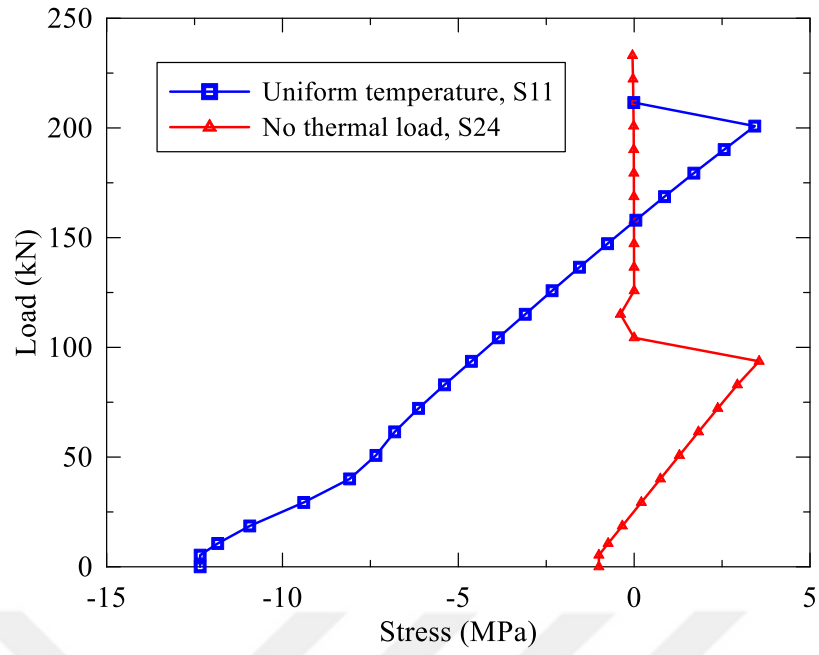


Figure 5.9 Effect of thermal loading on concrete stress at the bottom fiber at the center of restrained unbonded slab.

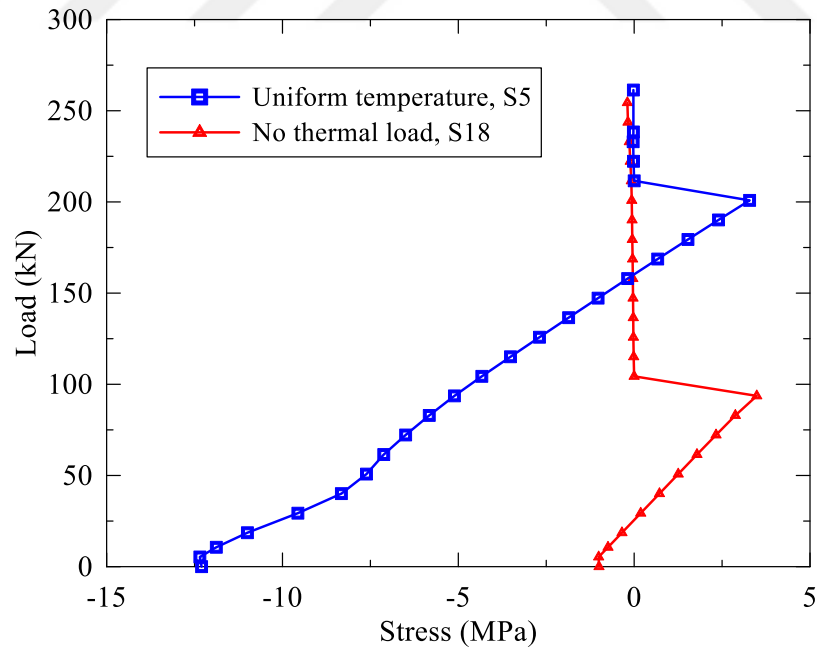


Figure 5.10 Effect of thermal loading on concrete stress at the bottom fiber at the center of restrained bonded slab.

From Figures 5.11-5.12, it can be observed that losses in prestress force in restrained slab are the smallest when the slab is bonded and subjected to top surface hotter load, while the losses are the highest when the slab is bonded and subjected to uniform temperature load. The losses in tendon force occur due to the increase in compressive stress at the bottom fiber and especially in restrained slab. From Table 5.3, it can be noted that the lowest compressive stress at the bottom fiber is 2.7 MPa for unbonded free slab with bottom surface hotter loading, while the highest compressive stress at the bottom fiber is 19.4 MPa for bonded restrained slab with uniform temperature loading.

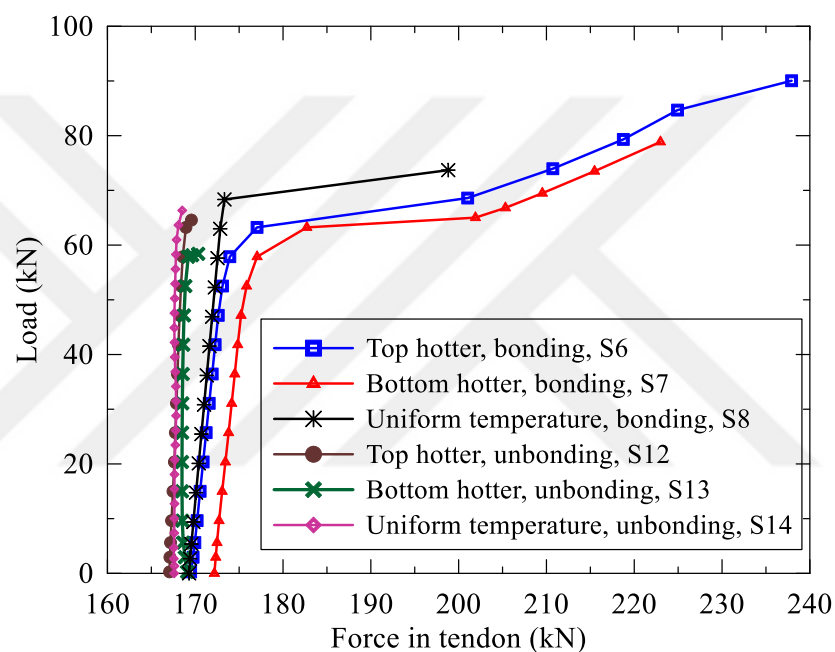


Figure 5.11 Effect of thermal loading on tendon force at the center of the free end slab.

5.4 Effect of Tendon Profile

The effect of the tendons profile was investigated by modelling twelve slabs S15-S26 as shown in Table 5.1. The groups of slabs are denoted as G4 and G5 in Table 5.1. Three types of tendons profiles are considered. These are the parabolic, the straight at middle and the straight at bottom profiles as shown in Figure 5.13. The central deflection for the three profiles are plotted in Figures 5.14-5.17. It is noted the straight bottom profile has the highest load capacity for the simply supported post tensioned slab. For the fixed post tensioned slab, the parabolic profile resulted in the maximum load capacity. Comparison between the simply supported slab and the

fixed slab shows that the slab with fix ends has the largest percentage of failure load to first cracking load (Figures 5.14-5.17).

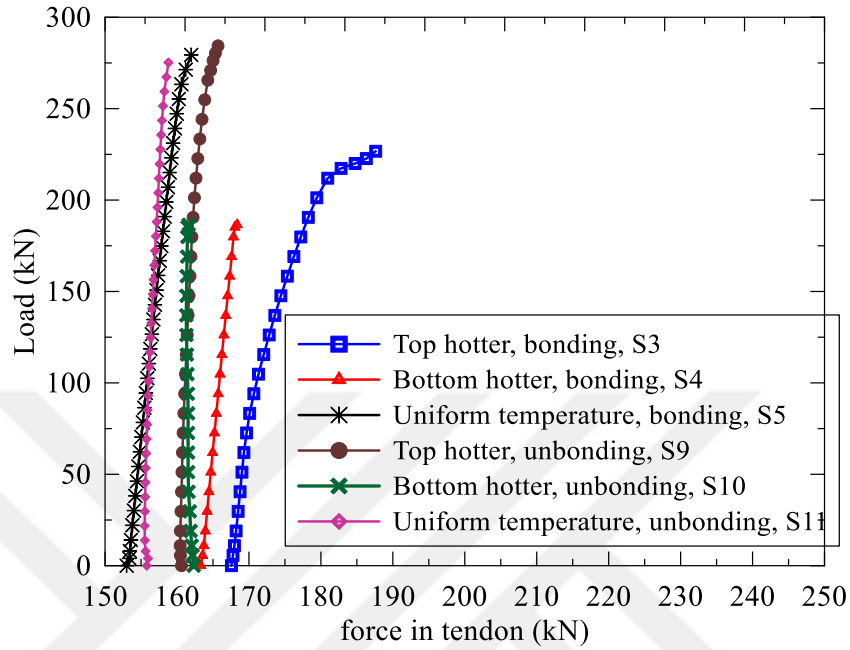


Figure 5.12 Effect of thermal loading on tendon force at the center of the restrained slab.

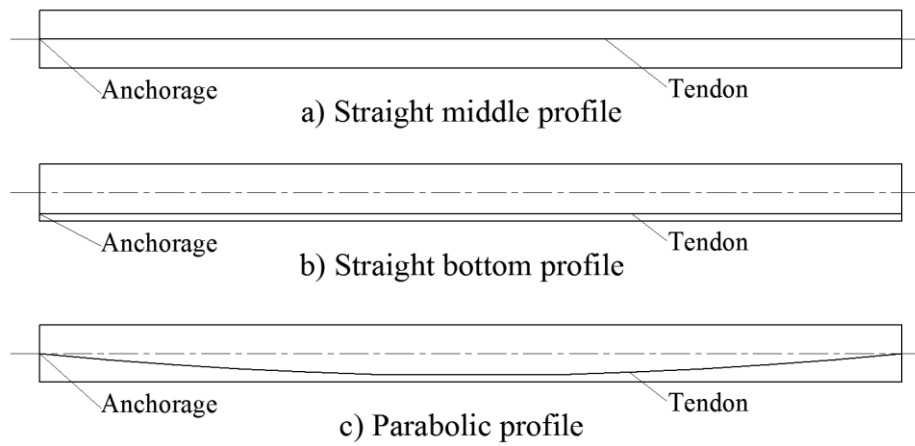


Figure 5.13 Proposed tendons profiles.

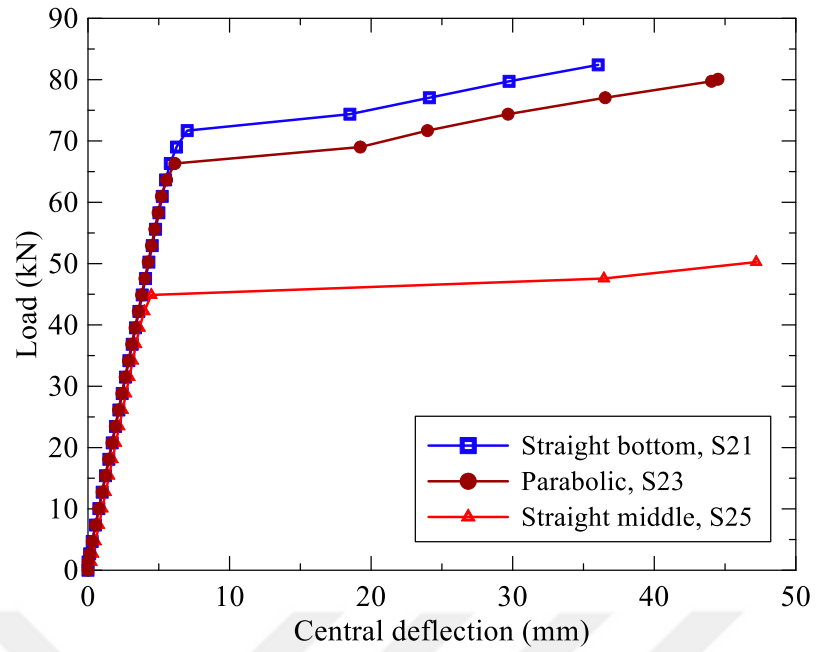


Figure 5.14 Effect of tendon profile on central deflection for simply supported unbonded slab.

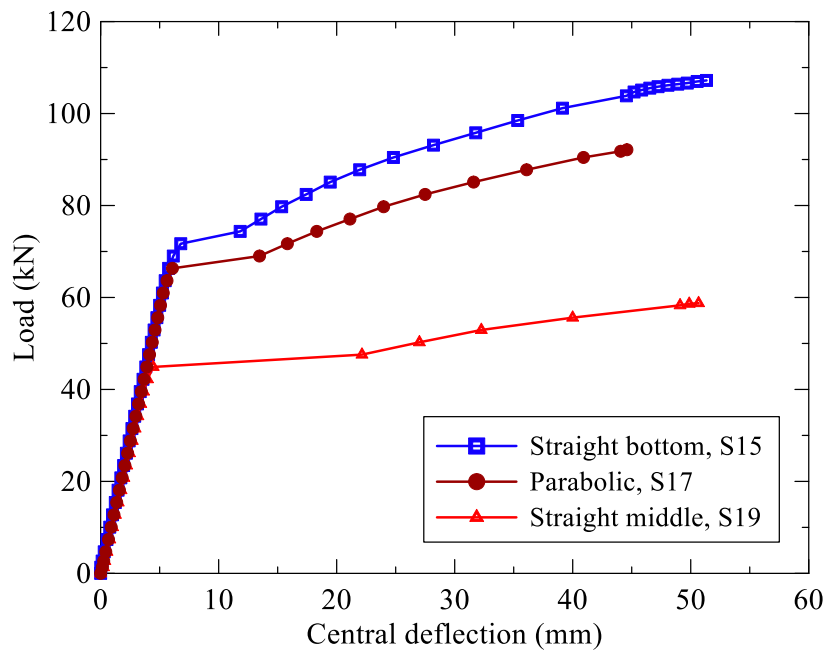


Figure 5.15 Effect of tendon profile on central deflection for simply supported bonded slab.

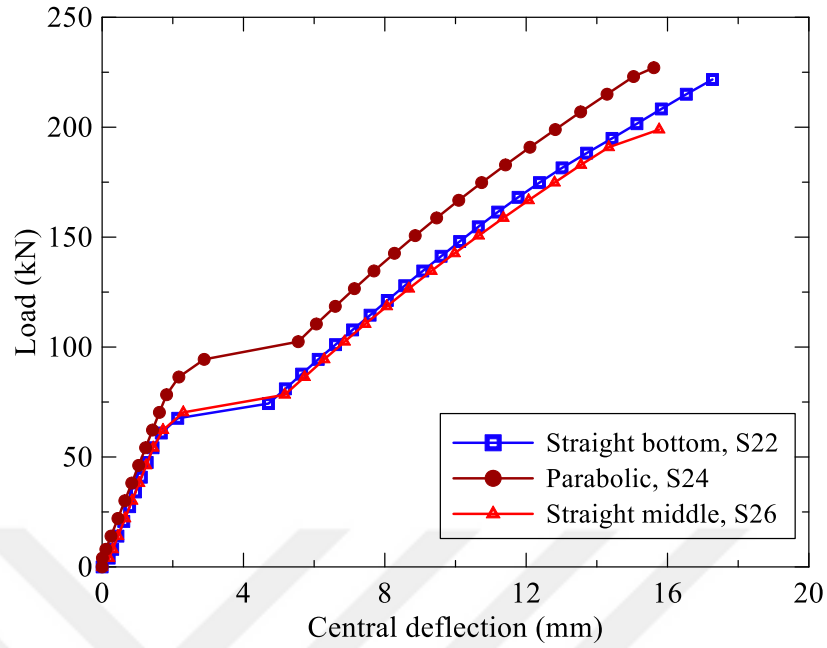


Figure 5.16 Effect of tendon profile on central deflection for fix supported unbonded slab.

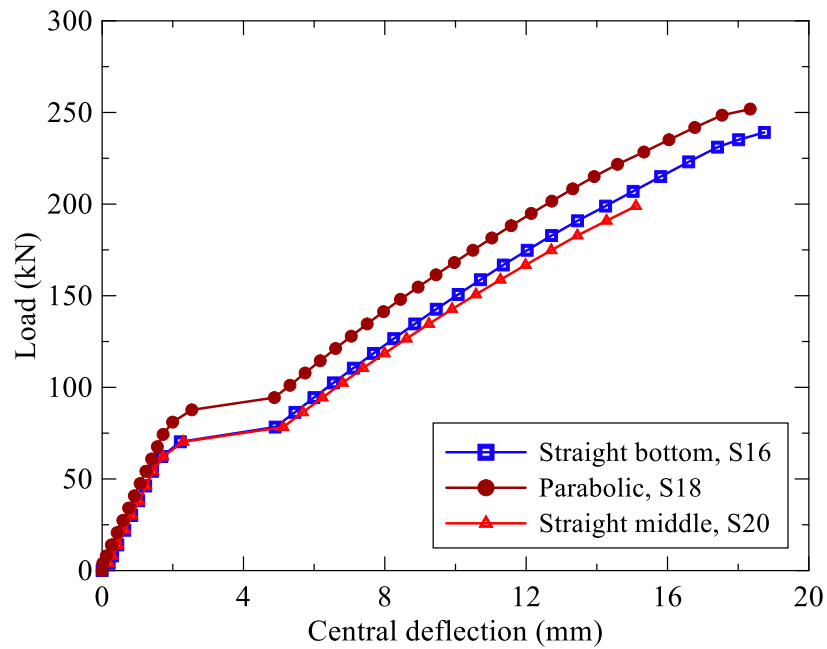


Figure 5.17 Effect of tendon profile on central deflection for fix supported bonded slab.

5.5 Summary of Parametric Study

The different parameters considered in the parametric study and their results are summarized in Table 5.4. The values presented in this table are the maximum values from the result analysis of all slabs. For the groups G2 and G3, it can be noted that the failure loads for the restrained slabs are greater than for the free end slabs. The higher ultimate capacity for restrained slabs are due to fixed support. In addition, thermal expansion in restrained slabs generates compressive stresses in the longitudinal direction that, at a result, decrease tensile stresses in the slab. Tensile stresses play a major role in the ultimate capacity of the concrete structures.

In addition, it can be noted that for groups G2 and G3 the unbonded restrained slab with top hotter (S9) has the highest failure load (284.3 kN), while the highest deflection (28.8 mm) occurs in bonded free slab with bottom hotter (S7). For groups G4 and G5, it was found that the bonded simply supported slab with a straight bottom profile (S15) has the highest deflection (51.3 mm). The highest tendon force (272.5 kN) occurs in center of simply supported bonded slab (S1).

5.5.1 Stress distribution in the concrete

The stress distribution in the concrete at ultimate state for the proposed PT slabs are shown in Figures 5.18-5.29. From this figures, it can be noted the compressive stress at mid-span for the thermal loading slabs (S7 and S13) are smaller than for the no-thermal loading slabs. The thermal strain coming from thermal load causes tensile stress at top and compressive stress at bottom that, at a result, decrease the top stresses in the slab. From the Figures 5.18-5.19, it is clear to observe the effect of bonding in the distribution of stress.

Table 5.4 Summary of the parametric study results.

Group	Slab	Type of slab	Type of supported	Tendon profile	Thermal loading	Longitudinal expansion	Max. deflection (mm)	Failure load (kN)	Max. force in tendon (kN)
G1	S1	Bonded	Simply	Parabolic	No thermal load	—	52.2	93	272.5
	S2	Unbonded					41.4	85.5	192.1
G2	S3	Bonded	Fixed	Parabolic	Top hotter	Restraint	11.6	227	187.6
	S4				Bottom hotter		8.1	187	168.4
	S5				Uniform		9.3	261.3	161.9
	S6		Simply		Top hotter	Free	28.0	91	237.9
	S7				Bottom hotter		28.8	78.9	222.9
	S8				Uniform		7	73.7	198.8
G3	S9	Unbonded	Fixed	Parabolic	Top hotter	Restraint	11.5	284.3	165.7
	S10				Bottom hotter		8.1	186.5	161.6
	S11				Uniform		7.5	216	158.8
	S12		Simply		Top hotter	Free	1.1	64	169.5
	S13				Bottom hotter		13.3	58.4	170.3
	S14				Uniform		4.5	66.3	168.5
G4	S15	Bonded	Simply	Straight	No thermal load	—	51.3	107.2	269.1
	S16		Fixed				Bottom	18.7	239.1
	S17		Simply	Parabolic			44.6	92.1	245.8
	S18		Fixed				18.3	251.8	198.2
	S19		Simply	Straight			50.7	58.8	242.8
	S20		Fixed	Middle			15.1	199	182.2
G5	S21	Unbonded	Simply	Straight	No thermal load	—	36	82.4	195.4
	S22		Fixed				Bottom	17.3	221.7
	S23		Simply	Parabolic			44.5	80.1	199.1
	S24		Fixed				15.6	227	178.2
	S25		Simply	Straight			47.2	50.3	189
	S26		Fixed	Middle			15.8	199	174.2

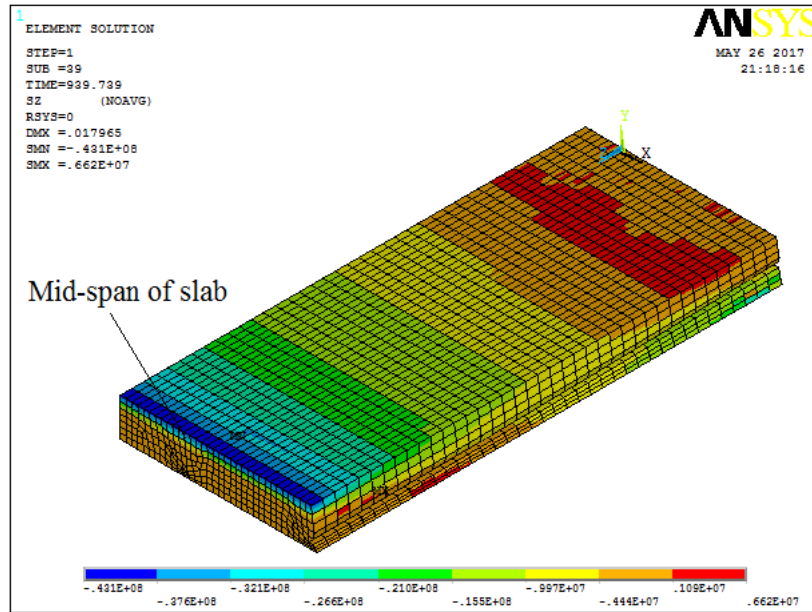


Figure 5.18 Stress distribution in the concrete at ultimate state for the slab S1.

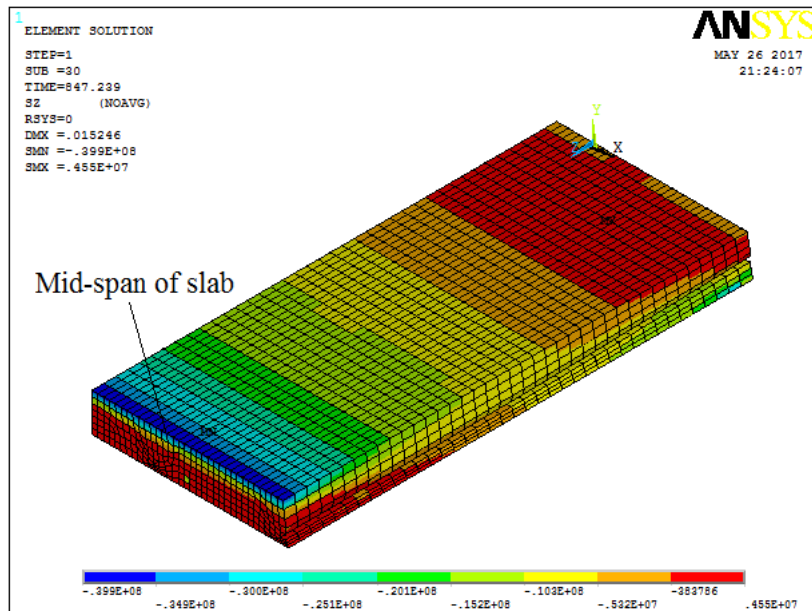


Figure 5.19 Stress distribution in the concrete for the slab S2.

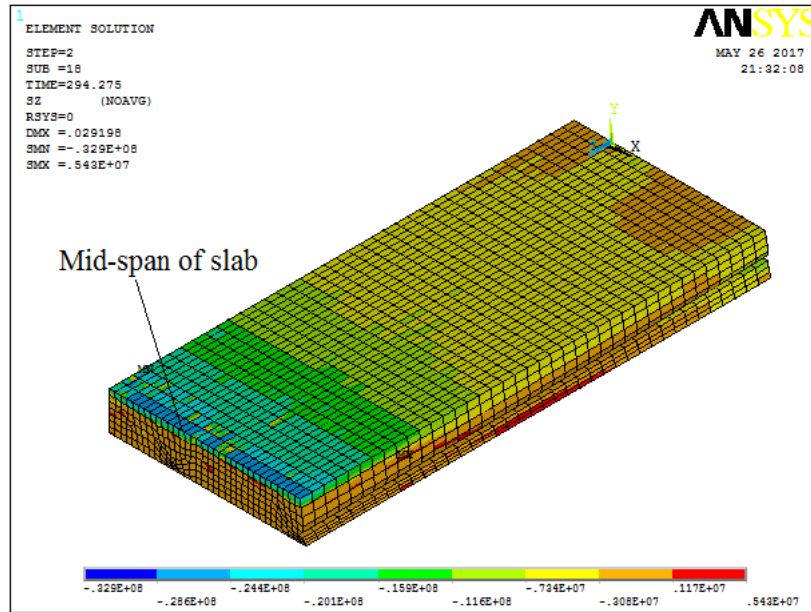


Figure 5.20 Stress distribution in the concrete for the slab S6.

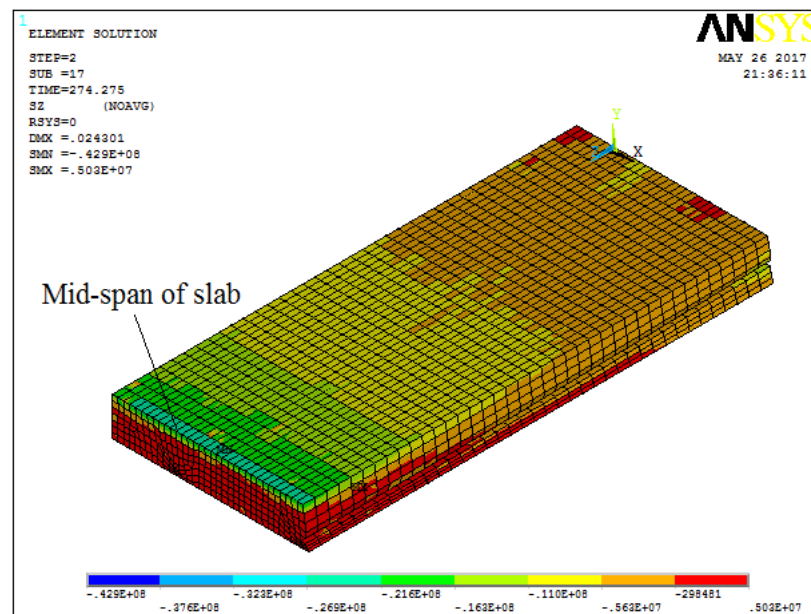


Figure 5.21 Stress distribution in the concrete for the slab S7.

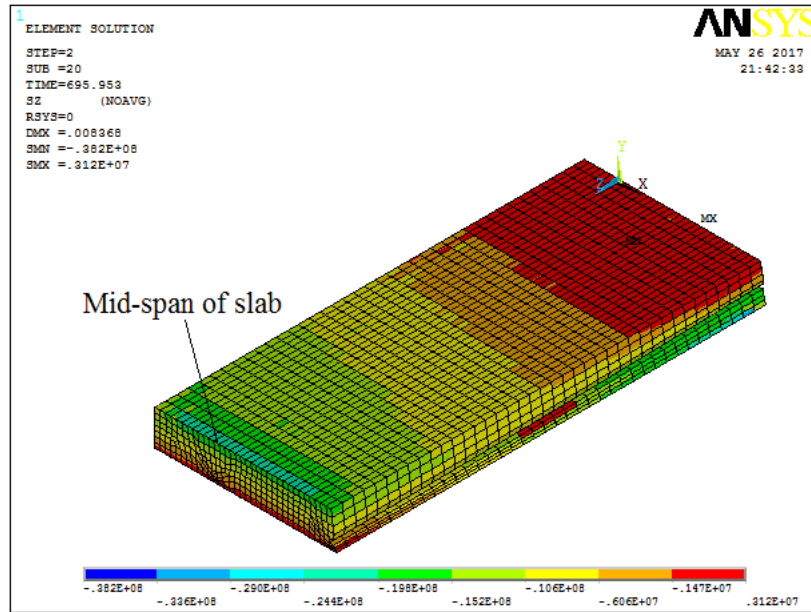


Figure 5.22 Stress distribution in the concrete for the slab S10.

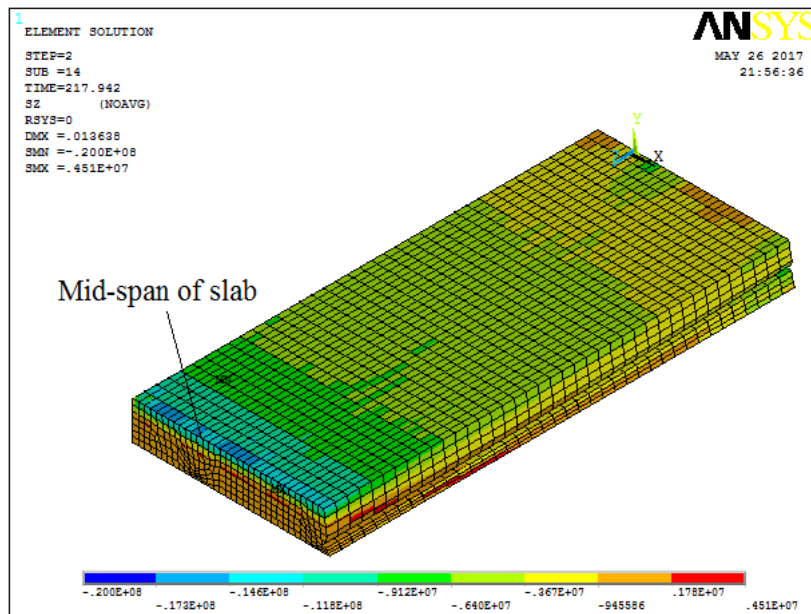


Figure 5.23 Stress distribution in the concrete for the slab S13.

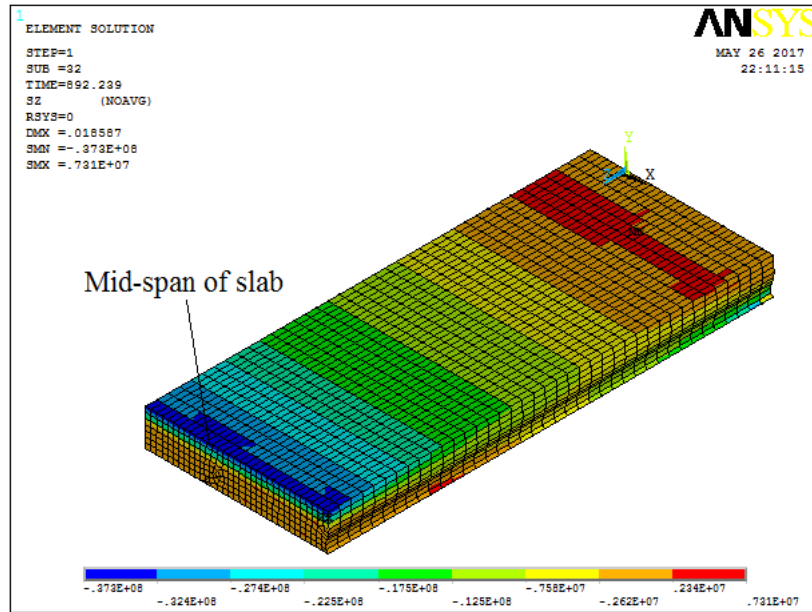


Figure 5.24 Stress distribution in the concrete for the slab S16.

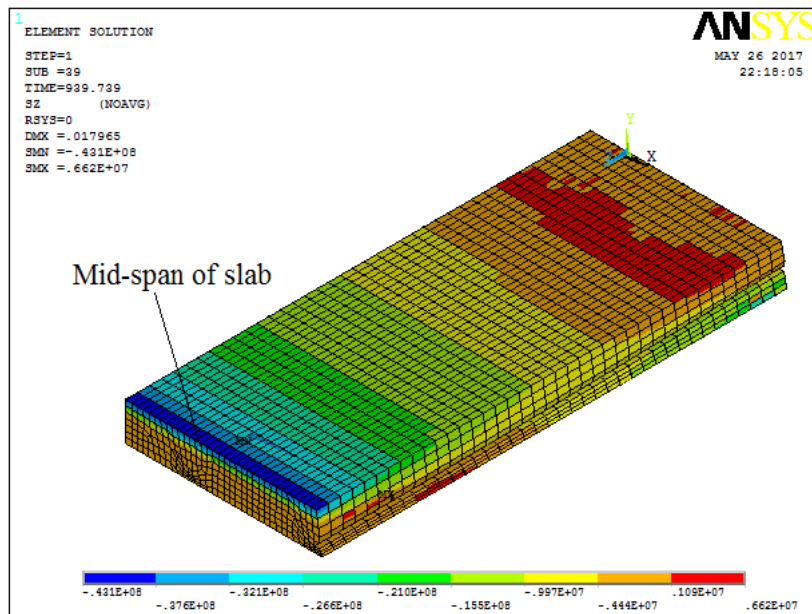


Figure 5.25 Stress distribution in the concrete for the slab S18.

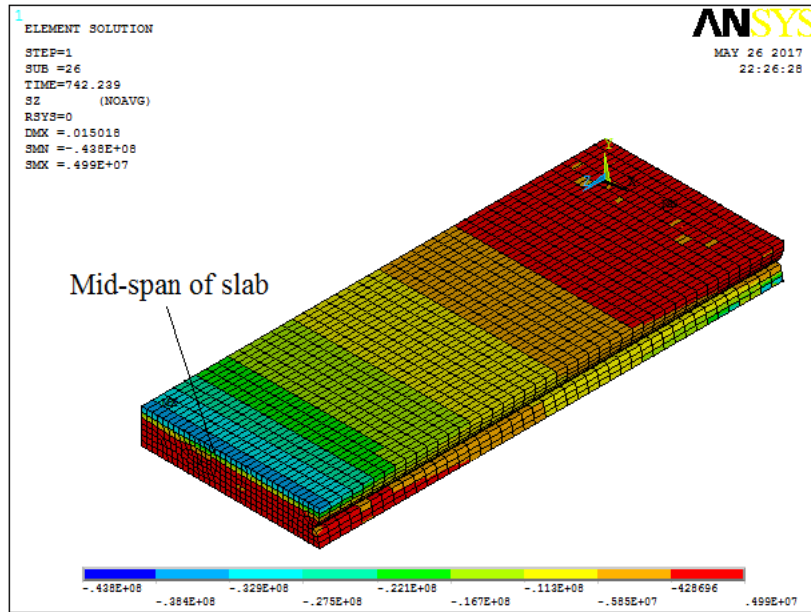


Figure 5.26 Stress distribution in the concrete for the slab S20.

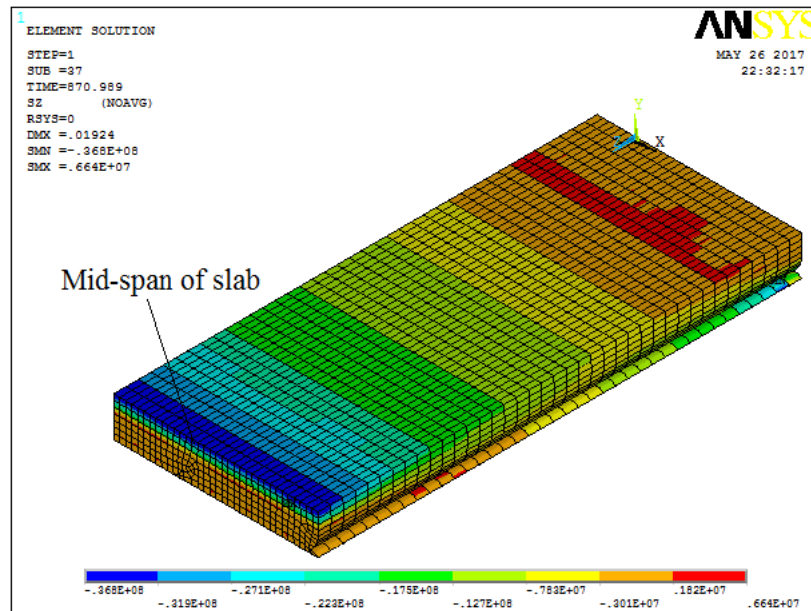


Figure 5.27 Stress distribution in the concrete for the slab S22.

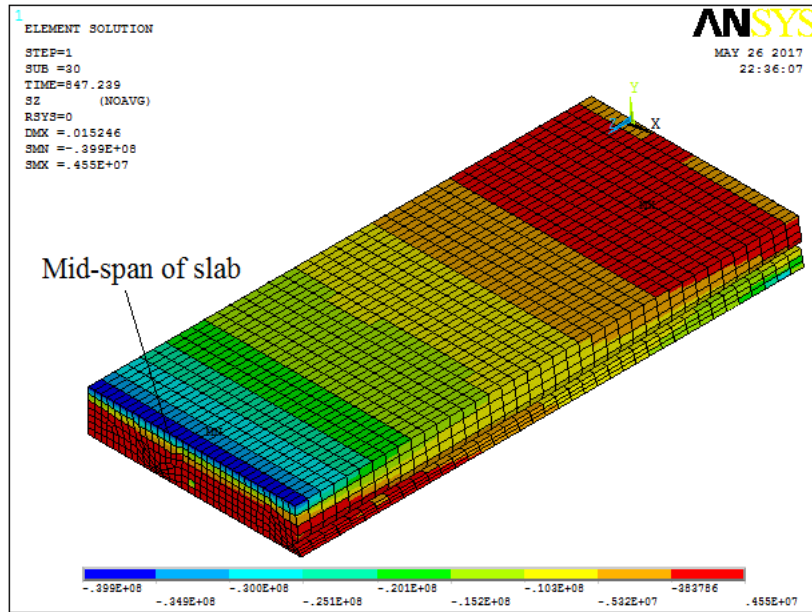


Figure 5.28 Stress distribution in the concrete for the slab S24.

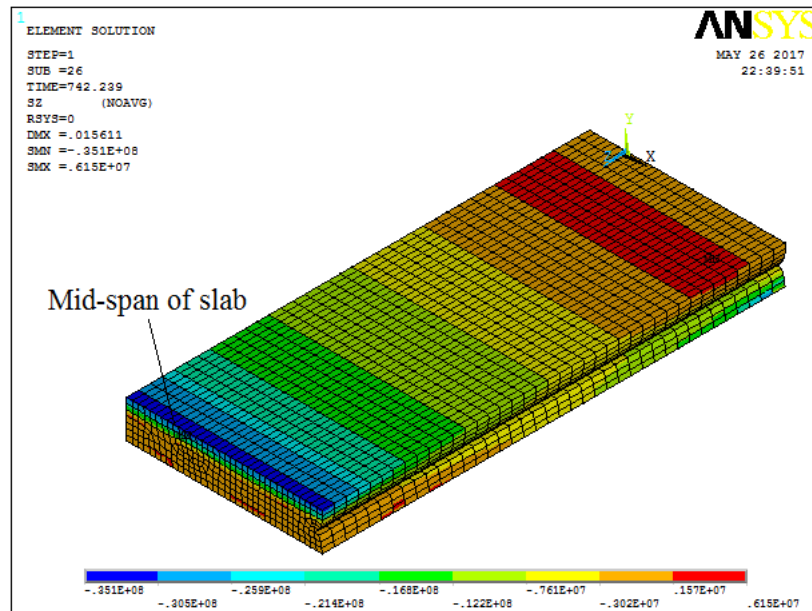


Figure 5.29 Stress distribution in the concrete for the slab S26.

5.5.2 Crack patterns

ANSYS computer program displays circles at locations of cracking or crushing in concrete elements. Cracking is shown with a circle outline in the plane of the crack, and crushing is shown with an octahedron outline. The first crack at an integration point is shown with a red circle outline, the second crack with a green outline, and the third crack with a blue outline (ANSYS, 2012). Figures 5.30-5.39 show crack and crushing patterns at ultimate state.

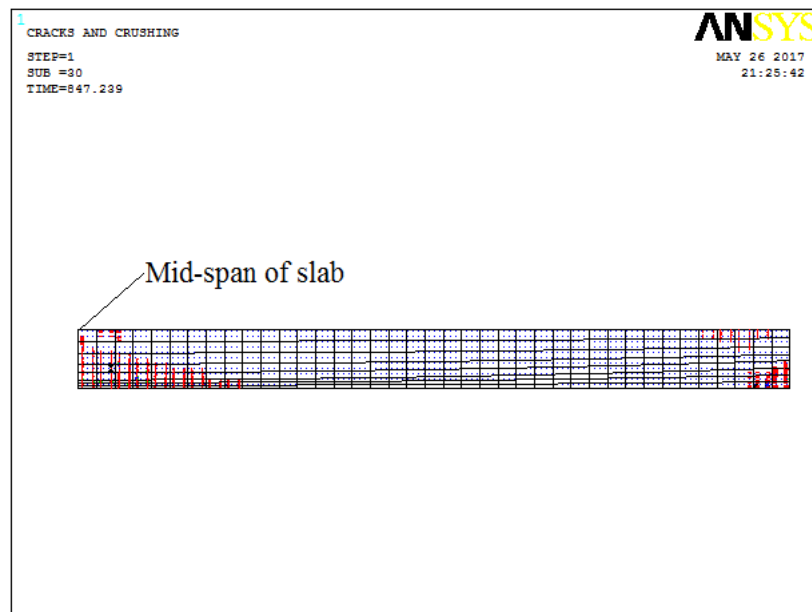


Figure 5.30 Cracks and crushing patterns of the slab S2 at ultimate state.

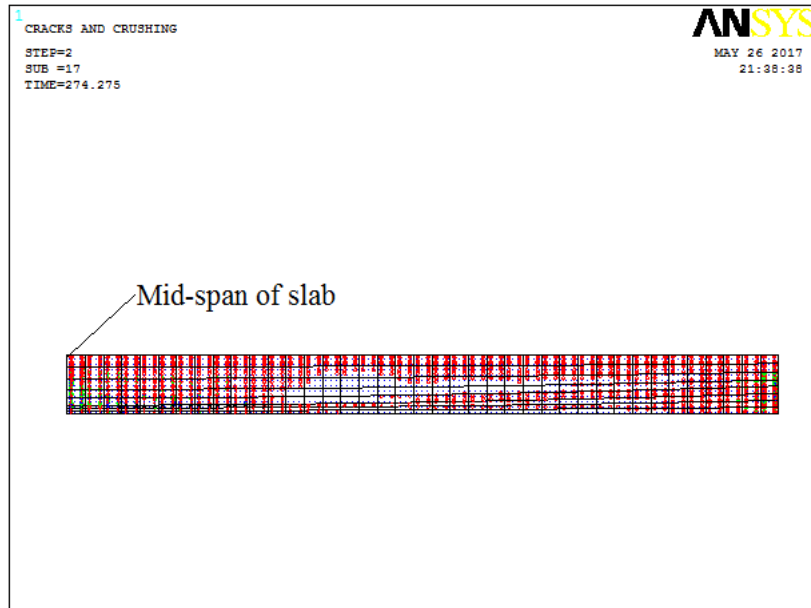


Figure 5.31 Cracks and crushing patterns of the slab S7.

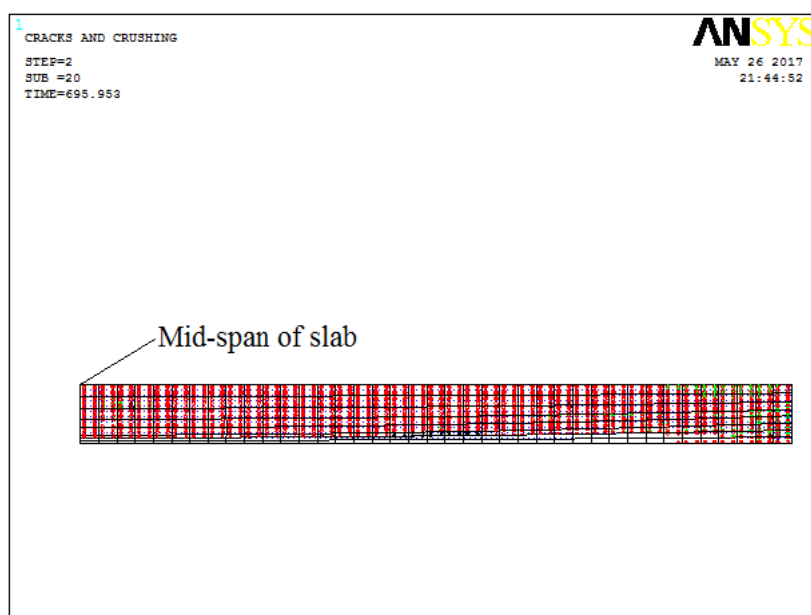


Figure 5.32 Cracks and crushing patterns of the slab S10.

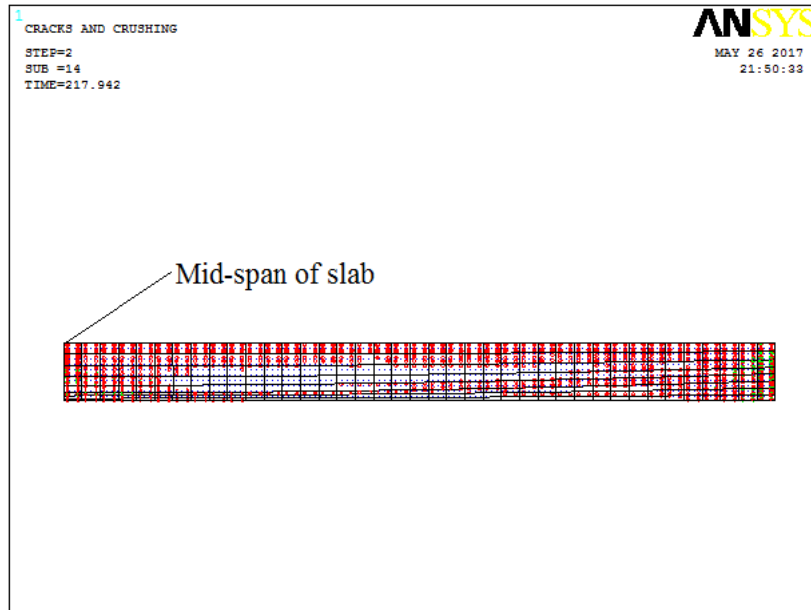


Figure 5.33 Cracks and crushing patterns of the slab S13.

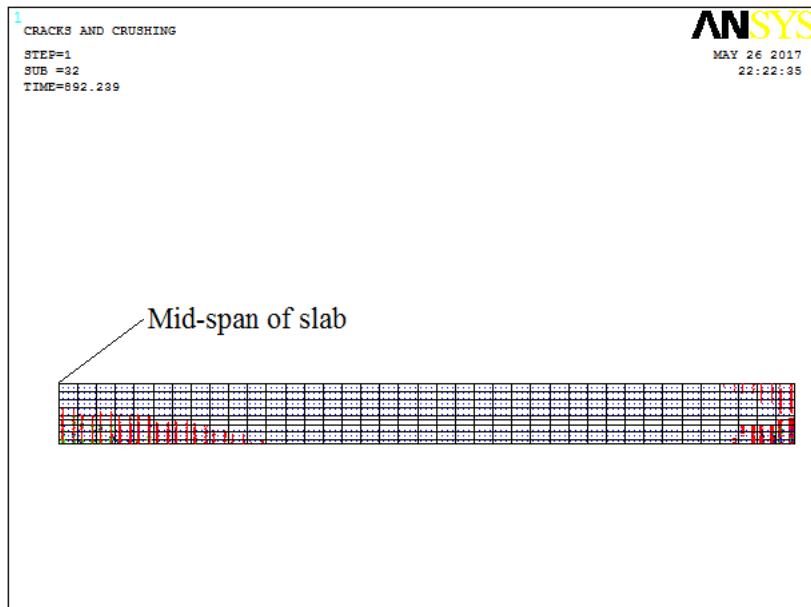


Figure 5.34 Cracks and crushing patterns of the slab S16.

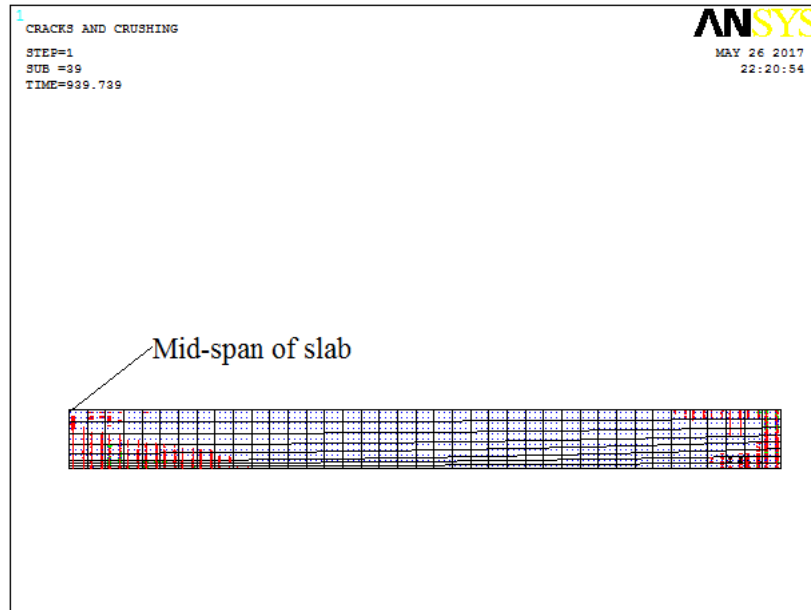


Figure 5.35 Cracks and crushing patterns of the slab S18.

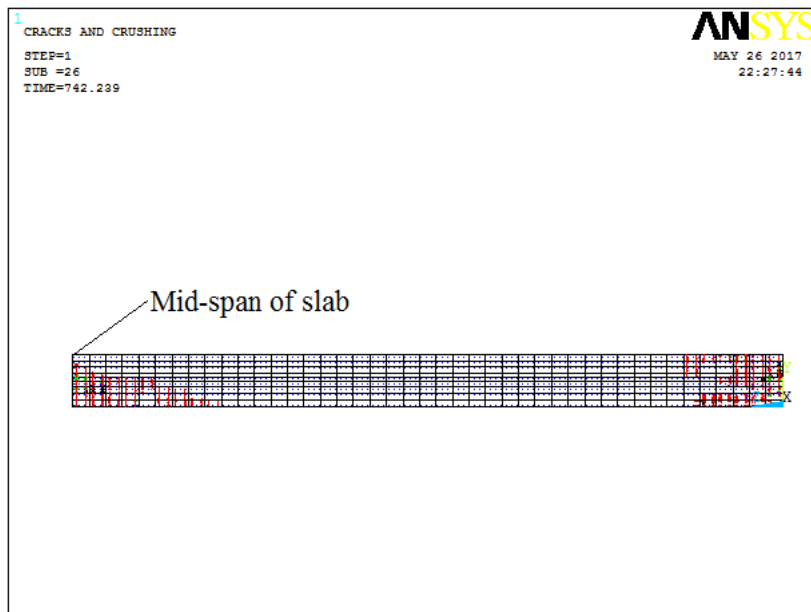


Figure 5.36 Cracks and crushing patterns of the slab S20.

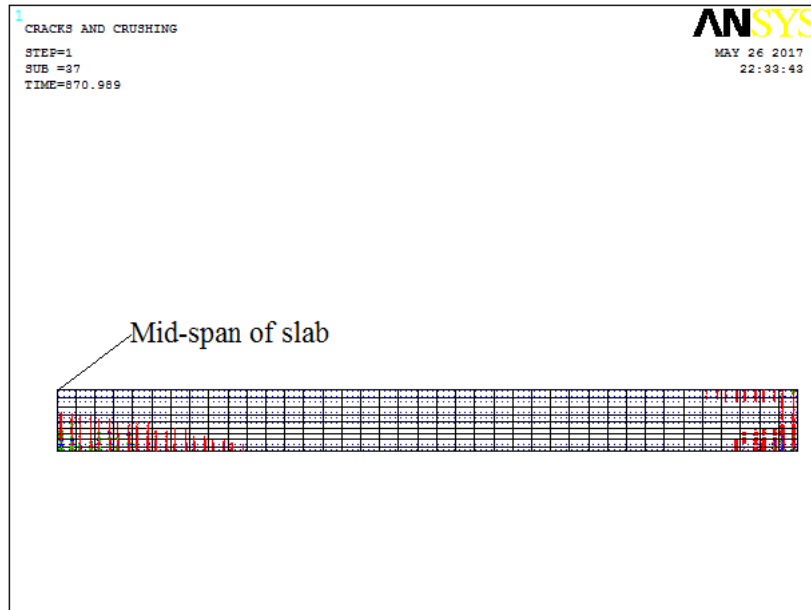


Figure 5.37 Cracks and crushing patterns of the slab S22.

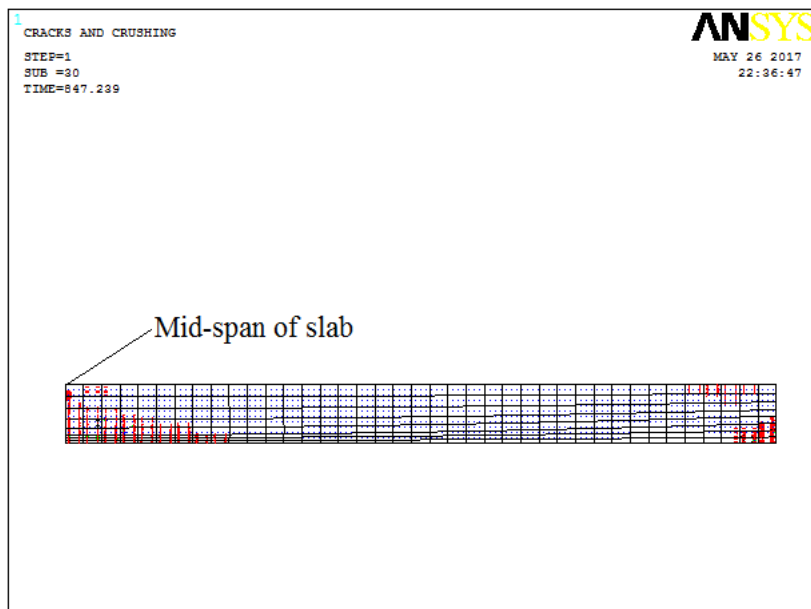


Figure 5.38 Cracks and crushing patterns of the slab S24.

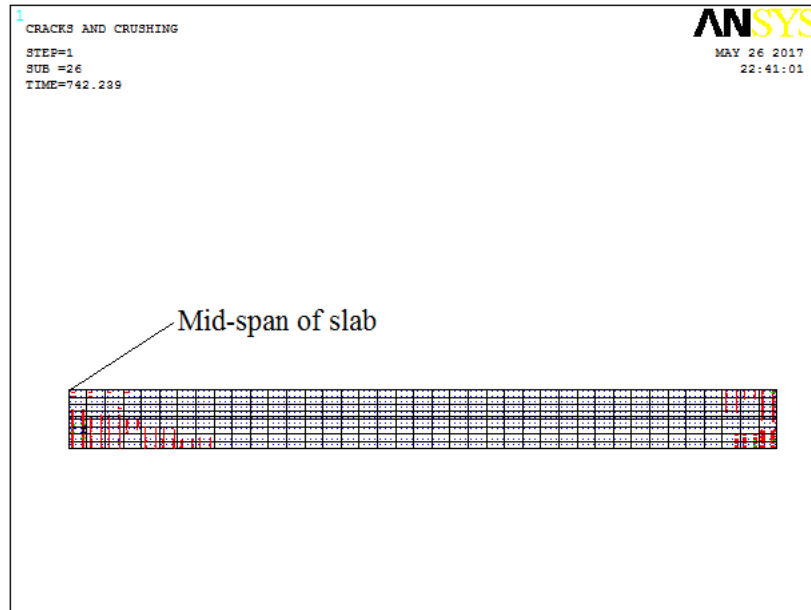


Figure 5.39 Cracks and crushing patterns of the slab S26.

5.5.3 Von-Mises stress in the concrete

Figures 5.40-5.44 show Von-Mises stress in the concrete at ultimate state.

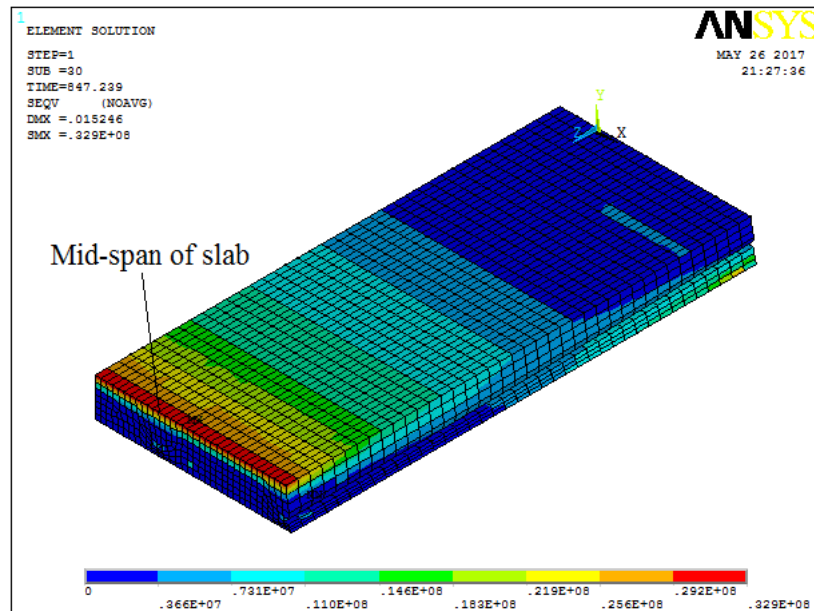


Figure 5.40 Von-Mises stress in the concrete of the slab S2 at ultimate state.

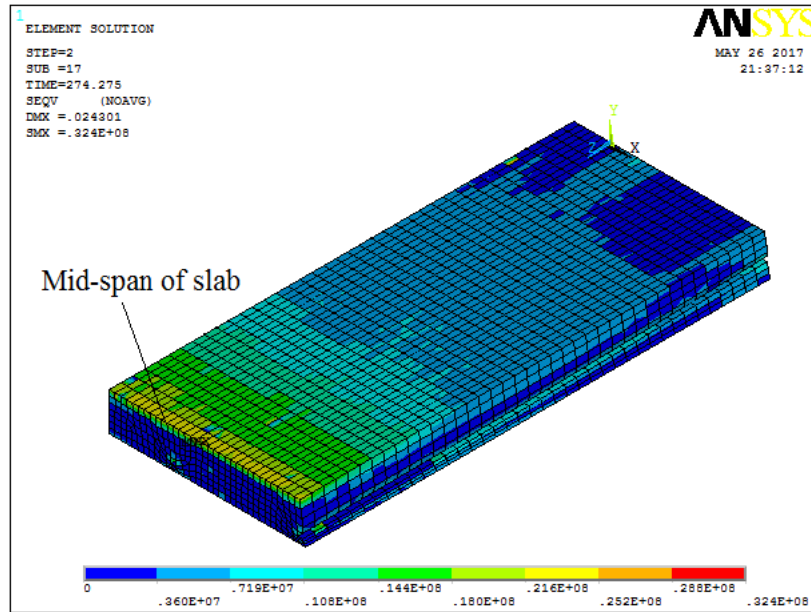


Figure 5.41 Von-Mises stress in the concrete of the slab S7.

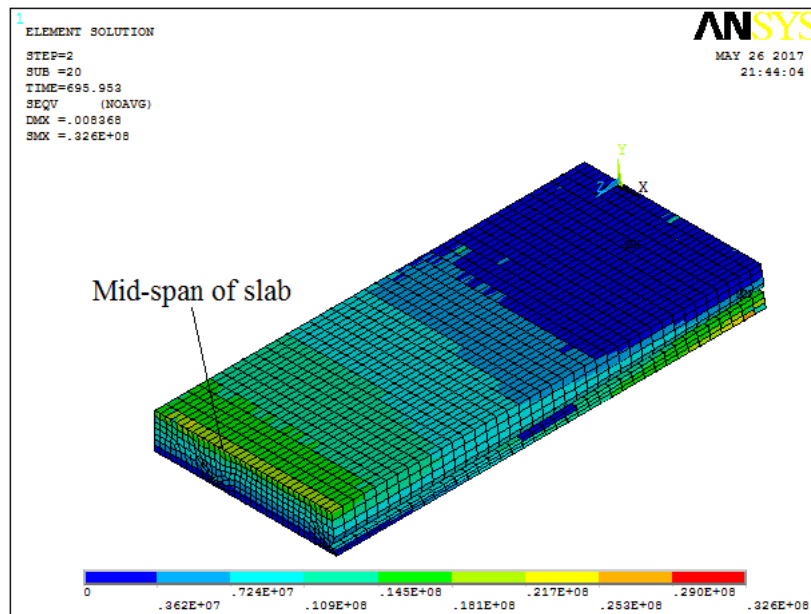


Figure 5.42 Von-Mises stress in the concrete of the slab S10.

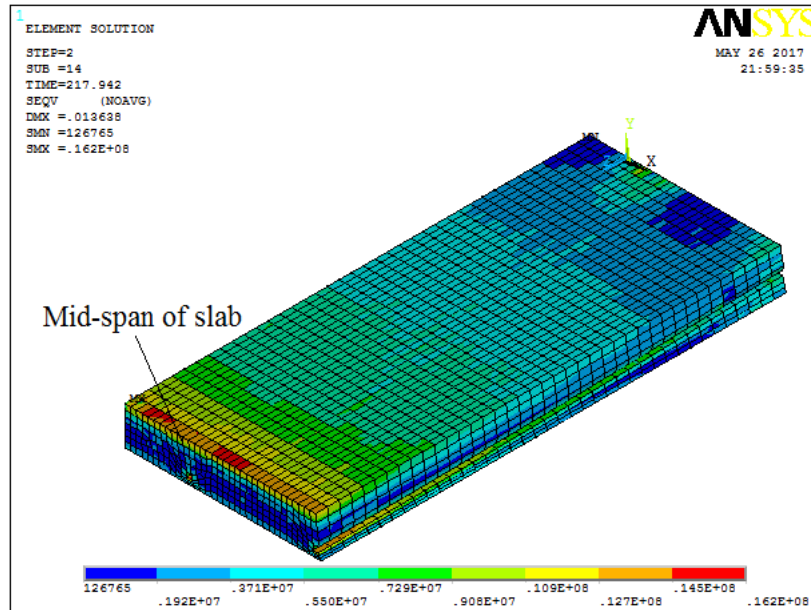


Figure 5.43 Von-Mises stress in the concrete of the slab S13.

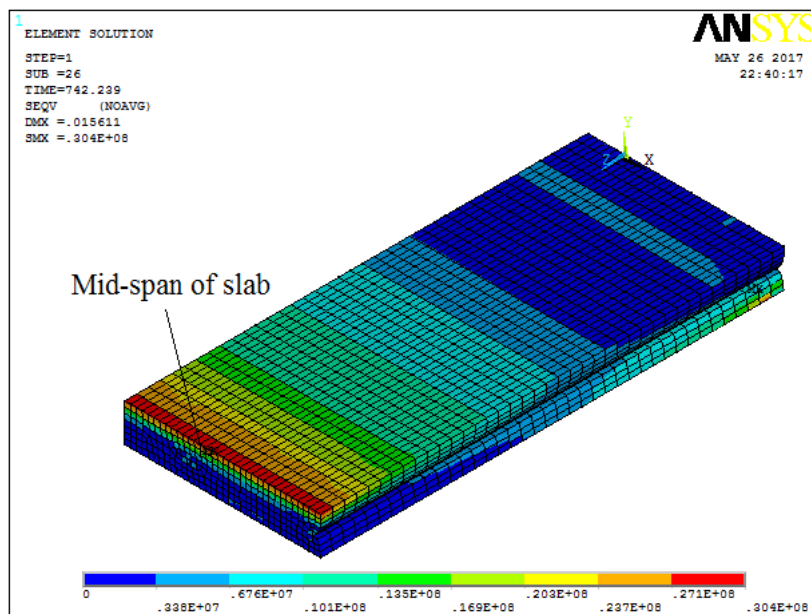


Figure 5.44 Von-Mises stress in the concrete of the slab S26.

CHAPTER 6

OPTIMIZATION OF POST-TENSIONED CONCRETE SLABS

6.1 General

PT concrete slab is broadly used for residential buildings, hotels, factories and hospitals because of its good performance and cost effectiveness compared with other slab types. The use of post-tensioning system allows for material savings due to reduced slab thickness. Moreover, cracking and deflection of the concrete slabs can be reduced by using post-tensioning. Several design variables and many practical constraints are contributory in the design of PT slab; so that the optimum design of PT slabs is challenging to the designers.

The techniques of optimization play a significant role in the design of structures, one of the most important objectives of optimization is finding the optimum solutions from which a designer can gain an utmost advantages from the available resources. There are a huge number of available designs, but the best design should be selected. The optimum design can be in terms of maximum performance, minimum weight, minimum cost or a combination of these (Rahul and Kumar, 2014).

6.2 Statement of an Optimization Problem

Majority of engineering problems often involve constrained minimization. An example of such constrained minimization problem is finding the minimum weight design of a structure subject to constraints on stress and deflection. Constrained problems may be expressed in the following general nonlinear programming form (Simpson et al., 2004):

$$\begin{aligned} & \text{minimize } f(\mathbf{x}) \\ & \text{subject to } g_i(\mathbf{x}) \leq 0 \quad i = 1, \dots, m \\ & \text{and } h_j(\mathbf{x}) = 0 \quad j = 1, \dots, l \end{aligned} \tag{6.1}$$

where $\mathbf{x} = (x_1, x_2, \dots, x_n)^T$ is a column vector of n real-valued design variables, f is the objective or cost function, g 's are inequality constraints, and h 's are equality constraints. The inequality constraints in Equation 6.1 include explicit lower and upper bounds on the design variables. We may also express Equation 6.1 in the form:

$$\begin{aligned} & \text{minimize } f(\mathbf{x}), \mathbf{x} \in \Omega \\ & \text{where } \Omega = \{\mathbf{x}: \mathbf{g} \leq 0, \mathbf{h} = \mathbf{0}\} \end{aligned} \quad (6.2)$$

Ω is the feasible region or feasible set. For unconstrained problems the feasible region is the entire space or $\mathbf{x} \in \mathbf{R}^n$. Objective function and constraints of linear programming problems involve linear functions of \mathbf{x} , where as objective function in quadratic programming problems is a quadratic function of the variables while the constraints are linear.

The design space or design variable space in an optimization problem can be considered as an n -dimensional Cartesian coordinate space where each coordinate axis represents a design variable x_i ($i = 1, \dots, n$). A design point is a point on the design space that may represent a possible or an impossible solution. Design variables cannot be chosen arbitrarily; they have to satisfy certain specific functional requirements to produce an acceptable design. These restrictions that must be satisfied in a design are called *design constraints*.

Design constraints are classified into two; one that represent limitations on the behavior or performance of the system and one that pose physical limitations on the design variables such as availability ,fabric ability, transportability etc. While the former is referred to as behavior or functional constraint, the latter is known as geometric or side constraints.

The values of the design variable belonging to the set \mathbf{x} that satisfy $g_i(\mathbf{x}) = 0$ forms a hyper-surface on the design space called the constraint surface. This is an $(n-1)$ dimensional subspace where n represents the number of design variables. The constraint surface divides the design space into two; one where $g_i(\mathbf{x}) < 0$ and the other in which $g_i(\mathbf{x}) > 0$. Design points on the hyper-surface i.e. points that satisfy $g_i(\mathbf{x}) = 0$ satisfy the constraint $g_i(\mathbf{x})$ critically. Those lying on the region where $g_i(\mathbf{x}) > 0$ are infeasible and unacceptable while those on the region belonging to $g_i(\mathbf{x}) < 0$ are feasible and acceptable. The collection of all constraint surfaces i.e. $g_i(\mathbf{x}) = 0$,

$i=1, \dots, m$ that separates the acceptable region is known as the *composite constraint surface*. A design point that lies on one or more constraint surfaces is known as a node point and its associated constraint as an *active constraint*. Those points that do not lie on the constraint surface are known as *free points*. Depending on the location of a design point on the design space, it can be classified into four as:

1. A free and acceptable point.
2. A free and unacceptable point.
3. A bound and acceptable point.
4. A bound and unacceptable point.

In general there will be more than one acceptable design point and our objective is to choose the best from the lot. This is obtained by specifying a criterion to compare the acceptable design and choosing the best one from it. This criteria or function is known as the cost or objective function of the optimization problem. When there are more than one objective function then the problem is known as a multi-objective programming problem. Like constraint surfaces, objective functions also form hyper surfaces known as objective function surfaces. Once the objective function surfaces are drawn along with constraint surfaces on the design space, the optimum point can be easily located graphically as shown in Figure 6.1.

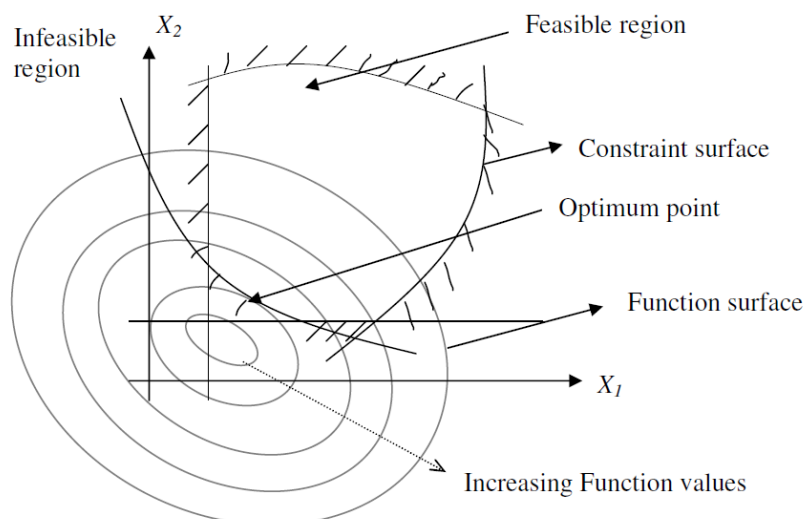


Figure 6.1 Function plot depicting optimum solution for a 2 design variable set.

6.3 Objective Function and Constraints

Nowadays FE method is often used to analyze structures and to find the stresses, strains and deformations of a structure subjected to different boundary conditions and loads. In all engineering fields, structural design techniques and especially the methods of numerical optimization have been developed during the last decades. Lucien Schmit (1960) explained the design of elastic structures by using the nonlinear programming techniques. Today, many FE codes that have optimization capabilities are usable.

The objective of the optimization procedures will develop herein is to minimize the total weight of PT tendons (w) while satisfying all relevant strength and serviceability limit states mandatory according to the code. The optimization problem will be defined as:

Minimize :

$$w = la\gamma \quad (6.3)$$

Subjected to:

$$g_i(\mathbf{x}) \leq 0 \quad i = 1, \dots, m \quad (6.4)$$

$$h_j(\mathbf{x}) = 0 \quad j = 1, \dots, l \quad (6.5)$$

where w is the objective function, l is the total length of PT tendons, γ is unit weight of PT tendons, a is the area of PT tendon, g_i is the inequality constraints, h_j is the equality constraints and \mathbf{x} is the design variable $\{x_1, x_2, \dots, x_n\}$. The design variables are as x_1 , which is the area of PT tendons, x_2 , which is the initial stress in tendons and x_3 , which is the eccentricity of the tendon profile at mid-span of the slab.

The constraints are defined as follows:

- Maximum normal stress in concrete
- Maximum normal stress in steel tendons
- Maximum shear stress in concrete
- Maximum displacement at mid-span of the slab

6.4 Optimization of PT Slabs using Sub-Problem Approximation Method

6.4.1 Optimization strategy

Many studies concerning the design optimization of concrete structural elements were published. Few studies were concerned with the design of PT concrete slabs. In this study, FE analysis is applied to optimize the total weight of PT tendons used to reinforce PT slab subjected to static loading. Optimization flow chart is given in Figure 6.2, it was noticed that in ANSYS package (ANSYS, 2012) that two optimization methods are available: the first order method and sub-problem approximation method.

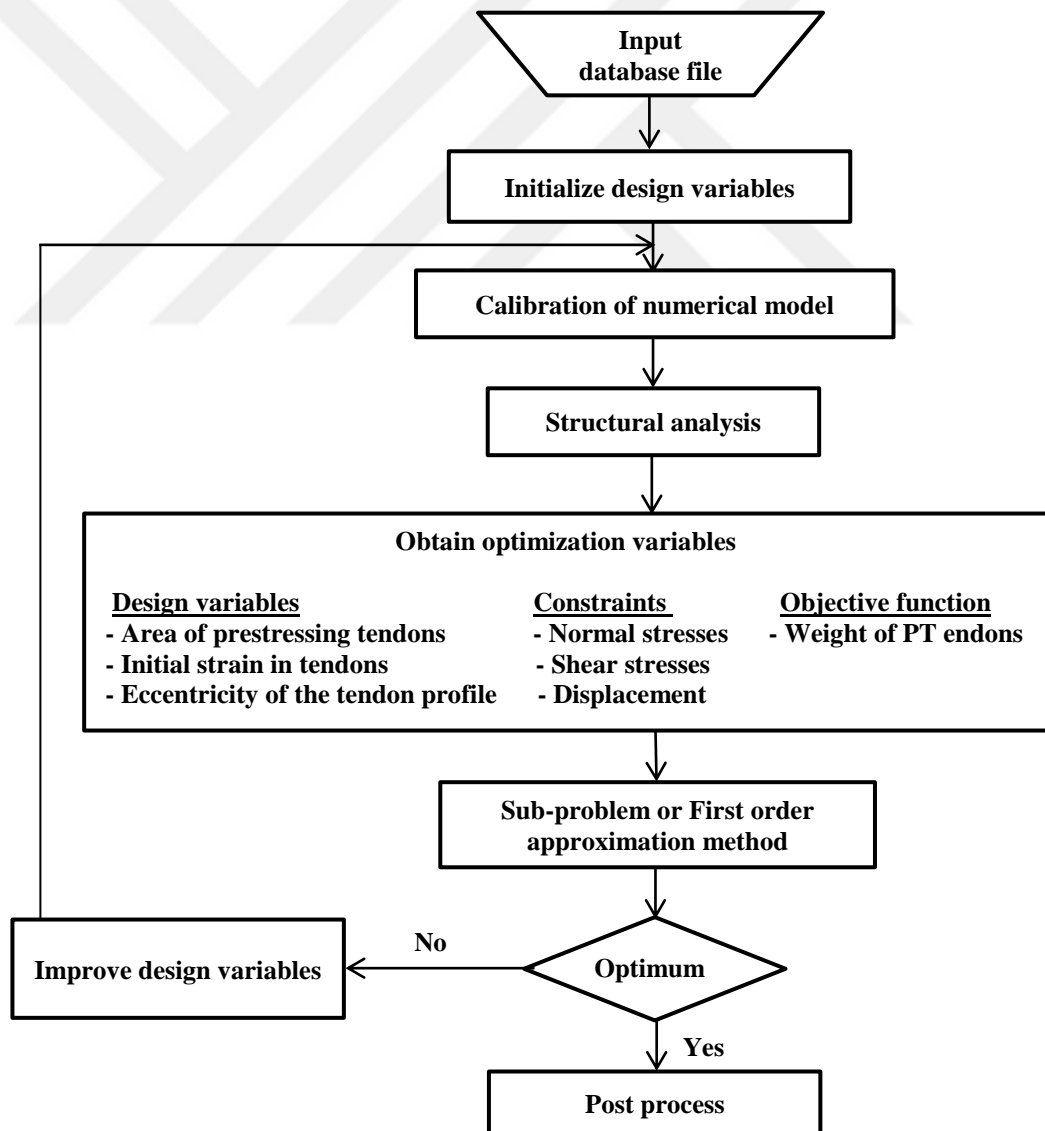


Figure 6.2 Optimization flow chart.

The first-order method utilizes gradients of the dependent variables with respect to design variables. The sub-problem approximation method could be explained as an advanced zero-order method that it needs only the dependent variable values, and not their derivatives. Three types of variables characterize the design process in both optimization methods: objective function, constraints and design variables.

6.4.2 Total weight of PT tendons minimization for bonded post-tensioned slab

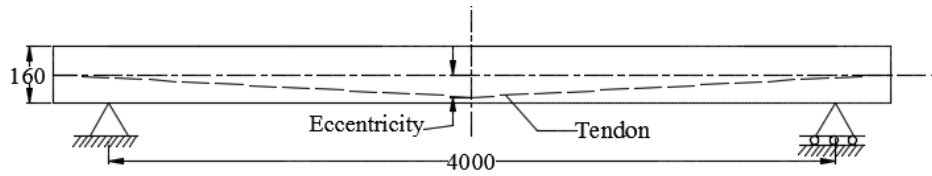
In this part, the BPT one-way concrete slab is optimized. The dimension of BPT slab is shown in Figure 6.3, and the loading considered for the proposed study is shown in Figure 6.4.

The slab is designed to behave as a fully PT concrete member, reinforced with fully BPT tendons with no regular rebar. The applied loads are the gravitational dead and static point loads. There are no lateral loads considered in the design. Pre-stressing was considered as a variable in the optimization process.

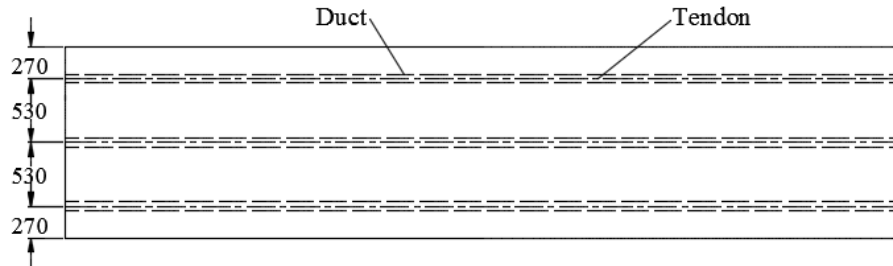
Design optimization was entirely conducted using the ANSYS Parametric Design Language (APDL). By adding penalty functions to the objective function, the optimization problem with constraints will be converted to unconstrained problem. For each iteration, various steepest descent and conjugate direction searches are performed until convergence is reached to determine a search direction. A line search strategy is adopted to minimize the unconstrained optimization problem. Total weight of PT tendons minimization and effect of area of tendons are investigated.

The objective of the design optimization procedures developed herein is to minimize the total weight of PT tendons. The design variables are the area of PT tendons, the initial stress in tendons and the eccentricity of the tendon profile at mid-span of the slab. Behavioral constraints dictated by the ACI 318 are explained in Table 6.1.

To minimize the total weight of PT tendons, it is necessary to respect the imposed constraints conditions: normal stress in concrete, stress in steel tendon, shear stress in concrete and displacement at mid-span of the slab. These parameters are evaluated according to the lower and upper limits of the design variables given in Table 6.2.



(a) General layout of slab



(b) Plan view of slab

Figure 6.3 Dimensions of BPT slab (mm).

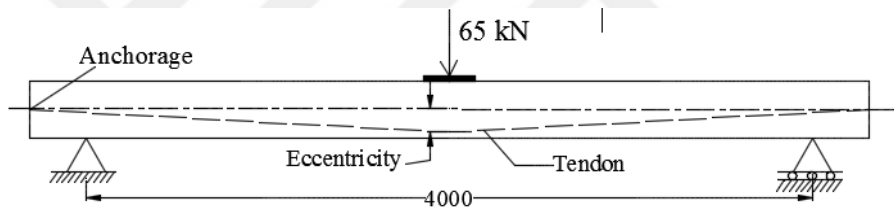


Figure 6.4 Loading of BPT slab for optimum design.

Table 6.1 Constraints specified by the ACI 318.

	Constraints	Limit
1	Compression stresses in concrete, f_c	$f_c > -0.6 f'_c$
2	Tension stresses in concrete, f_t	$f_t < 0.5\sqrt{f'_c}$
3	Stresses in steel tendons, f_{tendon}	$f_{tendon} < 0.7f_{pu}$
4	Shear stress, V_r	$V_r > V_f$
5	Displacement at mid-span of the slab, U_y	$U_y < l/360$

where: f'_c is the specified compressive strength of concrete; f_c is the compression stresses in concrete (obtained from FE analysis); f_t is the tensile stresses in concrete (obtained from FE analysis); f_{pu} is the specified tensile strength of PT tendons; f_{tendon} is the stresses in PT tendon (obtained from FE analysis); V_r is the factored shear stress resistance; V_f is the factored shear stress; U_y is the displacement at mid-span of the slab (obtained from FE analysis) and l is the span length.

Table 6.2 Initial, optimum and limits of design variables and constraints of BPT slab.

		Minimum	Initial value	Maximum	Optimum
Objective	w (g)	----	23736	----	18576
Design variables	a (m ²)	0.00005	0.00023	0.0005	0.00018
	i (MPa)	1025	1200	1332.5	1165
	e (m)	0.0	0.005	0.044	0.0437
Constraints	Max. f_c (MPa)	-20.0	-17.4	0.0	-14.5
	Max. f_t (MPa)	0.0	3.5	2.7	2.69
	Max. f_{tendon} (MPa)	0.0	1213	1430	1175
	Max. V_r (MPa)	0.0	10.2	9.0	8.3
	Max. U_y (mm)	0.0	4.75	11.0	3.2

where: a is the area of PT tendons, i is the initial stress in tendons and e is the eccentricity of the tendon profile.

After the calibration of our numerical model and clarification of the optimization strategy, minimization of the total weight of PT tendons can be performed. To establish total weight of PT tendons optimization, a random design iterations can be carried out against the material parameters limits. The initial data from the random design calculations can serve as starting points to feed the optimization methods described. Figure 6.5 shows the evolution of optimal total weight of PT tendons versus the number of iterations for sub-problem approximation method. From this figure, three distinctive zones can be recognized. The first zone is located between the first and the 6th iterations, which is characterized as a relatively high total weight of PT tendons, close to initial total weight of PT tendons (23736 g). The second zone is the incertitude zone located between the 6th and 12th iterations, and finally the feasible zone in which we have a stable value, which is 18576 g. Using this optimization, the total weight of PT tendons is reduced by almost 22 %.

In Figure 6.6 the optimized area of PT tendons is plotted against the number of iterations. Figure 6.6 has the same form as the total weight of PT tendons. A significant reduction in the area of PT tendons from 0.00023 m² for the initial state to 0.00018 m² for the converged solution is noticed. This reduction is significant, which (approximately equals 22 % of the initial area). In Figure 6.7 the eccentricity of the tendon profile is plotted against the number of iterations.

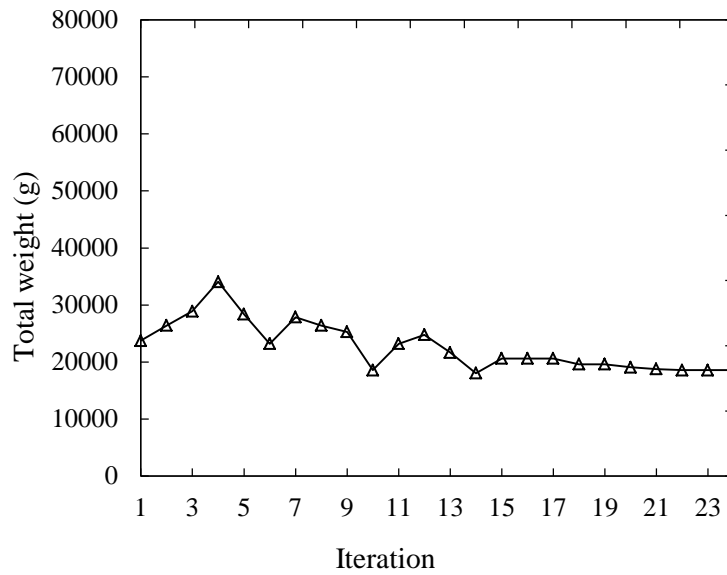


Figure 6.5 Evolution of optimal total weight of PT tendons for BPT slab versus number of iterations.

Figure 6.8 shows the evolution of mid-span deflection. The mid-span deflection at optimum design ($U_y = 3.2$ mm) is smaller than at initial design ($U_y = 4.75$ mm), which is attributed to the increase the eccentricity of tendons.

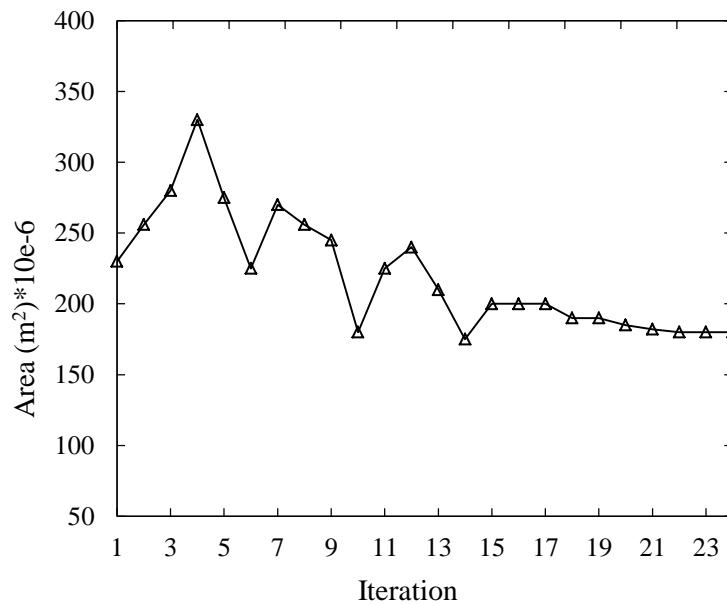


Figure 6.6 Evolution of the optimal area of PT tendons versus number of iterations.

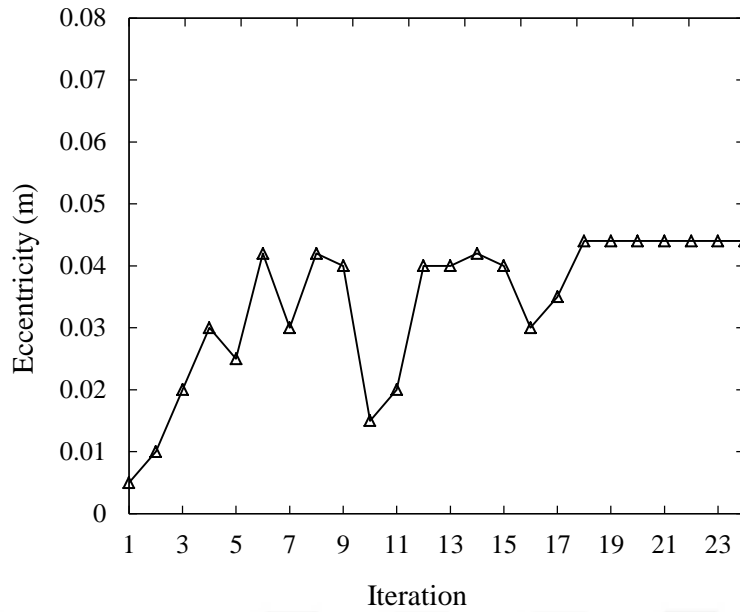


Figure 6.7 Evolution of the eccentricity of the tendon profile versus number of iterations.

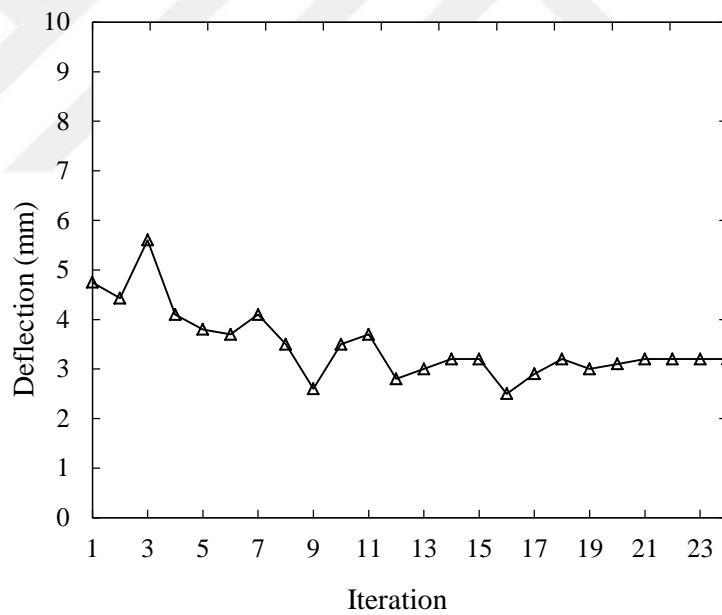


Figure 6.8 Evolution of mid-span deflection versus number of iterations.

The evolution of maximum compression stresses in concrete are plotted in Figure 6.9. It is noted the maximum compression stress in concrete at anchorage is decreased during the optimization iteration that is due to reduction in the prestressed force. A significant reduction in maximum compression stress at anchorage from 17.4 MPa for the initial state to 14.5 MPa for the converged solution is noticed. The

concentration of PT force leads to increase the compression stress in concrete at anchorage. Figure 6.10 shows the evolution of maximum tension stress in concrete. It is evident that the maximum tension stress is decreasing during the optimization iteration. The increase in eccentricity of tendons leads to this decrease in tension stress.

The initial and optimum design values for the total weight of PT tendons optimization are shown in Table 6.2. Optimization values for design variables and constraints are within the limits. From Table 6.2, it can be observed that the maximum tensile stress is decreased from 3.5 MPa for the initial state to 2.69 MPa for the optimum design state. From this table, it is obvious that the maximum tensile stress controls the optimization convergence. It is found that the optimum design value for the maximum tensile stress (2.69 MPa) is closed with the upper limit (2.7 MPa).

In addition, it can be noted that the smallest reduction occurs in initial stress in tendons, which is about 2.9 % while the highest reduction occurs in the mid-span deflection.

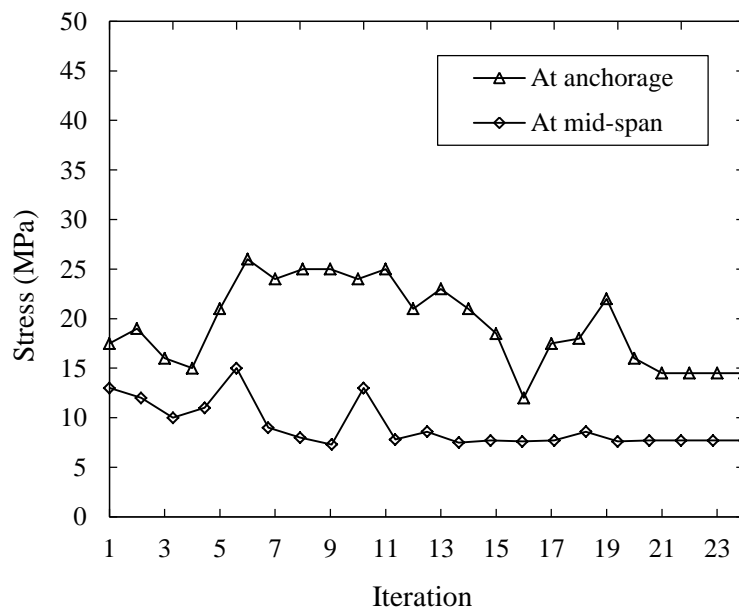


Figure 6.9 Evolution of maximum compression stress in concrete versus number of iterations.

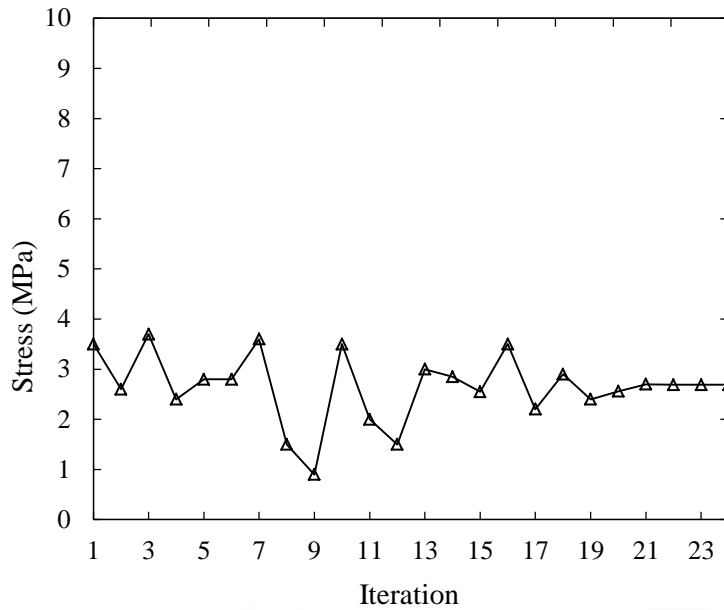


Figure 6.10 Evolution of maximum tensile stress at mid-span in concrete versus number of iterations.

6.4.2.1 Effect of the applied load on the optimization of bonded slab

To study the effect of the magnitude of applied load on the optimum values for BPT slab, the total weight of PT tendons optimization for the BPT slab is redesigned by specifying the applied total static loading to $P=55$, $P=65$ and $P=75$ kN. The loading of the BPT slab is shown in Figure 6.11. The objective, design variables and constraints developed herein are the same as those in Section 6.4.2. Behavioral constraints dictated by the ACI-318 code are explained in Table 6.1 and are evaluated according to the lower and upper limits of the design variables and constraints given in Table 6.2 for the maximal loading.

To establish total weight of PT tendons optimization, a random design iterations can be performed against the material parameters limits.

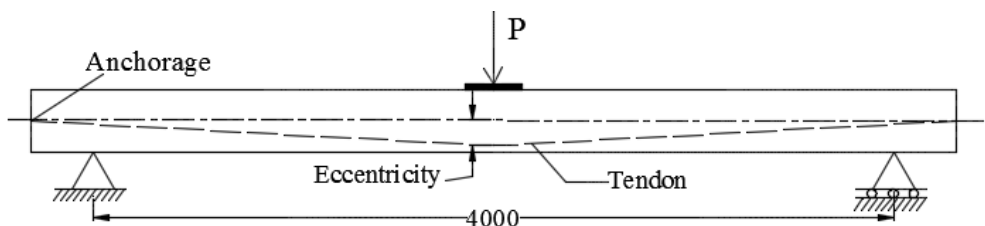


Figure 6.11 Loading of BPT slab for the load optimization.

The initial and optimum design values for the total weight of PT tendons optimization for the BPT slab are shown in Table 6.3. From Table 6.3, it can be observed that the value of the optimum area of tendon depends on the magnitude of applied load. From this table, it can be found that the optimum value of the area of tendons increases from 141 mm² for the applied loading P=55 kN to 215 mm² for the applied loading P=75 kN. The optimum area is increased when the applied load is increased.

The increases of the applied load on the one-way slab leads to increase in the tensile stress in concrete due to the increase in the positive bending moment and to keep the level of tensile stress in allowable limits it requires to increase the negative bending moment. For the increases of the negative bending moment it requires to increase in the area of tendons or the initial stress in tendons.

Table 6.3 Initial and design optimization values for BPT slab.

Total applied load (kN)	Initial values				Optimum value				Reduction	
	w (g)	a (mm ²)	i (MPa)	e (m)	w (g)	a (mm ²)	i (MPa)	e (m)	w	a
55	23736	230	1200	0.005	14551	141	1149	0.0438	38 %	38 %
65	23736	230	1200	0.005	18576	180	1165	0.0437	22 %	22 %
75	23736	230	1200	0.005	22188	215	1174	0.0437	6.5 %	6.5 %

6.4.2.2 Effect of number of applied point loads on the optimization of BPT slab

To study the effect of a number of applied point loads on the optimum values for BPT slab, the total weight of PT tendons optimization for the BPT slab is redesigned by applying four types of point loading. The four types of loading are one, two, three and four point loads. The loading of the BPT slab is shown in Figure 6.12. The objective, design variables and constraints developed herein are the same that in Section 6.4.2. Behavioral constraints dictated by the ACI-318 code are explained in Table 6.1 and are evaluated according to the lower and upper limits of the design variables given in Table 4.2 for the maximal loading.

Table 6.4 shows the initial and the design optimum values for BPT slab for different types of loading. From Table 6.4, it can be noted that the optimum values of total weight of PT tendons and area of tendons are affected by the number of applied point loads. From Table 6.4, it can be found that the optimum value of the area of tendons

decreases from 180 mm^2 for 1 point loading to 60 mm^2 for 4 point loading when the total applied load is kept constant. From this table, it is evident that the critical type of loading is when the load is applied near the mid-span of the BPT slab.

When the load is applied near the mid-span of the one-way slab leads to increase in the tensile stress in concrete due to the increase in the positive bending moment and because the maximum tensile stress controls the optimization convergence must keep the level of tensile stress in allowable limits. For the increases of the negative bending moment it requires to increase in the area of tendons or the initial stress in tendons.

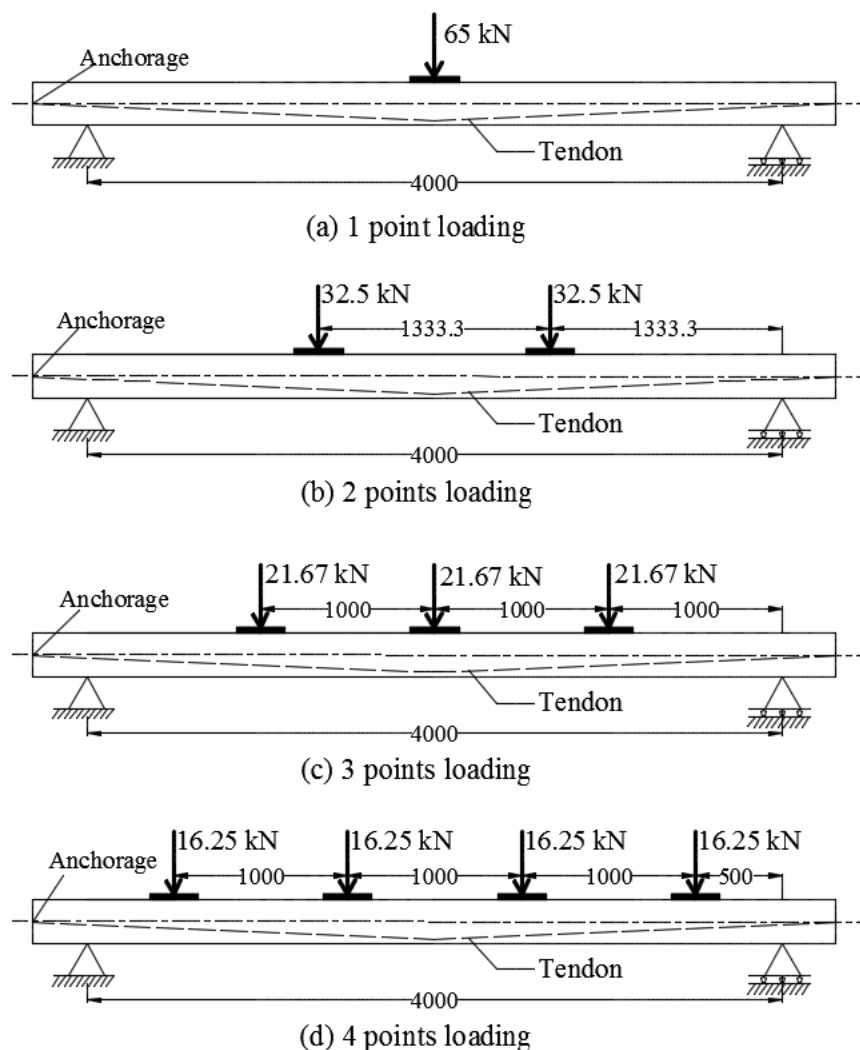


Figure 6.12 Loading of BPT slab for the number of applied point load optimization.

Table 6.4 Initial and design optimization values for BPT slab for different type of loading.

Type of loading	Initial values				Optimum value				Reduction	
	w (g)	a (mm ²)	i (MPa)	e (m)	w (g)	a (mm ²)	i (MPa)	e (m)	w	a
1 point loading	23736	230	1200	0.005	18576	180	1165	0.0437	22 %	22 %
2 points loading	23736	230	1200	0.005	10423	101	1180	0.0437	56 %	56 %
3 points loading	23736	230	1200	0.005	10216	99	1165	0.0439	57 %	57 %
4 points loading	23736	230	1200	0.005	6192	60	1159	0.0438	74 %	74 %

6.4.3 Total weight of PT tendons minimization for UPT slab.

In this part, the UPT one-way concrete slab is optimized. The dimension of UPT slab is shown in Figure 6.3, and the loading considered for the proposed study is shown in Figure 6.13.

The slab is designed to behave as a fully PT concrete member, reinforced with fully UPT tendons with no regular rebar. The applied loads are the gravitational dead and static point loads. There are no lateral loads considered in the design. Pre-stressing was considered as a variable in the optimization process.

Design optimization was entirely conducted using the APDL. By adding penalty functions to the objective function, the optimization problem with constraints will be converted to unconstrained problem. For each iteration, various steepest descent and conjugate direction searches are performed until convergence is reached to determine a search direction. A line search strategy is adopted to minimize the unconstrained optimization problem. Total weight of PT tendons minimization and effect of area of tendons are investigated.

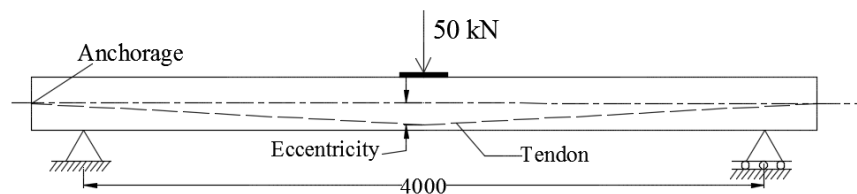


Figure 6.13 Loading of UPT slab for optimum design.

The objective of the design optimization procedures developed herein is to minimize the total weight of PT tendons. The design variables are the area of PT tendons, the initial stress in tendons and the eccentricity of the tendon profile at mid-span of the slab. Behavioral constraints dictated by the ACI 318 are explained in Table 6.1.

To minimize the total weight of PT tendons, it is necessary to respect the imposed constraints conditions: normal stress in concrete, stress in steel tendon, shear stress in concrete and displacement at mid-span of the slab. These parameters are evaluated according to the lower and upper limits of the design variables given in Table 6.5.

After the calibration of our numerical model and clarification of the optimization strategy, minimization of the total weight of PT tendons for the UPT one-way slab can be performed. To establish total weight of PT tendons optimization, a random design iterations can be carried out against the material parameters limits. The initial data from the random design calculations can serve as starting points to feed the optimization methods described. Figure 6.14 shows the evolution of optimal total weight of PT tendons versus the number of iterations for sub-problem approximation method. From this figure, three distinctive zones can be recognized. The first zone is located between the first and the 7th iterations, which is characterized as a relatively high total weight of PT tendons, close to initial total weight of PT tendons (23736 g). The second zone is the incertitude zone located between the 7th and 15th iterations, and finally the feasible zone in which we have a stable value, which is 17956 g. Using this optimization, the total weight of PT tendons is reduced by almost 24 %.

In Figure 6.15 the optimized area of PT tendons is plotted against the number of iterations. Figure 6.15 has the same form as the total weight of PT tendons. A significant reduction in the area of PT tendons from 0.00023 m^2 for the initial state to 0.000174 m^2 for the converged solution is noticed. This reduction is significant, which (approximately equals 24 % of the initial area). In Figure 6.16 the eccentricity of the tendon profile is plotted against the number of iterations.

Table 6.5 Initial, optimum and limits of design variables and constraints of UPT slab.

		Minimum	Initial value	Maximum	Optimum
Objective	w (g)	----	23736	----	17956
Design variables	a (m ²)	0.00005	0.00023	0.0003	0.000174
	i (MPa)	1010	1200	1220	1140
	e (m)	0.0	0.005	0.044	0.0438
Constraints	Max. f_c (MPa)	-20.0	-19.5	0.0	-15.5
	Max. f_t (MPa)	0.0	3.2	2.7	2.69
	Max. f_{tendon} (MPa)	0.0	1153	1430	1185
	Max. V_r (MPa)	0.0	11.1	9.0	6.1
	Max. U_y (mm)	0.0	5.7	11.0	2.9

where: a is the area of UPT tendons, i is the initial stress in tendons and e is the eccentricity of the tendon profile.

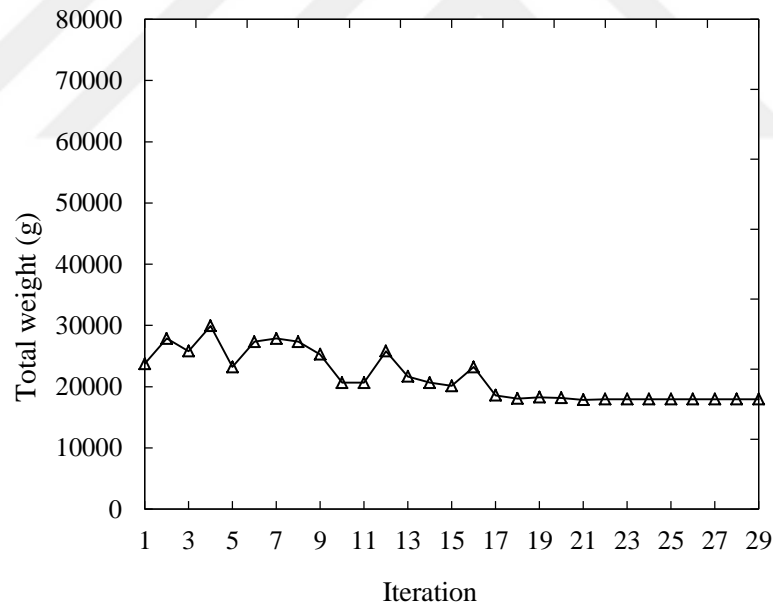


Figure 6.14 Evolution of optimal total weight of PT tendons for the UPT slab versus number of iterations.

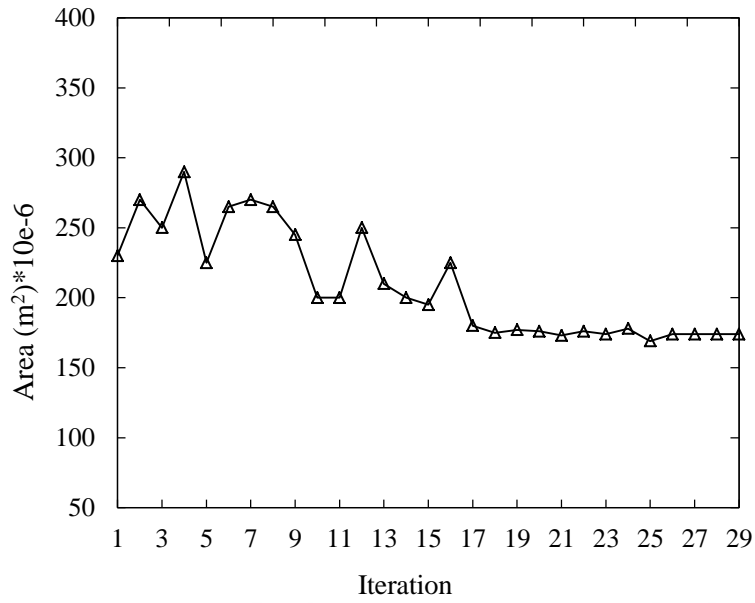


Figure 6.15 Evolution of optimal area of tendons for UPT slab versus number of iterations.

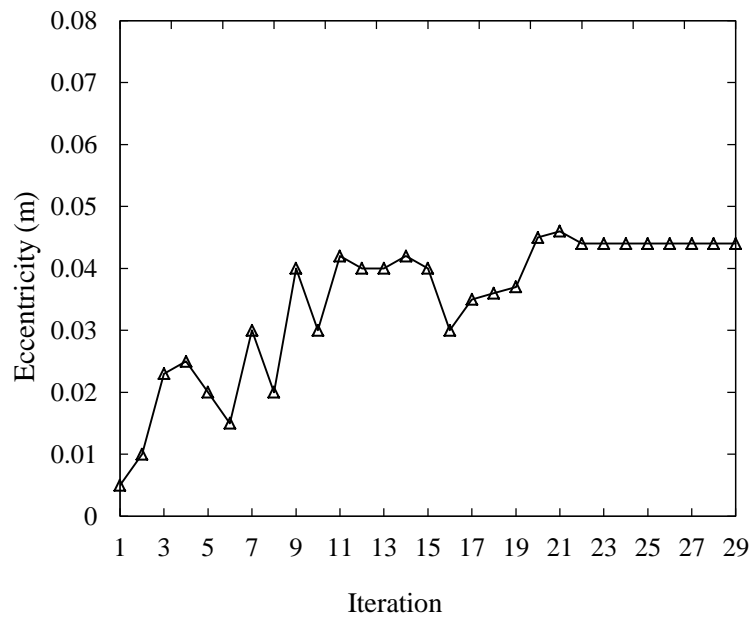


Figure 6.16 Evolution of eccentricity of the tendon profile of UPT slab versus number of iterations.

Figure 6.17 shows the evolution of mid-span deflection. The mid-span deflection at optimum design ($U_y = 2.9$ mm) is smaller than at initial design ($U_y = 5.7$ mm), which is attributed to the increase in the eccentricity of tendons.

The evolution of maximum compression stresses in concrete are plotted in Figure 6.18. It is noted the maximum compression stress in concrete at anchorage is decreased during the optimization iteration that is due to reduction in the prestressed force. A significant reduction in maximum compression stress at anchorage from 19.5 MPa for the initial state to 15.5 MPa for the converged solution is noticed. The concentration of PT force leads to increase the compression stress in concrete at anchorage. Figure 6.19 shows the evolution of maximum tension stress in concrete. It is evident that the maximum tension stress is decreasing during the optimization iteration. The increase in eccentricity of tendons leads to this decrease in tension stress.

The initial and optimum design values for the total weight of PT tendons optimization are shown in Table 6.5. Optimization values for design variables and constraints are within the limits. From Table 6.5, it can be observed that the maximum tensile stress is decreased from 3.2 MPa for the initial state to 2.69 MPa for the optimum design state. From this table, it is obvious that the maximum tensile stress controls the optimization convergence. It is found that the optimum design value for the maximum tensile stress (2.69 MPa) is closed with the upper limit (2.7 MPa).

In addition, it can be noted that the smallest reduction occurs in the tensile stress in concrete while the highest reduction occurs in the mid-span deflection.

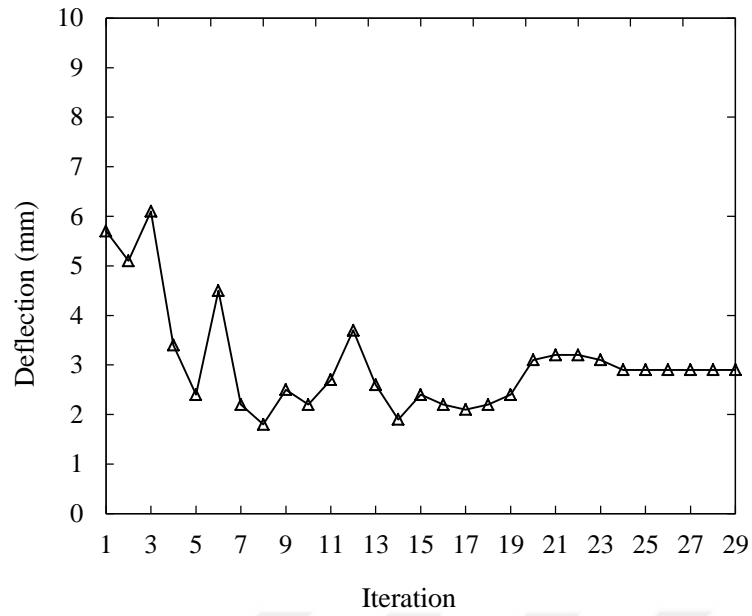


Figure 6.17 Evolution of mid-span deflection of UPT slab versus number of iterations.

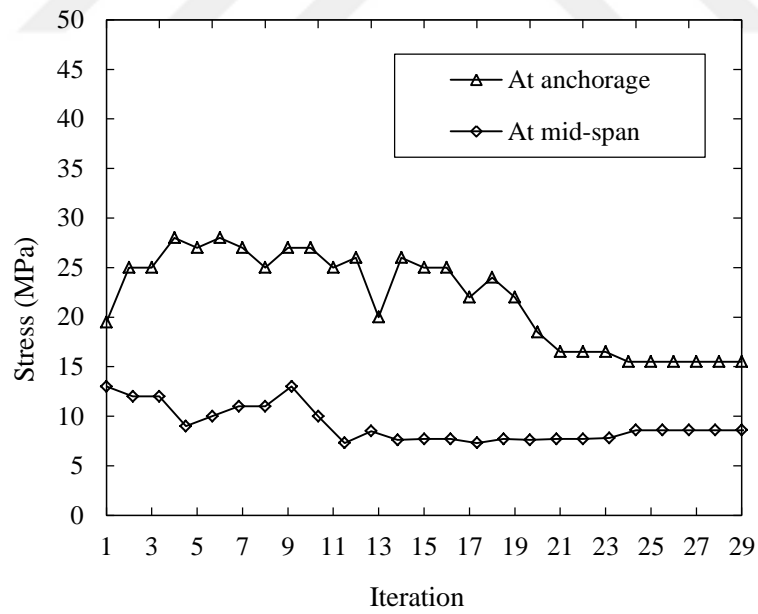


Figure 6.18 Evolution of maximum compression stress in concrete of UPT slab versus number of iterations.

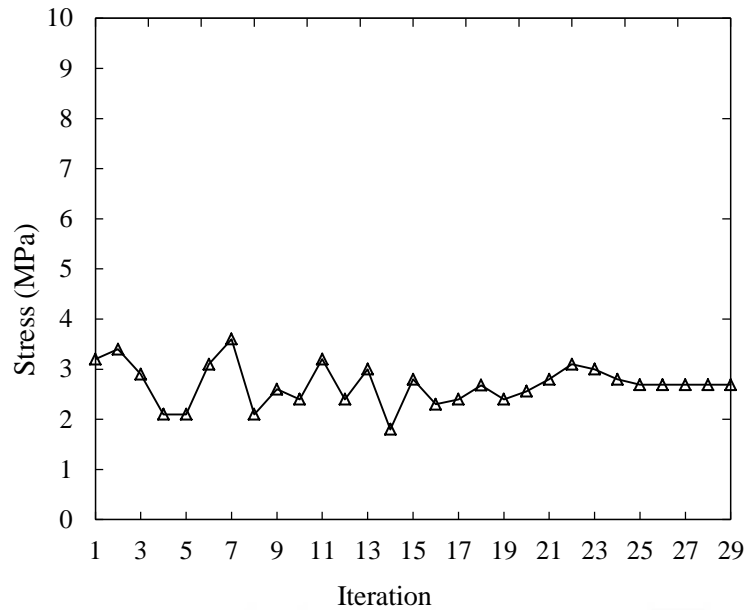


Figure 6.19 Evolution of maximum tensile stress at mid-span in concrete of UPT slab versus number of iterations.

6.4.3.1 Effect of the applied load on the optimization of UPT slab

To study the effect of the magnitude of applied load on the optimum values for UPT slab, the total weight of PT tendons optimization for the UPT slab is redesigned by specifying the applied total static loading to $P=45$, $P=50$ and $P=55$ kN. The loading of the UPT slab is shown in Figure 6.20. The objective, design variables and constraints developed herein are the same as those in Section 6.4.3. Behavioral constraints dictated by the ACI-318 code are explained in Table 6.1 and are evaluated according to the lower and upper limits of the design variables and constraints given in Table 6.5 for the maximal loading.

To establish total weight of PT tendons optimization, a random design iterations can be performed against the material parameters limits.

The initial and optimum design values for the total weight of PT tendons optimization for the UPT slab are shown in Table 6.6. From Table 6.6, it can be observed that the value of the optimum area of tendon depends on the magnitude of applied load. From this table, it can be found that the optimum value of the area of tendons increases from 155 mm^2 for the applied loading $P=45$ kN to 195 mm^2 for the

applied loading $P=55$ kN. The optimum area is increased when the applied load is increased.

The increases of the applied load on the one-way slab leads to increase in the tensile stress in concrete due to the increase in the positive bending moment and to keep the level of tensile stress in allowable limits it requires to increase the negative bending moment. For the increases of the negative bending moment it requires to increase in the area of tendons or the initial stress in tendons.

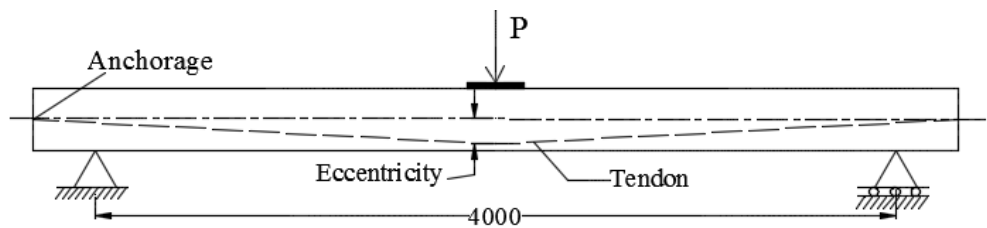


Figure 6.20 Loading of UPT slab for the load optimization.

Table 6.6 Initial and design optimization values for UPT slab.

Total applied load (kN)	Initial values				Optimum value				Reduction	
	w (g)	a (mm ²)	i (MPa)	e (m)	w (g)	a (mm ²)	i (MPa)	e (m)	w	a
45	23736	230	1200	0.005	15996	155	1155	0.0439	33 %	33 %
50	23736	230	1200	0.005	17956	174	1140	0.0438	24 %	24 %
55	23736	230	1200	0.005	20124	195	1160	0.0437	15 %	15 %

6.4.3.2 Effect of number of applied point loads on the optimization of UPT slab

To study the effect of a number of applied point loads on the optimum values for UPT slab, the total weight of PT tendons optimization for the UPT slab is redesigned by applying four types of point loading. The four types of loading are one, two, three and four point loads. The loading of the UPT slab is shown in Figure 6.21. The objective, design variables and constraints developed herein are the same that in Section 6.4.3. Behavioral constraints dictated by the ACI-318 code are explained in Table 6.1 and are evaluated according to the lower and upper limits of the design variables given in Table 6.5 for the maximal loading.

Table 6.7 shows the initial and the design optimum values for UPT slab for different types of loading. From Table 6.7, it can be noted that the optimum values of total

weight of PT tendons and area of tendons are affected by the number of applied point loads. From Table 6.7, it can be found that the optimum value of the area of tendons decreases from 175 mm² for 1 point loading to 75 mm² for 4 point loading when the total applied load is kept constant. From this table, it is evident that the critical type of loading is when the load is applied near the mid-span of the UPT slab.

When the load is applied near the mid-span of the one-way slab leads to increase in the tensile stress in concrete due to the increase in the positive bending moment and because the maximum tensile stress controls the optimization convergence must keep the level of tensile stress in allowable limits. For the increases of the negative bending moment it requires to increase in the area of tendons or the initial stress in tendons.

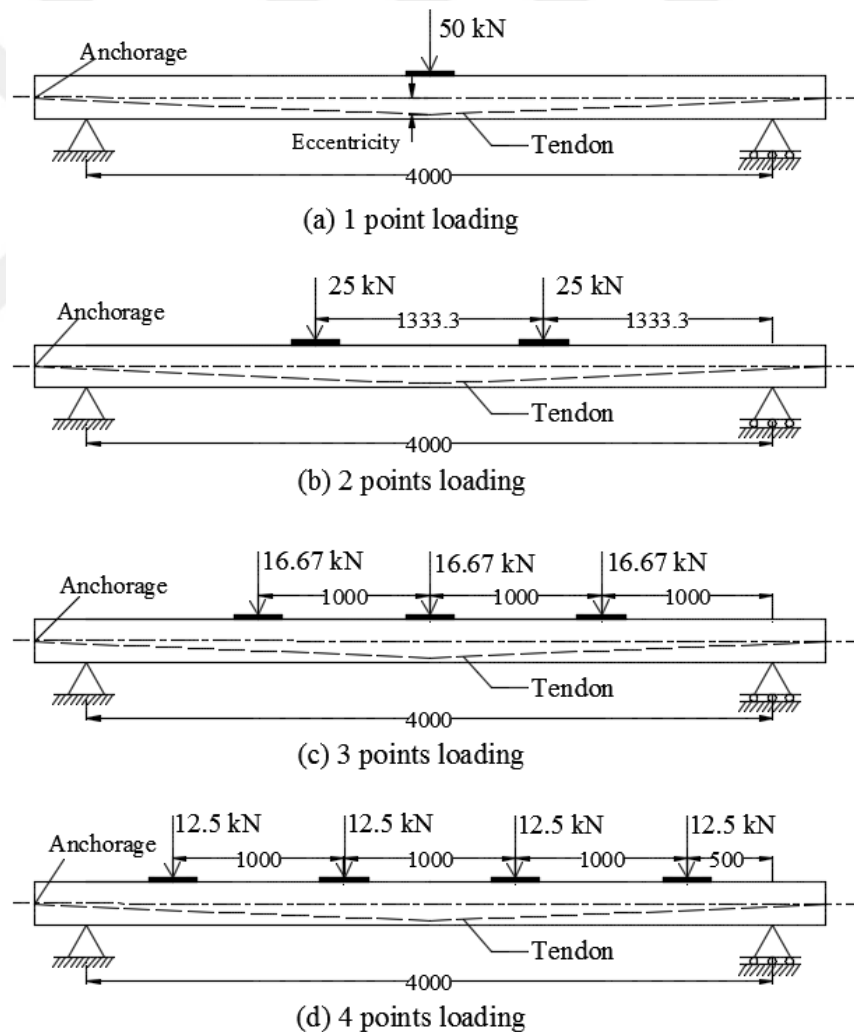


Figure 6.21 Loading of UPT slab for the number of applied point load optimization.

Table 6.7 Initial and design optimization values for UPT slab for different type of loading.

Type of loading	Initial values				Optimum value				Reduction	
	w (g)	a (mm ²)	i (MPa)	e (m)	w (g)	a (mm ²)	i (MPa)	e (m)	w	a
1 point loading	23736	230	1200	0.005	17956	174	1140	0.0438	24 %	24 %
2 points loading	23736	230	1200	0.005	11352	110	1155	0.0437	52 %	52 %
3 points loading	23736	230	1200	0.005	11145	108	1180	0.0438	53 %	53 %
4 points loading	23736	230	1200	0.005	7740	75	1194	0.0439	67 %	67 %

6.5 Optimization of Post-Tensioned Concrete Slabs Using Genetic Algorithm

Earlier, the engineers experience and their intuitions played the key role in designing a structure. But in the present stage, there are numerous techniques that helps to create an economical section, in which optimization techniques are the most efficient method. Optimization helps to achieve a feasible design, for a specified design objective. There are many optimization techniques based on mathematical programming to obtain optimum solutions. In the advanced optimization techniques, the GA is the most popular method. It is based on the theory of natural selection and genetics.

In the last three decades, heuristic methods have been rapidly developed to solve optimization problems. These methods are principally intuitive and do not have theoretical support. Heuristic methods such as GAs, simulated annealing and tabu search provide general ways to search for a good but not necessarily the best solution.

Manoharan and Shanmuganathan (1999) applied four different search mechanisms of simulated annealing, tabu search, GA and branch and bound technique to the design optimization of three different truss problems and compared them. They concluded that all three heuristic search methods simulated annealing, tabu search and GA, work well and produce an acceptable solution within a reasonable amount of time. Amongst these three methods, GA has a feature that it does not need an initial guess to search for the optimum. Branch and bound technique consumes an enormous amount of computing time to find optimum solution. Also, it is not viable for structures of any reasonable size (e.g. a truss structure with more than 6 bars).

6.5.1 Genetic algorithms

GAs were introduced by Holland in the 1960s (Holland, 1975). With the aid of his colleagues and students, he developed these algorithms during the 1970s in University of Michigan. He summarized the results of these researches in the book “Adaptation in natural and artificial systems” (Holland, 1975). GAs are numerical optimization techniques inspired by the natural evolution laws. A GA starts searching design space with a population of designs, which are initially created over the design space at random. In the basic GA, every individual of population (design) is described by a binary string (encoded form). GA uses four main operators, namely, selection, creation of the mating pool, crossover and mutation to direct the population of designs towards the optimum design.

In the selection process, some designs of a population are selected by randomized methods for GA operations, for example in creation of the mating pool, some good designs in the population are selected and copied to form a mating pool. The better (fitter) designs have a greater chance to be selected. Crossover allows the characteristics of the designs to be altered. In this process different digits of binary strings of each parent are transferred to their children (new designs produced by the crossover operation). Mutation is an occasional random change of the value of some randomly selected design variables. The mutation operation changes each bit of string from 0 to 1 or vice versa in a design’s binary code depending on the mutation probability. Mutation can be considered as a factor preventing from premature convergence.

A GA uses a discrete set of design variables in the optimization process. However, by defining the number of decimal digits for representation of continuous variables or step size between the sequential values of design variables this method can be applied to continuous problems as well.

GAs are based on the principles of natural genetics and natural selection. The basic elements of natural genetics, reproduction, crossover, and mutation, are used in the genetic search procedure. GAs differ from the traditional methods of optimization in the following respects (Rao, 2009):

1. A population of points (trial design vectors) is used for starting the procedure instead of a single design point. If the number of design variables is n , usually the size of the population is taken as $2n$ to $4n$. Since several points are used as candidate solutions, GAs are less likely to get trapped at a local optimum.
2. GAs use only the values of the objective function. The derivatives are not used in the search procedure.
3. In GAs the design variables are represented as strings of binary variables that correspond to the chromosomes in natural genetics. Thus the search method is naturally applicable for solving discrete and integer programming problems. For continuous design variables, the string length can be varied to achieve any desired resolution.
4. The objective function value corresponding to a design vector plays the role of fitness in natural genetics.
5. In every new generation, a new set of strings is produced by using randomized parents selection and crossover from the old generation (old set of strings). Although randomized, GAs are not simple random search techniques. They efficiently explore the new combinations with the available knowledge to find a new generation with better fitness or objective function value.

6.5.2 Interface MATLAB and ANSYS

The aim is to optimize the total weight of PT tendons for the PT one-way concrete slabs under constraint of limiting the stress to the allowable stress. The analysis of slab is carried out in ANSYS. ANSYS is coupled with MATLAB. The software helps to program FE model by using a text file to automate the optimization methodology. The coupling between MATLAB and ANSYS is done by a line-code.

The points of the interfacing process of ANSYS and MATLAB are presented in Appendix A.

The PT slab analysis will be carried out with ANSYS (ANSYS, 2012), which is FE software. It is worth highlighting that any other FE software (either licensed or opened source) may be used to be coupled with MATLAB. The requirement to be fulfilled is that the software must allow programming the FE model by means of a

text file in order to be able to automate the proposed optimization methodology shown in Figure 6.22.

The coupling between MATLAB and the FE software is done by means of line code which will be detailed in Appendix A. For the particular case analyzed in this study ANSYS has been used. The complete creation and solving of a structure may be done either by picking on the different menus or by programming in APDL. The main advantage of creating and solving a model by means of APDL is that the model can be defined in terms of variables, thus creating a parametric model. In terms of the optimization loop it is very convenient to create a parametric model as an automatic loop can be created without user intervention. The values of the different variables will be changing according to the optimization loop until a minimum is reached. APDL allows, among other features, creation of files in text format to store the results of the analyzed model. These files will be used by the optimization tool in order to redefine better values for the variables of the slab.

Figure 6.22 resumes the optimization loop. In the depicted figure the output of each of the steps is also shown. It can be seen that the information between ANSYS and MATLAB is based on text files which are overwritten in each loop. All of the created files must be placed on the same folder.

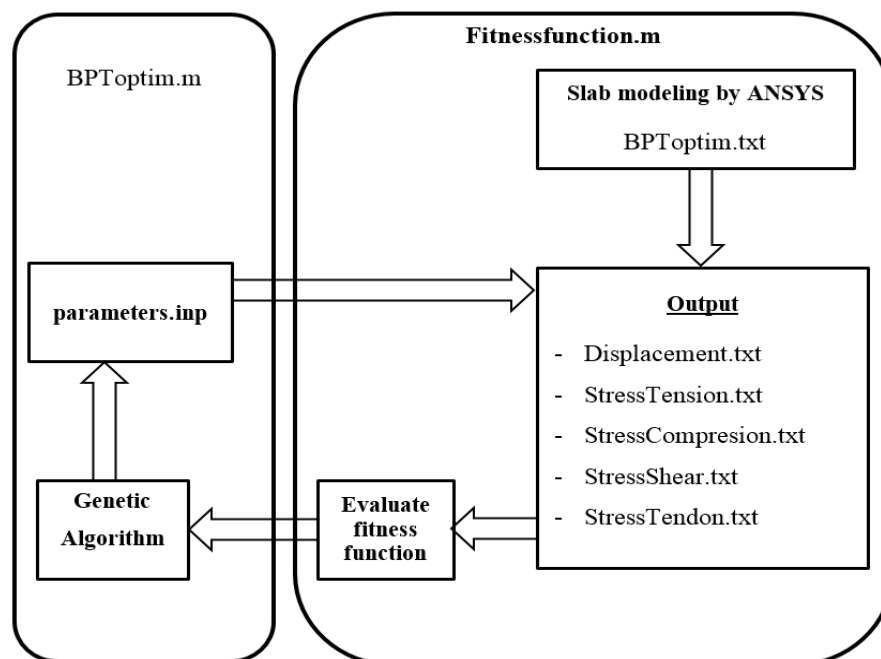
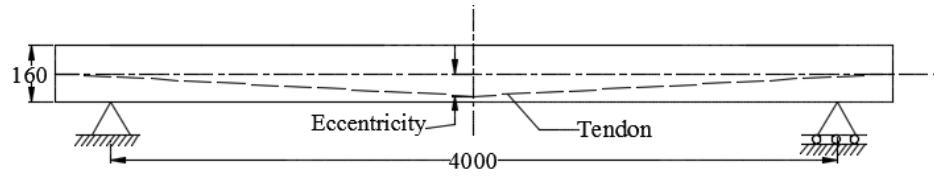


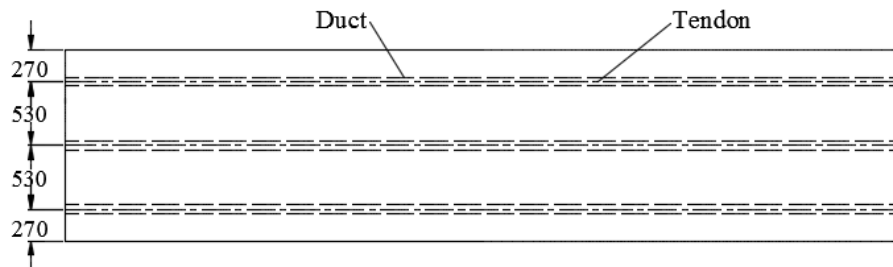
Figure 6.22 Optimization with GA.

6.5.3 Total weight of PT tendons minimization for the BPT slab using GA

In this part, the BPT one-way concrete slab is optimized. The dimension of BPT slab is shown in Figure 6.23, and the loading considered for the proposed study is shown in Figure 6.24.



(a) General layout of slab



(b) Plan view of slab

Figure 6.23 Dimensions of BPT slab (mm) for the optimization with GA.

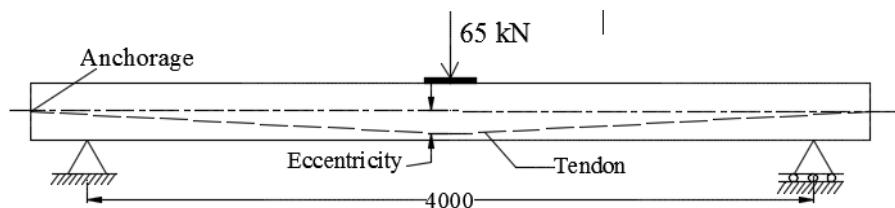


Figure 6.24 Loading of BPT slab for optimum design for the optimization with GA.

The slab is designed to behave as a fully PT concrete member, reinforced with fully BPT tendons with no regular rebar. The types of loads considered are the gravitational dead and static point loads. Lateral loading was not considered. Pre-stressing was considered as a variable in the optimization process.

The aim is to optimize the total weight of PT tendons for the BPT one-way slab under constraint of limiting the stress to the allowable stress. The analysis of slab is

carried out in ANSYS. ANSYS is coupled with MATLAB. The software helps to program FE model by using a text file to automate the optimization methodology. The coupling between MATLAB and ANSYS is done by a line-code.

The objective of the optimization procedures developed herein is to minimize the total weight of PT tendons. The design variables are the area of PT tendons, the initial stress in tendons and the eccentricity of the tendon profile at mid-span of the slab. Behavioral constraints dictated by the ACI 318 are explained in Table 6.8.

Table 6.8 Constraints specified by the ACI 318 for the optimization with GA.

	Constraints	Limit
1	Compression stresses in concrete, f_c	$f_c > -0.6 f'_c$
2	Tension stresses in concrete, f_t	$f_t < 0.5\sqrt{f'_c}$
3	Stresses in steel tendons, f_{tendon}	$f_{tendon} < 0.7f_{pu}$
4	Shear stress, V_r	$V_r > V_f$
5	Displacement at mid-span of the slab, U_y	$U_y < l/360$

where: f'_c is the specified compressive strength of concrete; f_c is the compression stresses in concrete (obtained from FE analysis); f_t is the tensile stresses in concrete (obtained from FE analysis); f_{pu} is the specified tensile strength of PT tendons; f_{tendon} is the stresses in PT tendon (obtained from FE analysis); V_r is the factored shear stress resistance; V_f is the factored shear stress; U_y is the displacement at mid-span of the slab (obtained from FE analysis) and l is the span length.

In order to minimize the total weight of PT tendons, it is necessary to respect the imposed constraints conditions: normal stress in concrete, stress in steel tendon, shear stress in concrete and displacement at mid-span of the slab. These parameters are evaluated according to the upper and lower limits of the design variables given in Table 6.9.

The optimized values obtained by interfacing ANSYS and MATLAB using GA is as shown in Table 6.9. The optimized values of design variables directly obtain in the MATLAB toolbox. It also displays the optimum value. The number of iterations carried out is also displayed in the toolbox.

The optimized parameters obtained for BPT one-way slab are as shown in Table 6.9. The optimization showed that by interfacing MATLAB and ANSYS 22 % reduction of total weight of PT tendons is obtained for the given design constraints.

Table 6.9 Initial, optimum and limits of design variables and constraints for the optimization with GA.

		Minimum	Initial value	Maximum	Optimum
Objective	w (g)	----	23736	----	18472
Design variables	a (m ²)	0.00005	0.00023	0.0005	0.000179
	i (MPa)	1030	1148	1250	1170
	e (m)	0.0	0.005	0.044	0.0439
Constraints	Max. f_c (MPa)	-20.0	----	0.0	----
	Max. f_t (MPa)	0.0	----	2.7	----
	Max. f_{iendon} (MPa)	0.0	----	1430	----
	Max. V_r (MPa)	0.0	----	9.0	----
	Max. U_y (mm)	0.0	----	11.0	----

where: a is the area of PT tendons, i is the initial stress in tendons and e is the eccentricity of the tendon profile.

From Table 6.9, it can be observed that a significant reduction in area of PT tendons from 0.00023 m² for the initial state to 0.000179 m² for the converged solution. This reduction is significant, which (approximately equals 22 % of the initial area).

CHAPTER 7

CONCLUSIONS

7.1 Conclusions

The PT slabs commonly used in building and bridge construction are grouped into two basic categories. These are the unbonded and bonded systems. The use of post-tensioning system allows for material savings due to reduced slab thickness. Moreover, cracking and deflection of the concrete slabs can be reduced by using post-tensioning. Post-tensioning of concrete slabs can be conducted using unbonded or bonded tendons. In bonded systems, the tendons are fully bonded to the surrounding material. The tendons are inserted into the ducts and after the pre-stressing load is applied, the ducts are filled with cementitious grout to achieve the required bond between the tendon and the concrete. For bonded systems, there is in principle uniform steel-concrete force transfer along the length of the tendons and full strain compatibility is assumed, implying that steel strains are equal to concrete strains.

A nonlinear FE model for the analysis of PT unbonded and bonded concrete slabs at elevated temperatures was developed in this study. The interface between the tendon and surrounding concrete was also modelled, allowing the tendon to retain its profile shape during the deformation of the slab. The computer program ANSYS is used to model and analyze PT concrete one-way slab. SOLID65 (or 3D reinforced concrete solid) is utilized for 3D modelling of concrete, which is capable of crushing in compression and cracking in tension. Tendons and reinforcement were represented using 2-node discrete link elements (LINK8), which are included within the properties of 8-node brick elements. To prevent stress concentration, steel plates were added at location of loading. SOLID45 is used for 3D modelling of steel plates having 8-nodes with 3-degrees of freedom at each node. The contact between the concrete and the tendon is modeled by contact elements (using the CONTACT PAIR MANAGER). The method requires the definition of two surfaces that are the target

and the contact surfaces. Several contact behaviour are available in ANSYS. For the unbonded tendons the standard behavior was used, while the bonded behaviour was used for bonded tendons. To avoid the ends from crushing the shell plates must be applied at ends. SHELL181 is suitable for analyzing shell structures.

Thermal-stress applications are treated in a so-called coupled-field analysis, which consider into account the interaction between thermal expansion/contraction and mechanical stress. The transfer from structural to thermal analysis is done in ANSYS as the elements are switched from SOLID65 structural element to SOLID70 thermal element. The distributions of thermal elastic stress components are then calculated by switching the thermal SOLID70 element to structural SOLID65 element which is used for 3D modelling of solid structures. The FE solution performed via ANSYS calculates nodal temperatures, and then use the nodal temperatures to obtain other thermal quantities.

For the verification of the current numerical model, experimental unbonded and bonded PT concrete slabs were chosen from literature. The load–deflection behaviour, load–force behaviour in the tendon, and the failure modes are presented. The experimental and numerical load deflection curves obtained for slabs show good agreement between the experimental and the FE results.

The verified FE model was used to investigate the effect of several selected parameters on the overall behaviour of PT one-way concrete slabs. These parameters include the effect of tendon bonding, the effect of thermal loading and the effect of tendon profile.

From the analytical results obtained in this study the following conclusions can be drawn:

- 1- The behaviour of BPT concrete slabs is more complicated by reason the presence of ducts, the bond between concretes and ducts, the bond between ducts and grout, and the bond between grout and tendons. Two stages of analysis are needed for bonded slabs. At the first stage the slab is analyzed as UPT slab under prestress loading and gravity loading only. Next the slab is analyzed as bonded post tensioned slab. The two stages are needed because the grout is added after the prestressing of the strands.

- 2- It was observed that the ultimate load capacity for slab with a bonded tendon increased by 9 % compared to the same slab with unbonded tendon. The higher ultimate capacity for bonded slab is due to the additive stiffness obtained by tendon-concrete bond. The force in bonded tendon is higher than the force in unbonded tendon in the center of the slab, while the opposite stands at the support.
- 3- It was found that the failure loads for the restrained slabs are greater than free end slabs.
- 4- It was observed, for restrained slabs under thermal loading, that the failure load capacity for slab with bottom surface hotter load is the smallest due to the effect of thermal strain. The thermal strain coming from the bottom surface hotter load causes tensile stress at top and high compressive stress at the bottom which is the in the opposite sign with prestress stress, and hence decreases the prestress stress.
- 5- It was found that losses in prestress force on restrained slab under thermal loading is smaller when the slab is bonded and subjected to top surface hotter load, while the losses is higher when the slab is bonded and subjected to uniform temperature load. The losses in tendon force occur due to increase in compressive stress at bottom fiber and especially for restrained slab.
- 6- For free slabs under thermal loading, it was found also that the failure load capacity for slab with bottom surface hotter load is the smallest.
- 7- For the effect of tendon profile, it was observed that the straight bottom profile resulted in the maximum load capacity for the simply supported post tensioned slab. For the fixed end post tensioned slab, the parabolic profile showed the maximum load capacity.

Optimization in its wide sense can be used to solve many engineering problems and to find the best solutions that a designer can gain a maximum benefit from the available resources. A 3D FE model for the optimization of bonded and unbonded PT concrete one-way slab was also developed in this study. The total weight of PT tendons for the PT concrete slab was considered as the objective function. The design variables are the area of PT tendons, the initial stress in tendons and the eccentricity of the tendon profile while the constraints are the normal stress in concrete, the stress in steel tendon, the shear stress in concrete and the displacement

at mid-span of the slab. From the optimization procedures developed in this study the following conclusions can be drawn:

- 1- The data developed in this study indicated that the total weight of PT tendons reduction was more evident in the optimized bonded and unbonded PT concrete slab than the non-optimized slab. As the result, the total weight of PT tendons was reduced approximately 22 % and 24 % for the bonded and unbonded respectively. A significant reduction in the area of PT tendons was also reached which was approximately 22 % and 24 % for the bonded and unbonded respectively.
- 2- The mid-span deflection and maximum tension stress were decreased during the optimization iterations within the allowable limits due to the decrease in the eccentricity of the tendons. It was also noticed that the optimum area has increased when the magnitude of applied load is increased.
- 3- The optimum values of total weight of PT tendons and the area of tendons are affected by the number and location of the applied point loads. It is obvious that the critical type of loading is when the load is applied near the mid-span of the BPT slab.

In this study an optimization technique, GA is implemented by coupling MATLAB and ANSYS. Thus the FE analysis of ANSYS can be effectively utilized in the search algorithm in MATLAB. In this study a BPT slab is optimized using the above methodology. It helps to obtain an optimum design complying with the design constraints. The total weight of PT tendons of PT slab is optimized under constraint of stress limited to the allowable stress.

7.2 Recommendations for Future Study

To follow up this study, the following topics can be suggested:

- 1- Study the flexure behavior of two-way PT concrete slabs.
- 2- Study the behavior of PT concrete slabs subjected to fire.
- 3- Study the behavior of PT bubbled concrete slabs.
- 4- Study the behavior of PT concrete slabs with opening.

REFERENCES

- Abdullah, A. B. (2015). A tendon monitoring framework for unbonded post-tensioned bridges based on anchor strain response, Doctoral dissertation, University of Florida.
- Abeles, P.W. (1965). An introduction to prestressed concrete, *Concrete Publication Ltd*, **2**, 555.
- ACI Committee 318 (2011). Building code requirements for structural concrete (ACI 318-11) and commentary, Farmington Hills.
- Al-Gahtani, A. S., Al-Saadoun, S. S., Abul-Feilat, E. A. (1995). Design optimization of continuous partially prestressed concrete beams, *Computers & Structures* , **55(2)**, 365-370.
- Aimin, Y., Yuli, D., Litang, G. (2013). Behavior of unbonded prestressed continuous concrete slabs with the middle and edge span subjected to fire in sequence, *Fire safety journal*, **56**, 20-29.
- Allouche, E. (1999). Tendon stressed in continous unbonded prestressed concrete members, *PCI journal*, **44(1)**, 60-73.
- Al-Thebhawe, H. W. (2001). Nonlinear finite element analysis of prestressed concrete members, M.Sc. Thesis, University of Technology, Iraq.
- Amir, O. (2013). A topology optimization procedure for reinforced concrete structures, *Computers and Structures*, **114–115**, 46–58.
- ANSYS (2012). ANSYS Help, Release 14.5, Copyright.
- Atabay, S., Gulay, F. G. (2009). The study of the effect of changes in cost of the materials used in 3-D shear-wall reinforced concrete structures on the optimum dimensions, *Expert Systems with Applications*, **36(3)**, 4331–4337.
- Ayoub, A., Filippou, F. C. (2009). Finite-element model for pretensioned prestressed concrete girders, *Journal of structural engineering*, **136(4)**, 401-409.
- Bailey, C. G., Ellobody, E. (2009a). Fire tests on unbonded post-tensioned one-way concrete slabs, *Magazine of Concrete Research*, **6**, 67-76.
- Bailey, C. G., Ellobody, E. (2009b). Fire tests on bonded post-tensioned concrete slabs, *Engineering Structures*, **31**, 686-696.
- Bathe, J. (1996). Finite Element Procedures, Prentice-Hall Inc., U.S.A.
- Bennegadi, M.L., Sereir, Z., Amziane, S. (2013). 3D nonlinear FE model for the volume optimization of a RC beam externally reinforced with a HFRP plate, *Construction and Building Materials*, **38**, 1152-1160.

- Bums, N. H., Helwig, T., Tsujimoto, T. (1991). Effective prestress force in continuous post-tensioned beams with unbonded tendons, *ACI Structural Journal*.
- Campbell, T. I., Chouinard, K. I. (1991). Influence of nonprestressed reinforcement on the strength of unbonded partially prestressed concrete members, *ACI Journal*, **88**(5), 546-551.
- Chaitanya Kumar, J.D, Venkat, L. (2013). Genetic algorithm based optimum design of prestressed concrete beam, *International Journal of Civil and Structural Engineering*, **3**(3), 644-654.
- Chakrabarti, P. R., Whang, T. P. (1989). Study of partially prestressed beams with unbonded post-tensioning, *In Structural Design Analysis and Testing*, 189-200.
- Chakrabarti, P. R., Whang, T. P., Brown, W., Arsad, K. M., Amezeua, E. (1994). Unbonded Post-Tensioning Tendon and Partially Prestressed Beams, *ACI Structural Journal*, **91**(5), 616-625.
- Chen W. F. (1982). *Plasticity in Reinforced Concrete*, McGraw-Hill Book Company.
- Chen W. F., Saleeb A. F. (1982). *Constitutive equations for engineering materials*, John Wiley and Sons Inc.
- Desayi, P., Krishnan, S. (1964). Equation for the stress-strain curve of concrete, *Journal of the American Concrete Institute*, **61**, 345- 350.
- Díaz, J., Hernández, S., Fontán, A. Romera, L. (2010). A computer code for finite element analysis and design of post-tensioned voided slab bridge decks with orthotropic behavior, *Advances in Engineering Software*, **41**, 987–999.
- Ellobody, E. A., Bailey, C. G. (2008). Modelling of bonded post-tensioned concrete slabs in fire, *Proceedings of the Institution of Civil Engineers-Structures and Buildings*, **161**(6), 311-323.
- Ellobody, E., Bailey, C. G. (2009). Modelling of unbonded post-tensioned concrete slabs under fire conditions, *Fire Safety Journal*, **44**, 159–167.
- European Committee for Standardization (CEB), Eurocode 3 (1993). *Design of Steel Structures, Part 1.1: General Rules and Rules for Buildings*, DD ENV, 1-1, EC3.
- Euser, M. K., Mehlhorn, G., Cornelius, V. (1983). Bond between prestressed steel and concrete—computer analysis using ADINA, *Computers & Structures*, **17**(5-6), 669-676.
- Fanning, P. (2001). Nonlinear models of reinforced and post-tensioned concrete beams, *Electronic Journal of Structural Engineering*, **2**, 111-119.
- Gilbert R. I., Mickleborough N. C. (1990). *Design of prestressed concrete*, Spon Press, London .
- Gribniak V., Kaklauskas G., Hung Kwan, A. K., Bacinskas, D., Ulbinas, D. (2012). Deriving stress– strain relationships for steel fibre concrete in tension from tests of beams with ordinary reinforcement, *Engineering Structures*, **42**, 387–395.

- Harajli, M. H. (1990). Effective of span-depth ratio on the ultimate steel stress in unbonded prestressed concrete member, *ACI Structural Journal*, **87**(3), 305-312.
- Harajli, M., Khairallah, N., Nassif, H. (1999). Externally prestressed members: evaluation of second-order effects, *Journal of Structural Engineering*, **125**(10), 1151-1161.
- Harajli, M. H. (1993). Strengthening of Concrete Beams by External Prestressing, *PCI Journal*, **38**(6).
- Harajli, M.H., Kanj, M.Y. (1991). Ultimate flexural strength of concrete members prestressed with unbonded tendons, *ACI Structural Journal*.
- Hegger, J., Roggendorf, T., Teworte, F. (2010). FE analyses of shear-loaded hollow-core slabs on different supports, *Magazine of concrete research*, **62**(8), 531-541.
- Holland, J.H. (1975). Adaptation in natural and artificial systems, University of Michigan, Ann Arbor.
- Hoyer, E. A. (1939). Contribution towards the question of bond strength, in *Beton und Eisen, Berlin*, **38**(6), 107-110.
- Hussien, O. F., Elafandy, T. H. K., Abdelrahman, A. A., Baky, S. A., Nasr, E. A. (2012). Behavior of bonded and unbonded prestressed normal and high strength concrete beams, *HBRC Journal*, **8**(3), 239-251.
- Kang, T., Huang, Y. (2012). Computer modeling of post-tensioned structures, *4th International Conference on Computer Modeling and Simulation (ICCMS 2012), Singapore*, **22**, 41-45.
- Kasat, A. S., Varghese V. (2012). Finite element analysis of prestressed concrete beams, *International Journal of Advanced Technology in Civil Engineering*, **1**(3,4), 2231 –5721.
- Kim, K. S., Lee, D. H. (2012). Nonlinear analysis method for continuous post-tensioned concrete members with unbonded tendons, *Engineering Structures*, **40**, 487–500.
- Kim, M. S., Lee, Y. H. (2016). Flexural behavior of posttensioned flat plates depending on tendon layout, *Advances in Materials Science and Engineering*, **2016**.
- Kim, N. H. (2014). Introduction to nonlinear finite element analysis. New York: Springer Science and Business Media.
- Kim, U., Chakrabarti, P. R., Choi, J. H. (2012). Nonlinear finite element analysis of unbonded post-tensioned concrete beams, Challenges, Opportunities and Solutions in Structural Engineering and Construction “, Chapter 16 ,Taylor & Francis Group, London, ISBN 978-0-415-56809-8, 99-104.
- Koziey B. L., Mirza F. A. (1995). Consistent thick shell element, *Computers and Structures*, **65**(4), 531–549.
- Krauser, G. (2009). Optimization of two-way post-tensioned concrete floor systems , M.Sc. Thesis , Faculty of California Polytechnic State University.

- Kupfer H., Hilsdorf K., Rusch H. (1969). Behavior of concrete under biaxial stress, *Journal of American Concrete Institute*, **66** (8), 656-666.
- Kuyucular, A. (1991). Prestressing optimization of concrete slabs, *Journal of Structural Engineering*, **117**(1), 235–254.
- Litvan, G. G. (1996). Waterproofing of parking garage structures with sealers and membranes, *Construction and Building Materials*, **10**(1), 95-100.
- Lou, T. J., Xiang, Y. Q. (2006). Finite element modeling of concrete beams prestressed with external tendons, *Engineering structures*, **28**(14), 1919-1926.
- Lou, T., Lopes, S. M. R., Lopes, A. V. (2013). Nonlinear and time-dependent analysis of continuous unbonded prestressed concrete beams, *Computers and Structures*, **119**, 166–176.
- Lounis, Z., Cohn, M. Z. (1993). Multiobjective optimization of prestressed concrete structure, *Journal of Structural Engineering*, **119**(3), 794–808.
- MacRae, A. J., Cohn, M. Z. (1987). Optimization of prestressed concrete flat plates, *Journal of Structural Engineering*, **113**(5), 943–957.
- Manalip, H., Pinglot, M., Lorrain, M. (1994). Behavior of the compressed zone of reinforced and prestressed high-strength concrete beams, *Special Publication*, **149**, 209-226.
- Manoharan, S., Shanmuganathan, S. (1999). A comparison of search mechanisms for structural optimization, *Computers & Structures*, **73**(1-5), 363-372.
- Merritt F. S., Ricketts J.T. (2001). Building design and construction handbook, Sixth Edition, McGraw-Hill.
- Moaveni, S. (1999). Finite element analysis theory and application with ANSYS, Upper Saddle River, New Jersey, U.S.A.
- Naghipour, M., Nemati, M., Doostdar, H. M. (2010). Experimental study and modeling of reinforced concrete beams strengthened by post-tensioned external reinforcing bars, *International Journal of Engineering*, **23**(2), 127-144.
- Nan Zhanga, N., Fub, C. C., Chec H. (2011). Experiment and numerical modeling of prestressed concrete curved slab with spatial unbonded tendons, *Engineering Structures*, **33**, 747–756.
- Nawy, E.G. (2010). Prestressed concrete: a fundamental approach, 5th edition, Prentice Hall, Pearson Education, Inc., Upper Saddle River, N.J..
- Nowak, A. S. (1994). Calibration of the Ontario highway bridge design code, *Canadian Journal of Civil Engineering*, **21**(1), 25-35.
- Öztorun, N. K., Utku, M. (2002). Computer aided design of post-tensioned concrete reservoirs, *Computers and Structures*, **80**, 2195–2207.
- Park, R., Paulay (1975). Reinforced concrete structures. John Wiley and Sons.

- Peng, Q., Liu, W. (2013). Inverse analysis of related parameters in calculation of concrete drying shrinkage based on ANSYS design optimization, *Journal of Materials in Civil Engineering*, **25** (6), 683-692.
- Rabczuk, T., Belytschko, T. (2006). Application of particle methods to static fracture of reinforced concrete structures, *International Journal of Fracture*, **137**(1-4), 19-49.
- Rabczuk, T., Eibl, J. (2004). Numerical analysis of prestressed concrete beams using a coupled element free Galerkin/finite element approach, *International Journal of Solids and Structures*, **41**(3), 1061-1080.
- Rahul, Kumar, K. (2014). Design and optimization of portable foot bridge”, *Procedia Engineering*, **97**, 1041 – 1048.
- Ranzi, G., Al-Deen, S., Ambrogi, L., Uym, B. (2013). Long-term behaviour of simply-supported post-tensioned composite slabs, *Journal of Constructional Steel Research*, **88**, 172-180.
- Ranzi, G., Al-Deen, S., Hollingum, G., Hone, T., Gowripalan, S., Uy, B. (2013). An experimental study on the ultimate behaviour of simply-supported post-tensioned composite slabs, *Journal of Constructional Steel Research*, **89**, 293-306.
- Rao, S. S. (2009). Engineering Optimization Theory and Practice, 4th edition, John Wiley & Sons, Inc., U.S.A.
- Rozvany, G. I. N., Hampson, A. J. K. (1963). Optimum design of prestressed plates, *Journal of the American Concrete Institute*, **60**(8), 1065–1082.
- Sahab M.G., Ashourb A.F., Toropov V.V. (2005). Cost optimisation of reinforced concrete flat slab buildings, *Engineering Structures*, **27**, 313–322.
- Sahab, M. G., Ashour, A. F., Toropov, V. V. (2005). A hybrid genetic algorithm for reinforced concrete flat slab buildings, *Computers & Structures*, **83**(8-9), 551–559.
- Schmit L. A. (1960). Structural design by systematic synthesis”, Proceedings, 2nd conference on electronic computation, *ACSE*, 105-122.
- Semelawy, M. El, Nassef, A.O., El Damatty, A. A. (2012). Design of prestressed concrete flat slab using modern heuristic optimization techniques, *Expert Systems with Applications*, **39**, 5758–5766.
- Simpson, T. W., Booker, A. J., Ghosh, D., Giunta, A. A., Koch, P. N., Yang, R., J. (2004). Approximation methods in multidisciplinary analysis and optimization-a panel discussion, *Structural and Multidisciplinary Optimization*, **27**, 302-313.
- Tan, K. H., Ng, C. K. (1997). Effects of deviators and tendon configuration on behaviour of externally prestressed beams, *ACI Structural Journal*, **94**(1), 13-22.
- Tao, X., Du, G. (1985). Ultimate stress of unbonded tendons in partially prestressed concrete beams, *PCI Journal*, **30**(6), 72-91.
- Tavarez, F.A. (2001). Simulation of behavior of composite grid reinforced concrete beams using explicit finite element methods, M.Sc. Thesis, University of Wisconsin-Madison.

The Post-Tensioning Institute (PTI), formed in 1976, provides research, technical development, marketing, and promotional activities for companies engaged in post-tensioned prestressed construction. Their website is <http://www.post-tensioning.org>

Vu, N. A., Castel, A., François, R. (2010). Response of post-tensioned concrete beams with unbonded tendons including serviceability and ultimate state, *Engineering Structures*, **32(2)**, 556-569.

Willam, K., Warnke, E. (1975). Constitutive model for the triaxial behavior of concrete, *International Association for Bridge and Structural Engineering*, **19**, ISMES.

Williams, M.S., Waldron, P. (1989). Movement of unbonded post-tensioning tendons during demolition, *Proceedings of the Institution of Civil Engineers*, Part 2, **87**, 225-253.

Wolanski, A. J. (2004). Flexural behavior of reinforced and prestressed concrete beams using finite element analysis, M.Sc. Thesis, University of Marquette.

Yang, K. H., Mun, J. H., Kim, G. H. (2013). Flexural behavior of post-tensioned normal-strength lightweight concrete one-way slabs, *Engineering Structures*, **56**, 1295–1307.

Zebun, M. A. (2006). Behavior and strength of steel-concrete-steel sandwich beams with partial shear connection, Ph.D. Thesis, University of Al-Mustansiriya, Iraq.

Zhang, N., Fu, C. C., Che, H. (2011). Experiment and numerical modeling of prestressed concrete curved slab with spatial unbonded tendons, *Engineering Structures*, **33(3)**, 747-756.

Zheng, W., Hou, X. (2008). Experiment and analysis on the mechanical behaviour of PC simply-supported slabs subjected to fire, *Advances in Structural Engineering*, **11(1)**, 71-89.

APPENDIX A

Interfacing process of ANSYS and MATLAB

In this work optimization toolbox is used to implement GA. The following are the points summarizing the interfacing process of ANSYS and MATLAB:

1. Initially the algorithm creates a random population.
2. This initial population then becomes the scalar parameter for ANSYS.
3. ANSYS is then run in batch mode from MATLAB and produce the output files.
4. The output files from ANSYS is then read into MATLAB for checking the constraint conditions.
5. If the check is satisfied then the total weight of PT tendons is accepted, else MATLAB returns an invalid value.
6. The algorithm then creates a new sequence of populations. In every step, the algorithm utilizes the individuals in the current generation to obtain the next population.
7. Finally the algorithm comes to a stops when any one of the stopping criteria is met.

The fitness function is defined in a MATLAB file which is the one that will call ANSYS so that it runs in batch mode, that is, so that it runs under the operating system without intervention of the user. The file “fitnessfunction.m” stores the optimized parameters in the file “parameters.inp”, executes ANSYS in batch mode and evaluates the fitness function.

During the first part the developed program stores the provided values of design variables from the GA (“BPToptim.m”) to individual variables. Next, these individual variables are stored in the file “parameters.inp” which will be used to create the slab geometry. Afterwards, ANSYS is executed from “fitnessfunction.m” by means of the command specified following command code: (!"C:\Program Files\ANSYS Inc\v121\ansys\bin\WINX64\ANSYS.exe" -b -

```
J BPTOPTIM -DIR "D:\PhD\Semester No 8\TB1-Optim" -i "D:\PhD\Semester  
No 8\GA optim\BPToptim.TXT")
```

In addition, it must be checked on the help tool how to run the FE software in batch mode. Batch mode allows the software to be run under system without specifically opening it by providing an input text file in which the FE model is programmed. For ANSYS, batch mode is run with the specific commands described above. The third part of the code provided above the file route that points to the input FE model text file in which the FE model is programmed. When using different FE software the programming written in the input file will vary as it has to follow the appropriate commands for the specific employed FE software.

The optimization loop will flow through the following steps:

- The file “BPToptim.m” creates the file “parameters.inp” which stores the value of the design variables of the slab. This file is the one that runs the GA, which needs to evaluate the fitness function.
- Once the file “parameters.inp” stores the assigned values of the design variables of the slab the FE model can be run. The FE model is programmed, by means of APDL, in a text file (“BPToptim.txt”). This text file retrieves the values of the design variables of the slab from file “parameters.inp”. Once the model is solved, the results (“Displacement.txt”, “StressTension.txt”, “StressCompresion.txt”, “StressShear.txt” and “StressTendon.txt”) are stored in different files. These results will be used to evaluate the fitness function, which represents the objective function that has to be minimized.
- Next, the GA mutates the value of the design variables so as to achieve a minimum in the fitness function. The new values for the design variables are stored and overwritten in “parameters.inp”.
- The loop will continue until a stopping criteria or minimum is achieved.

APPENDIX B

PERSONAL INFORMATION

Name and Surname : Abbas Haraj Mohammed
Nationality : Iraq
Birth place and date : Diyala/1974
Marital status : Married – 1 kids
Mobile number : +90 538 032 14 76 in Turkey
+964 770 929 60 73 in Iraq
E-mail : abbas_haraj@yahoo.com

EDUCATION

Degree	Graduate School	Year
Master	University of Baghdad	2001
Bachelor	University of Baghdad	1998
High School	Al- Muqdadiya High School	1993

WORK EXPERIENCE

Year	Place	Enrollment
2005-Present	University of Diyala	Assistant Lecturer

PUBLICATIONS

A. Journals

Mohammed, A. H., Tayşi, N., (2017). Modelling of bonded and unbonded post-tensioned concrete flat slabs under flexural and thermal loading. *Structural Engineering and Mechanics, An International Journal*, **62(5)**, 595-606.

Nassani, D. E., Hussein, A. K., **Mohammed, A. H.** (2017). Comparative Response Assessment of Steel Frames With Different Bracing Systems Under Seismic Effect. *Structures*, **11**, 229-242.